Synthesis of Rotorcraft Noise from Flyover Data

Jonathan Robert Hardwick

Thesis submitted to the faculty of the Virginia Polytechnic Institute and State University
in partial fulfillment of the requirements for the degree of

Master of Science
In
Mechanical Engineering

Christopher R. Fuller
Stephen A. Rizzi
Pablo A. Tarazaga
Eric Greenwood

August 21, 2014
Hampton, VA

Keywords: rotorcraft, synthesis, flyover noise

Synthesis of Rotorcraft Noise from Flyover Data

Jonathan Robert Hardwick

ABSTRACT

Flyover noise is a problem that affects citizens, primarily those that live near or around places with high air traffic such as airports or military bases. Such noise can be of great annoyance. The focus of this thesis is in determining a method to create a high fidelity sound source simulation of rotorcraft noise for the purpose of producing a complete flyover scenario to be used in psychoacoustic testing. The focus of the sound source simulation is simulating rotorcraft noise fluctuations during level flight to aid in psychoacoustic testing to determine human perception of such noise. Current methods only model the stationary or time-average components when synthesizing the sound source. The synthesis process described in this thesis determines the steady-state waveform of the noise as well as the time-varying fluctuations for each rotor individually. The process explored in this thesis uses an empirical approach to synthesize flyover noise by directly using physical flyover recordings. Four different methods of synthesis were created to determine the combination of components that produce high fidelity sound source simulation. These four methods of synthesis are:

a) Unmodulated main rotor
b) Modulated main rotor
c) Unmodulated main rotor combined with the unmodulated tail rotor
d) Modulated main rotor combined with the modulated tail rotor

Since the time-varying components of the source sound are important to the creation of high fidelity sound source simulation, five different types of time-varying fluctuations, or modulations, were implemented to determine the importance of the fluctuating components on the sound source simulation. The types of modulation investigated are a) no modulation, b) randomly applied generic modulation, c) coherently applied generic modulation, d) randomly applied specific modulation, and e) coherently applied specific modulation. Generic modulation is derived from a different section of the source recording to which it is applied. For the purposes of this study, it is not clearly

dominated by either thickness or loading noise characteristics, but still displays long-term modulation. Random application of the modulation implies that there is a loss of absolute modulation phase and amplitude information across the frequency spectrum. Coherent application of the modulation implies that an attempt is made to line up the absolute phase and amplitude of the modulation signal with that which is being replaced (i.e. that which was stripped from the original recording and expanding or contracting to fit the signal to which it is applied). Specific modulation is the modulation from the source recording which is being reconstructed.

A psychoacoustic test was performed to rank the fidelity of each synthesis method and each type of modulation. Performing this comparison for two different emission angles provides insight as to whether the ranking will differ between the emission angles. The modulated main rotor combined with the modulated tail rotor showed the highest fidelity and had a much higher fidelity than any of the other synthesis methods. The psychoacoustic test proved that modulation is necessary to produce a high fidelity sound source simulation. However, the use of a generic modulation or a randomly applied specific modulation proved to be an inadequate substitute for the coherently applied specific modulation. The results from this research show that more research is necessary to properly simulate a full flyover scenario. Specifically, more data is needed in order to properly model the modulation for level flight.

Acknowledgements

I would like to thank my advisor, Dr. Christopher Fuller, and my mentor, Dr. Stephen Rizzi, for supporting and guiding me through my research. I would like to thank Dr. Eric Greenwood for support and guidance in understanding rotorcraft noise and for the use of the synchronous time-average method as a starting point for my computer program to complete my research. I would like to thank my committee member, Dr. Pablo Tarazaga for his help and advice in regard to my thesis.

I would like to thank Andy Christian for his insight and guidance in the analysis of the psychoacoustic results. I would like to thank Dan Palumbo for his help in understanding the demodulation process. I would like to thank NASA Langley Research Center, specifically the Structural Acoustics Branch, the National Institute of Aerospace (NIA), and Virginia Tech for a place to better myself through higher education and financial support. I would like to thank Gail Coe, Cathy Hill, and Mandy Collins for help and support at Virginia Tech. Being a distance education student presents a unique set of challenges and your support helped to bridge that gap. I would like to thank Rita Aguillard for all of her help with the distance learning classes. This opportunity has been made possible by all of the aforementioned people for which I am so grateful.

Table of Contents

List of Figures

List of Tables

1. Introduction

Flyover noise is a problem that affects many citizens, primarily those that live near or around places with high air traffic such as airports or military bases. Such noise can be of great annoyance. As the world trade grows and the interest to explore new areas of the world increases so does the air traffic that causes such disturbances. Fixed and rotary wing aircraft contribute to this noise pollution. The areas of annoyance, detection, and sleep disturbance, among others, are particularly important to researchers designing the next generation of aircraft. Human subject tests are used to evaluate whether the noise from a particular aircraft is considered to be a nuisance. Before a human subject test can be performed, the researchers must be able to aurally present a sound that realistically resembles that of the aircraft of interest for the test subjects. The creation of this realistic sound is called sound source simulation. Realism is a very subjective, or qualitative, way to describe a sound. Sounds can be described through mathematical equations; therefore sounds can be compared through quantitative metrics. The best term that combines both the qualitative and quantitative metrics of sound is fidelity. The higher the fidelity of a sound, the more realistic the sound is. The desire is to use high fidelity sounds when creating sound source simulation. The purpose of the high fidelity sound source simulation is to aid in the understanding of the human response to aircraft flyover noise, specifically rotorcraft noise. The focus of this thesis is determining a method to create a high fidelity sound source simulation of rotorcraft flyover noise. The objective and subjective metrics of the methods, discussed in the following chapters, will be evaluated to determine the best method to create such a sound source simulation.

The overall goal for this research is to synthesize or create a realistic digital representation of time-varying rotorcraft noise. This ability will allow the realistic rotorcraft noise to be generated without the need to record the physical aircraft. The hypothesis is that by adding time-varying (aperiodic) components to a time-invariant (periodic) signal, the noise will become perceptibly more realistic. The focus of the sound source simulation is simulating a fluctuating sound source. A fluctuating or time-

varying sound source can be thought of as having two separate pieces. The first piece is a steady, or stationary, sound source consisting of one or more independent frequencies. The second piece is a sound source that fluctuates, or varies with time. These two pieces can be combined to match the original signal. Currently, acoustic analyses such as those found in the Aircraft NOise Prediction Program (ANOPP) [1] and PSU-WOPWOP [2] only create the stationary or time-average components when predicting source noise. The current method does not include the important fluctuations of the sound. Time-varying fluctuations alert us to changes in our environment. These fluctuations are not only important in simulating aircraft noise but are also important in everyday life.

Understanding rotorcraft noise, specifically the impact of various flight conditions on such noise, is an important topic in the area of aeroacoustics. Recently, the noise of the XV-15 was analyzed with regard to rotor operating conditions, specifically how the noise levels change as the angle of the nacelle varies [3]. Also, Ram JanakiRam and Hamza Khan explored a method to model helicopter descent as heard by an observer on the ground [4]. These are two examples of research in an immense array of research topics pertaining to rotorcraft noise. Both of these articles analyze how the rotorcraft noise changes with changing operating conditions and flight paths. However, people experience rotorcraft annoyance when the aircraft is in level flight since this flight condition makes up the majority of the flight path, depending on the duration of the flight.

Rotorcraft noise simulation is a growing field. Brentner and Farassat discuss recent improvements in methods to predict helicopter noise. The authors conclude that advances in the understanding of and the ability to predict impulsive noise sources, such as blade-vortex interaction (BVI) and high speed impulsive (HSI) noise, has been achieved. However, the calculations necessary to determine the aerodynamic interactions along the rotor blade surface are complex and difficult. Also, a greater understanding of the different types of vortices generated by helicopter rotors is necessary. The authors are optimistic for the future of rotorcraft noise prediction methods [5].

The hope is to eventually create a full flyover simulation. A full flyover can consist of ascending flight, such as takeoff or climb, level flight, or cruising flight, and descending flight. This thesis specifically analyzes level flight. However, the synthesis

process described throughout this document can be applied to any type of rotorcraft flyover noise. The components that contribute the most to flyover noise should be determined first in order to simulate any form of flight. According to Fredric H. Schmitz et al. [6], of all the various noise sources on present day helicopters, the main and tail rotors have the largest influence on the overall acoustic signature of the helicopter during the majority of operating conditions. In descending flight conditions, unsteadiness in acoustical sources is present partially due to the pilot making corrections to stay on course [4]. The same unsteadiness may be present in level flight. Franklin Harris describes the unsteadiness as the waveform "dancing," which causes distortion of the signal, however the fundamental behavior is easily recognized [7]. Therefore, steady-state (or stationary) and unsteady (or time-varying) acoustical sources must be simulated to create an accurate representation of the rotorcraft noise. The periodic noise of a rotorcraft consists of three different noise sources which are thickness noise, loading noise, and impulsive noise sources, such as BVI and HSI noise [8]. Thickness noise and loading noise will be directly analyzed in this thesis. Defining these two types of noise sources will further aid in understanding sound source simulation. Thickness noise is generated from the way air interacts with the rotor blades in the plane of the rotor disk [9]. Loading noise is generated by the aerodynamic forces acting perpendicular to the rotor disk plane [9].

The synthesis process described in this thesis determines the steady-state waveform of the noise as well as the unsteady components separately. This allows the engineer to decide whether to use the steady-state waveform determined by the process explored in this thesis or to simply use the superposition principle to combine the time-varying fluctuations and the steady-state waveform determined via some other analysis method.

This synthesis process utilizes an empirical approach to synthesize flyover noise by directly using physical flyover recordings. The Bell 206B3 is the source of the flyover data used in the analysis. The Bell 206B3 is a conventional helicopter, which uses a main and tail rotor for lift and propulsion. The benefit of using an empirical approach is that the time-varying fluctuations, or modulation, of the flyover noise can be extracted from the recording, whereas the use of a theoretical model may struggle with the

characterization of such modulation. However, empirical methods are not without certain limits. The drawback to using empirical data is that the rotorcraft being modeled (whether a current or future design) must have geometrically similar rotors to the rotorcraft that produced the data. Also, the rotorcraft being modeled must have undergone the same flight conditions as the rotorcraft that produced data being used. The flight conditions are characterized by non-dimensional flight characteristics, such as coefficient of thrust, the hover tip Mach number, advance ratio, and rotor tip path plane angle of attack. The use of this empirical data cannot be used to characterize or approximate any aircraft design that does not share similar rotor geometries and flight conditions as the data. If the desired aircraft does match with these characteristics, the empirical data can be appropriately scaled to approximate the desired aircraft design [10].

The synthesis process explored in this thesis uses the flyover data to create a flying hemisphere that represents the source noise. It is determined from sound radiated from the source to an observer on the ground. This is accomplished by correlating tracking data of the source with the pressure-time history of the flyover noise. The sound, heard by the observer on the ground, is corrected for Doppler shift and spherical spreading to create a sound that is representative of the sound heard by a "virtual observer" that is located on the flying hemisphere at a specified distance away from the main rotor hub. The synthesis process isolates the sound of each rotor. The individual rotor signatures are then separated into the steady-state components and the unsteady components, or modulation. The steady-state components consist of the time-average frequency, amplitude, and the initial phase of each harmonic. The unsteady components describe how the frequency and amplitude shift over the time record. This separation of components allows for each rotor to be reconstructed separately with or without the unsteady components using different methods of synthesis. Also, various types of modulation may be combined with the steady-state content to determine if a generic form of modulation is adequate in representing all modulation for this particular helicopter. The various methods of synthesis and types of modulation are used in a psychoacoustic test to determine the relative ranking of fidelity, or realism. The general overview of the process is shown in Figure 1.

Since the creation of a realistic sound source simulation is the primary focus of this work, it is important to understand what is meant by realism. Realism is a subjective measure of how closely the synthesized, or reconstructed, signal mirrors that which one might experience in the "real world." A more inclusive term to describe the aim of this research is "fidelity". Fidelity includes objective and subjective measures to aid in the determination of what is to be considered realistic [11].

Before continuing it is important understand what is meant by synthesis, which is discussed in Chapter 2. An additive synthesis method is used as the basis for the deconstruction, analysis, and synthesis of rotorcraft noise. This method is founded on the principles that sound can be deconstructed using Fourier analysis and reconstructed using the process of superposition. Six objective metrics are chosen to facilitate the comparison of the reconstructed signals to the reference signal. This comparison is done to determine the accuracy of the reconstructed signals, as compared to the reference. The sound to be synthesized is chosen to be rotorcraft flyover noise from a Bell 206B3 helicopter. The sound is processed through a back-propagation algorithm to create a signal indicative of the sound that would be heard near the helicopter. Two methods will be used to determine steady-state signal. The first method, the synchronous time-averaged method, employs an ensemble averaging technique to determine the time-averaged main and tail rotor pulses. The second method, the demodulation method, employs band-pass filtering, amplitude demodulation, and frequency demodulation to determine the average main rotor and tail rotor signals, as well as the time-varying portion of the rotorcraft noise. Four reconstruction methods are employed to reconstruct the rotorcraft noise.

Two considerations in regard to facilitating a complete flyover scenario are evaluated. The first consideration is to develop a method to extend the pressure-time histories of modulation data for an arbitrary length of time. The second consideration is to develop a method that allows for the capability to transition the sound between adjacent emission angles. In order to validate these methods, a psychoacoustic test is performed. The goal of this test is to indicate the method by which high fidelity rotorcraft noise is synthesized.

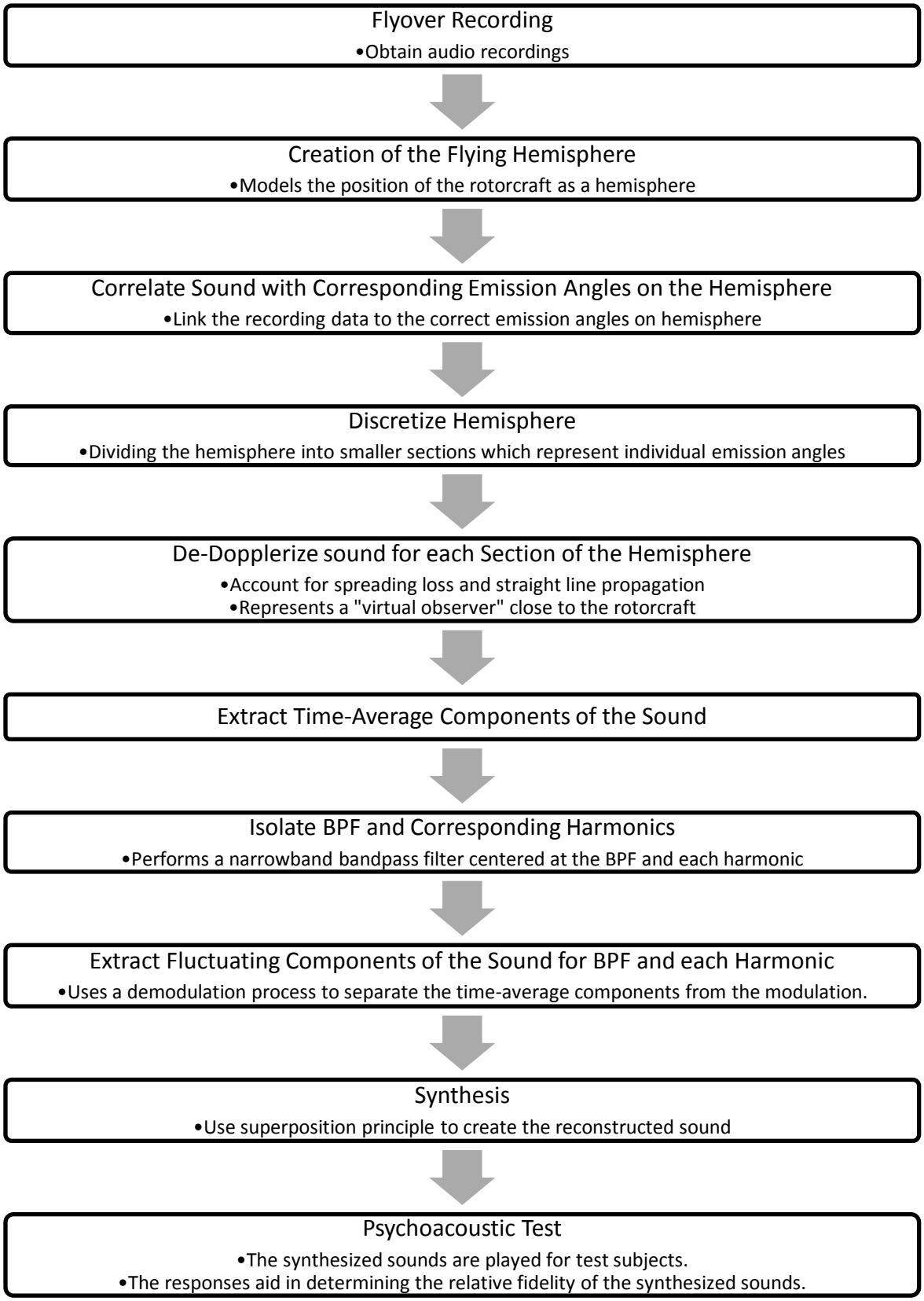

Figure 1: Flow chart of synthesis process.

2. Synthesis Overview

In this chapter, an additive method for synthesizing rotorcraft main and tail rotor noise is proposed. It is amenable to the synthesis of time-invariant (periodic) harmonic signals and time-varying (aperiodic) harmonic signals. The means for determining the synthesis input parameters are discussed in Chapters 3 and 4. Irrespective of the input, a means of measuring the fidelity of the synthesized signals vis-à-vis recordings is necessary to judge the merits of one synthesis method over another. Some objective measures of fidelity are offered for this purpose.

2.1 Additive Synthesis Method for Application to Rotorcraft Noise

The pressure time history of rotorcraft source noise can be deconstructed into a series of sine and cosine waves via Fourier analysis. A sinusoidal wave with a constant amplitude (A), frequency (f), and phase (ϕ) for all time t is classified as a time-invariant signal or wave [12]. A time-invariant (periodic) wave is described by

$$p(t) = A\cos(2\pi f t + \phi_0). \tag{1}$$

Once these values begin to change with time, the sinusoidal wave is reclassified as a time-varying (aperiodic) signal and Equation (1) becomes

$$p(t) = A(t)\cos\big(2\pi f(t)t + \phi(t)\big). \tag{2}$$

This is accomplished by applying amplitude and/or frequency fluctuations to a time-invariant base signal. A more detailed equation to describe a time-varying signal and the one ,which will be used to create the synthesized signal is shown as

$$p(t) = \big[\bar{A} + \tilde{A}(t)\big]\cos\left(2\pi\bar{f}t + 2\pi\int_0^t \tilde{f}(\tau)d\tau + \phi_0\right). \tag{3}$$

Here, the total amplitude is broken into two parts; the time-invariant component, or mean amplitude ($\bar{A}$), and the time-varying component, or amplitude fluctuation ($\tilde{A}(t)$). The total frequency, in the same way, consists of two components; mean frequency ($\bar{f}$) and frequency fluctuation ($\tilde{f}$). The fluctuations are also known as modulations. An important note to make is that frequency is the derivative of the phase, as seen in Equation (4), and that is why the frequency modulation and any phase modulation will be assumed to be characterized by the frequency modulation term ($\tilde{f}$) [13, 14].

$$\phi(t) = 2\pi \int_0^t \tilde{f}(\tau) d\tau + \phi_0 \tag{4}$$

By using Equation (3) to describe the noise, it is assumed that any and all fluctuations in phase are completely due to fluctuations in frequency. This is why the phase term ϕ_0 is constant and does not vary with time. Also, Equation (3) only describes each individual sinusoidal wave that is used to create the rotorcraft noise. In order to synthesize or reconstruct the rotorcraft noise, or at least the parts of interest, the individual sinusoidal waves must be summed together through the process of superposition. This is the discrete inverse Fourier transform. Such a process is described by

$$p(t) = \sum_{i=1}^{N} \left[\bar{A}_i + \tilde{A}_i(t)\right] \cos\left(2\pi \bar{f}_i t + 2\pi \int_0^t \tilde{f}_i(\tau) d\tau + \phi_{0,i}\right). \tag{5}$$

Equation (5) is merely a summation of Equation (3) for all of the sinusoidal waves that make up the signal of interest. For the purposes of this thesis, only the noise produced by the main rotor and tail rotor are of interest. The harmonic series is the group of sinusoidal waves that make up the noise for each rotor. The lowest tonal frequency present that is greater than zero is called the blade passing frequency (BPF). All other tonal frequencies, which are multiples of the BPF, are referred to as overtones. Equation (5) sums the BPF and all harmonics in order to reproduce the original signal. The N in Equation (5) is the maximum number of harmonics present, including the BPF. The main rotor and tail rotor, typically, have different BPFs. The BPF of the main rotor and tail rotor are typically not integer multiples of one another.

The BPF is equal to the multiplication of the number of blades in the rotor disk (n) and the angular velocity (rad/s), which is characterized by

$$BPF = n\omega. \tag{6}$$

How does one go about finding the components in order to build the desired synthesized signal? One option is to use a time-averaged signal to act as a surrogate for the fluctuations. This base signal is a time domain signal containing the mean frequency, mean amplitude, and relative phase of all of the frequencies of interest, which represents the general characteristic of the rotorcraft noise for each rotor individually. Therefore the engineering analysis that produces the base signal must provide each of these three components in some manner. The time-averaged signal may be created from either a

theoretical model of the noise or from empirical data. Engineering analysis codes such as PSU-WOPWOP [2] or the most current version of the Aircraft NOise Prediction Program (ANOPP2) [1] provide a time-averaged signal derived from a theoretical model. In contrast, the synchronous time-averaging method utilized by Greenwood [15] and implemented in this research to extract the back-propagated signal from the original flyover data, utilizes an empirical method. Analysis methods such as those contained in the Rotorcraft Noise Model (RNM) [16] only provide the relationship between amplitude and frequency while neglecting phase, which is insufficient for the purposes of this research. Once the base signal is established, the next step is to determine a manner in which to capture the time-varying nature of the noise of interest. This is explained in Chapter 4.

2.2 Objective Measures of Fidelity

In the subsequent chapters, each synthesized waveform is analyzed using six different comparison metrics. The metrics are loudness, roughness, sharpness, specific loudness, specific roughness, and tonality. Loudness is a measure of how the human ear perceives sound intensity [17]. Specific loudness is the representation of loudness in the frequency domain. Roughness describes the time-varying characteristics, such as the frequency or amplitude, of a sound [18]. Sharpness describes the way in which the human ear perceives the high frequency content of a particular sound. Tonality describes the amount and amplitude of the pure tones present. The objective measures and the standards used for each metric are shown in Table 1.

Table 1: Objective metrics of fidelity

Metric	Standard	Units
Loudness	ANSI S3.4-2007	phon
Roughness	Sottek hearing model	asper
Sharpness	ANSI S3.4-2007(loudness method), Aures(sharpness method)	acum
Specific Loudness	ANSI S3.4-2007	sone/ERB
Specific Roughness	N/A	asper/Bark
Tonality	Publications by Terhardt and Aures [18]	tu

The calculations for each metric were performed in the ArtemiS Suite from HEAD Acoustics [18, 19]. For each of the metrics, all synthesized waveforms were compared to the reference sound using the percent root mean square error calculated over a signal length of interest.

3. Synthesis of Time-Invariant Rotorcraft Noise

The time-average signal was obtained using the method described in reference [15]. The process is summarized below. The flyover data used in this work was recorded from a Bell 206B3 helicopter at straight and level flight over the eight microphone linear ground array. This microphone array is located perpendicular to the flight path of the helicopter. However, only the center microphone (M5) is used to create the time-average and unsteady signals used later in this work. The Bell 206B3 consists of two rotors, a main rotor and a tail rotor. More information can be obtained from [6].

The purpose of the following signal analysis is two-fold. First, it is used as a means of determining the "base" signal from recorded flyover noise. Here, the "base" signal contains both mean and fluctuating amplitude and frequency components. The second purpose is the processing of that signal to determine the time-averaged blade passage signals for each rotor of the helicopter. Note that the latter is one of two methods offered for determining the mean values. The other method is described in Chapter 4.

3.1 Base Signal Preparation

The first step in establishing the "base" signal is to create a hemispherical surface around the source based on the tracking data and the microphone locations. The hemisphere is then divided into different sections. Each section of the hemisphere must include enough rotor blade passages to effectively represent rotor harmonic noise when the individual blade passages are averaged together and the noise emitted from a single section of the hemisphere must be indicative of a single emission angle within that section of the hemisphere [15]. This means that enough continuous blade passages must be included in each section to sufficiently reduce any noise that is not harmonic with the rotor when the blade passages are averaged together. Included in that other noise are time-varying components. The second condition implies that the blade passages for each section must originate from the same portion of the hemisphere and be in close proximity

to the other blade passages. Both parameters are selected when sectioning the hemisphere. The pressure-time history is superimposed onto the hemisphere by correlating the pressure-time history with the tracking data. This allows one to determine which section of the hemisphere corresponds to the correct section of the pressure time history. The tracking data consists of the time record and the three-dimensional location, in Cartesian coordinates, of the rotorcraft during the flyover. It is desirable to reorient the coordinate system from the Cartesian coordinate system whose origin is located at the observer (or microphone), which is located on the ground plane, to spherical coordinates whose origin is located at the main rotor hub. Since the flyover data used is from only one microphone and that microphone is located directly in line with the helicopter's flight path, the flyover can be considered two-dimensional where the third dimension is held constant. Figure 2 illustrates the relationship between the noise source and the observer with regard to the Cartesian coordinate system (blue) and the spherical coordinate system (red).

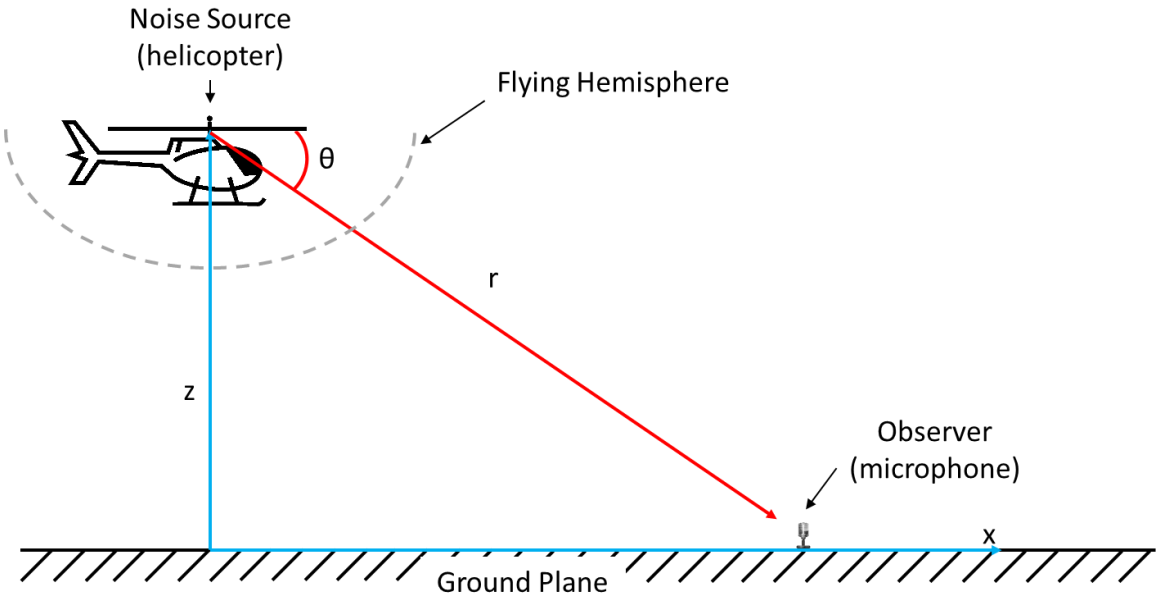

Figure 2: Reorienting the coordinate system from a observer centered Cartesian coordinate system to a noise source centered spherical coordinate system.

By knowing the location of the observer (x_{mic}, y_{mic}, z_{mic}) during the flyover, the Cartesian coordinates of the rotorcraft (x_{source}, y_{source}, z_{source}) can be converted to

spherical coordinates whose origin is located at the origin of the hemisphere, using the relations

$$r = \sqrt{(x_{mic} - x_{source})^2 + (y_{mic} - y_{source})^2 + (z_{mic} - z_{source})^2} \tag{7}$$

$$\theta = \tan^{-1}\left(\frac{|z_{mic} - z_{source}|}{\sqrt{(x_{mic} - x_{source})^2 + (y_{mic} - y_{source})^2}}\right) \tag{8}$$

$$\psi = \tan^{-1}\left(\frac{y_{mic} - y_{source}}{x_{mic} - x_{source}}\right). \tag{9}$$

The distance between the rotorcraft and the observer is represented by r. The elevation angle (θ) spans from zero degrees to 90 degrees, whereas the azimuth angle (ψ) spans from 0 degrees at the tail to 180 degrees at the nose to 360 degrees at the tail, which is illustrated by Figure 3.

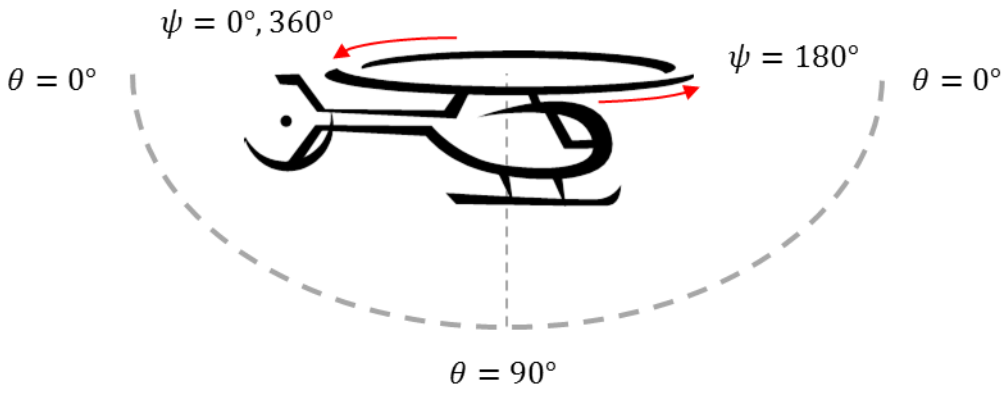

Figure 3: Elevation angle and azimuth angle convention as used in this work

Tracking data is now in the form of the emission angles (θ and ψ) versus time. Once the time record of the tracking data is correlated with the time record of the pressure-time history, the angles of the hemisphere will be linked to the corresponding pressure. Since the data used in this work was obtained from the centerline microphone, equations (7)-(9) reduce to

$$r = \sqrt{(x_{mic} - x_{source})^2 + (z_{mic} - z_{source})^2} \tag{10}$$

$$\theta = \tan^{-1}\left(\frac{|z_{mic} - z_{source}|}{|x_{mic} - x_{source}|}\right) \tag{11}$$

$$\psi = \tan^{-1}(0). \tag{12}$$

The next step is to convert the noise heard by the observer (in this case a ground microphone) to a signal that is representative of the noise emitted at the source. This

process is accomplished through a time domain back-propagation process. A monopole in motion generates a pressure field described by [15]

$$p'(\mathbf{x},t) = \frac{Q(\tau)}{4\pi r(\tau)} \frac{1}{|1 - M_r|} \tag{13}$$

where $r(\tau)$ is the time-varying propagation distance, Q is the source strength of an arbitrary source, and M_r is the Mach number in the direction along r. The back-propagation process corrects for the Doppler shift that occurs between an observer on the ground and a noise source in a flyover scenario due to the variation in time delay

$$t - \tau - \frac{r(\tau)}{a_0} = 0 \tag{14}$$

where a_o is the speed of sound. The signal is corrected to a "virtual observer" located at a user specified distance away from the source by using the following modified retarded time equation.

$$t_v = t - \frac{r(\tau) - r_v}{a_0} \tag{15}$$

The noise that occurs at the "virtual observer" at time t_v is representative of what would be heard by a microphone at distance r_v from the source

$$p'_v(\mathbf{x_v}, t_v) = \frac{r(\tau)}{r_v} p'(\mathbf{x}, t). \tag{16}$$

The pressure at the "virtual observer", or "virtual microphone", is resampled to a constant sampling rate using simple linear interpolation, which is shown in Figure 4 [15].

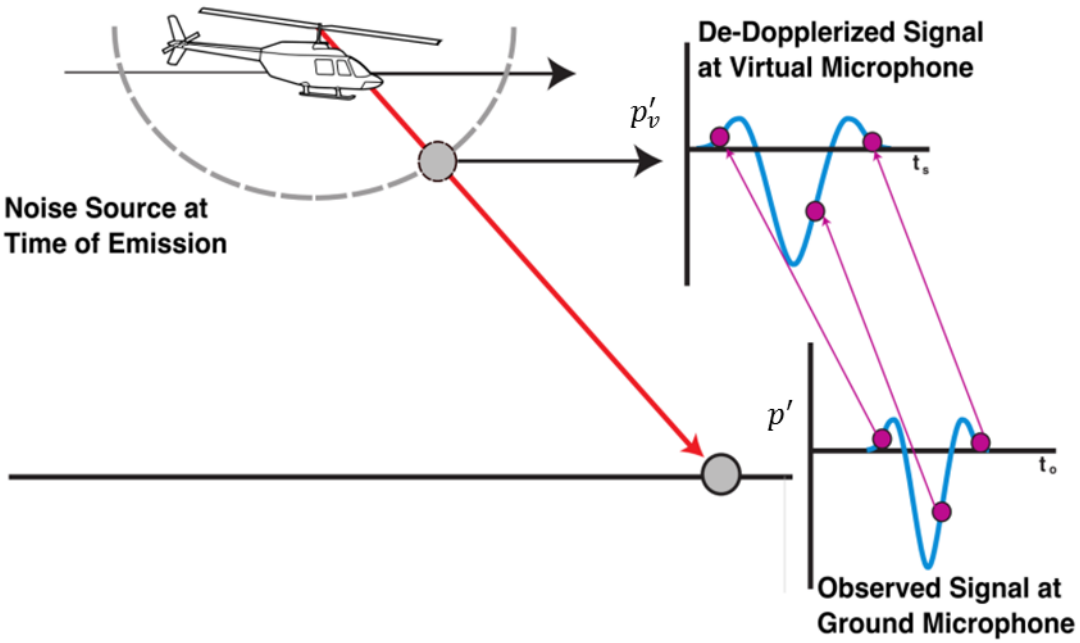

Figure 4: Back-propagation process [15]

The back-propagation process accounts for straight line propagation between the source and the observer, as well as spherical spreading at the source but does not compensate for atmospheric attenuation. Compensation for atmospheric attenuation is deemed unnecessary because the propagation distances are generally short and the frequency content is low. Further, since the microphones are located on the ground plane, no correction other than removal of pressure doubling is needed. The method assumes that the noise source, in this case the main rotor and the tail rotor, is a compact source. This allows the hemisphere, which flies with the helicopter, to describe the noise characteristics of the helicopter as heard by an observer in the far-field [15]. The use of a compact source model is a valid assumption when the helicopter is significantly far from the observer or when the angle between the straight-line path (red line in Figure 2) and the ground plane is significantly small. This allows the noise source to be modeled as a compact source since the wavelength of the source noise is much longer than the dimensions of the source [17]. The location of the far-field is determined by the wavelength (λ) of the sound source. The far-field for higher frequencies is located closer to the sound source compared to the location of the far-field for lower frequencies. The far-field is located at a distance far enough away from the sound source such that the

sound pressure (p) and particle velocity (u) are in phase. Sound pressure and particle velocity are defined by

$$p(r,t) = \frac{Ae^{-ikr}}{r} e^{i\omega t} \tag{17}$$

$$u(r,t) = \frac{1}{\rho c}\frac{A}{r}\left(1 + \frac{i}{kr}\right) e^{-ikr} e^{i\omega t}. \tag{18}$$

The sound pressure and particle velocity are described in terms of the amplitude (A), wave number (k), frequency (ω) in rad/sec, and characteristic impedance of the medium (ρc). The amplitude (A), for a simple spherical source, is related to the source-strength ($Q(\tau)$) in Equation (13) by [20]

$$Q(\tau) = \frac{4\pi A(\tau)}{\omega\rho}. \tag{19}$$

In order for the sound pressure and the particle velocity to align in phase, the term $\left|\frac{i}{kr}\right| \ll 1$, where

$$kr = \frac{2\pi r}{\lambda} \tag{20}$$

and λ represents the wavelength of the source noise

$$\lambda = \frac{v}{f}. \tag{21}$$

The frequency of the sound source is represented by f and the phase velocity is represented by v. The phase velocity is assumed to be equal to the speed of sound in air (nominally 1125 ft/s). The lowest frequency (90% of the BPF) used in this work is 11.0159Hz, which has a corresponding wavelength of 102.13ft. The Bell 206B3 main rotor (noise source) radius is approximately 16.67 ft long. The wavelength of the lowest frequency is much longer than the largest dimension of the sound source. Therefore, the helicopter can be modeled as a compact source (monopole). However, do the phase velocity and the sound pressure align in phase? The far-field criteria for the lowest frequency in the spectrum of interest satisfy the far-field criteria for all other frequencies of interest since the far-field location is closer to the sound source for higher frequencies as compared to lower frequencies. During the flyover, the shortest distance between the helicopter and the observer is 159.49 ft.

$$\frac{i}{kr} = \frac{i}{\frac{2\pi r}{\lambda}} = 0.1019i \tag{22}$$

Since $\frac{i}{kr}$ is in fact much less than unity, the particle velocity and the sound pressure do align in phase. This means that the helicopter can be characterized as a compact source in the far field [21]. However, the compact source is beginning to violate this condition as the rotorcraft moves close to the observer at 159.49 ft.

A few parameters must be set to create this flying hemisphere. A reference distance of 30 feet was used to create the data that will be later used to synthesize the rotorcraft noise. Also, the minimum number of revolutions of the main rotor and the minimum angular distance required for each section of the hemisphere were specified as 20 revolutions and 10°, respectively. Table 2 displays the emission angles and the length of time for three of the sections of the hemisphere, which were determined from the back-propagation method described earlier. The three segments shown in Table 2 will be specifically used in the analysis later in this work. The character of the thickness noise (section 2 of the hemisphere) and the character of the loading noise (section 4 of the hemisphere) are captured in audiofile25.wav and audiofile26.wav, respectively.

Table 2: A few hemisphere section characteristics.

Section of the Hemisphere	Dominant Noise Type	Emission Angles (°)	Section Length (s)
2	thickness noise	12.72- 21.78	2.3463
3	thickness and loading noise	21.7809-34.5251	1.3394
4	Loading noise	36.98-80.91	1.6349

Now that the hemisphere has been created and the pressure-time history has been linked with the corresponding sections of the hemisphere, the next step in the analysis determines the number of samples in each blade passage through the use of the continuous wavelet transform. For the each rotor, this is based on the blade passage frequency (BPF), that is,

$$S(b, t_v) = \int_{-\infty}^{\infty} s(t_v') \frac{1}{\sqrt{b}} \xi^* \left(\frac{t_v - t_v'}{b} \right) \mathrm{d}t_v' \tag{23}$$

where the wavelet scales are represented by b and the complex conjugate of the basis wavelet function, also known as the mother wavelet, is denoted by ξ^*. The wavelet scales are inversely related to the frequency. For this application, the mother wavelet is the Ricker wavelet, as seen given by

$$\xi(y) = \frac{1}{\sigma^3 \sqrt{2\pi}} \left(1 - \frac{y^2}{\sigma^2} \right) e^{-\frac{y^2}{2\sigma^2}}. \tag{24}$$

The shape of this wavelet is controlled by σ, which is usually chosen to be approximately unity [15]. The wavelet transform allows for the frequencies of interest to be specified. In this case, ± 10% of the nominal blade passage was evaluated. The wavelet transform sweeps through the frequencies of interest and evaluates the magnitude of the wavelet transform for each of the corresponding wavelet scales. The transformed signal is used to generate a wavelet power spectrogram. The peaks of this spectrogram are determined by comparing the magnitude of the wavelet transform for all frequencies. These peaks correspond to the location of the end points of each blade passage in time [15]. The time difference between the each blade passage denotes the period of the each blade passage and is later used to determine the actual BPF.

3.2 Time-Averaged Main Rotor Identification

Figure 5 displays a one-second section of the back-propagated source signal on the hemisphere and corresponds to a shallow elevation angle where thickness noise is dominant. The locations of the end points of several blade passages, as identified by the above process, are shown in Figure 5 and are designated by the vertical red lines. The leading grey section of the signal is an example of a partial blade passage, which is discarded from further calculations. Partial blade passages may occur when the rotorcraft is close enough to the observer for the noise to be of interest and the rotor disk has not completed a full blade passage at this the time of interest. This may also occur when the hemisphere is divided into multiple sections and a blade passage is split between two adjacent sections of the hemisphere. The latter case is most likely to occur when the minimum angle parameter is the deciding parameter on the boundaries of the sections

within the hemisphere. Partial blade passages occur at either the beginning of the sound wave, at the end of the sound wave, or both locations.

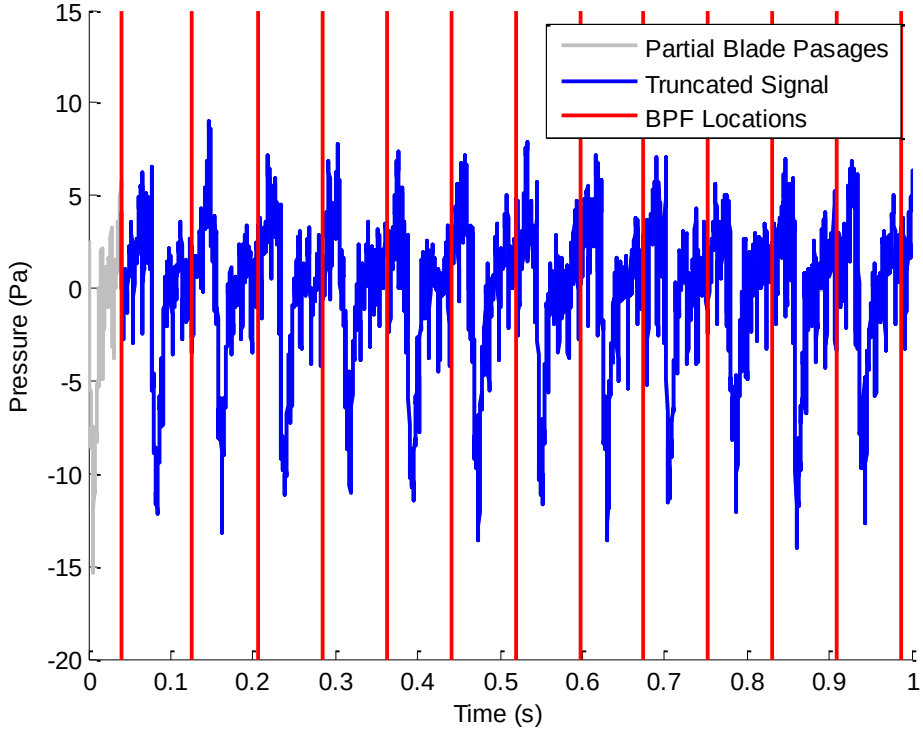

Figure 5: Division of signal into individual blade passages for section 2.

Figure 6 shows a close-up view of Figure 5 to allow for better clarity. The alternating color pattern is used to show the individual blade passages.

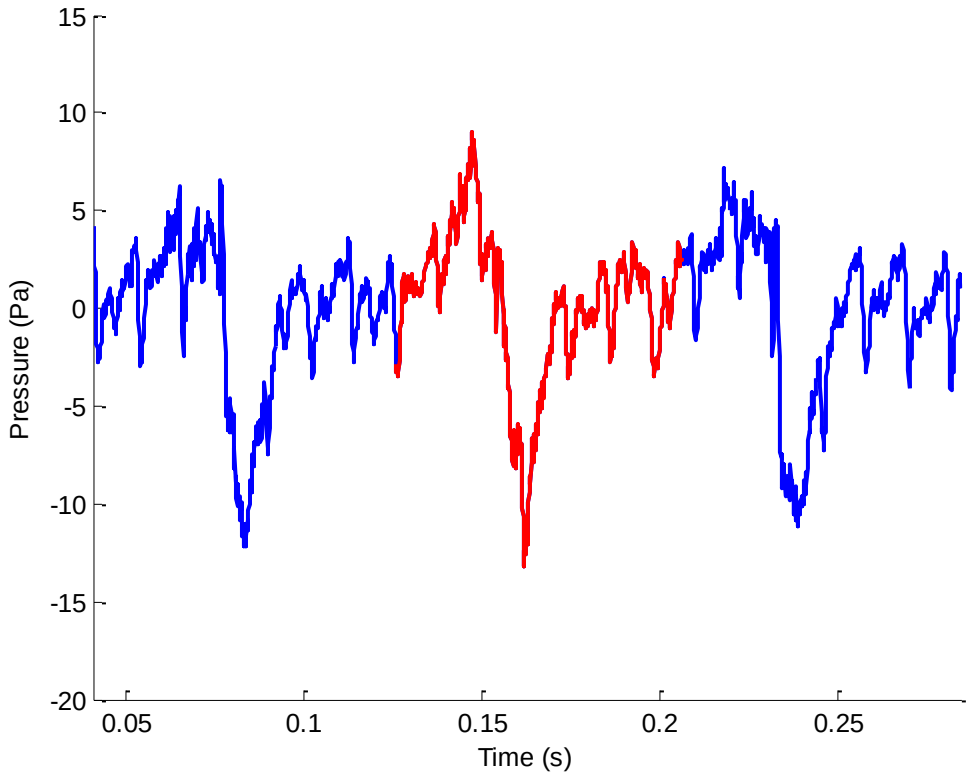

Figure 6: A close-up of the individual blade passages for section 2. Alternating colors designate each full blade passage.

In order to develop the time-averaged signal, each blade passage is time aligned at slice points indicated in Figure 5. When the waveform is divided into each individual blade passage, all blade passages may not have the same number of samples since the slice points determined by the wavelet analysis may not be uniformly spaced in the pressure-time history of the signal. Therefore, each blade passage window is individually resampled to the average block size using linear interpolation. This insures that all of the blade passages contain the same number of samples for computing the synchronous time average. The averaging process performs a point-by-point average for each sample across all blade passages associated with a particular emission angle. Examples of resampled blade passages are shown in Figure 7.

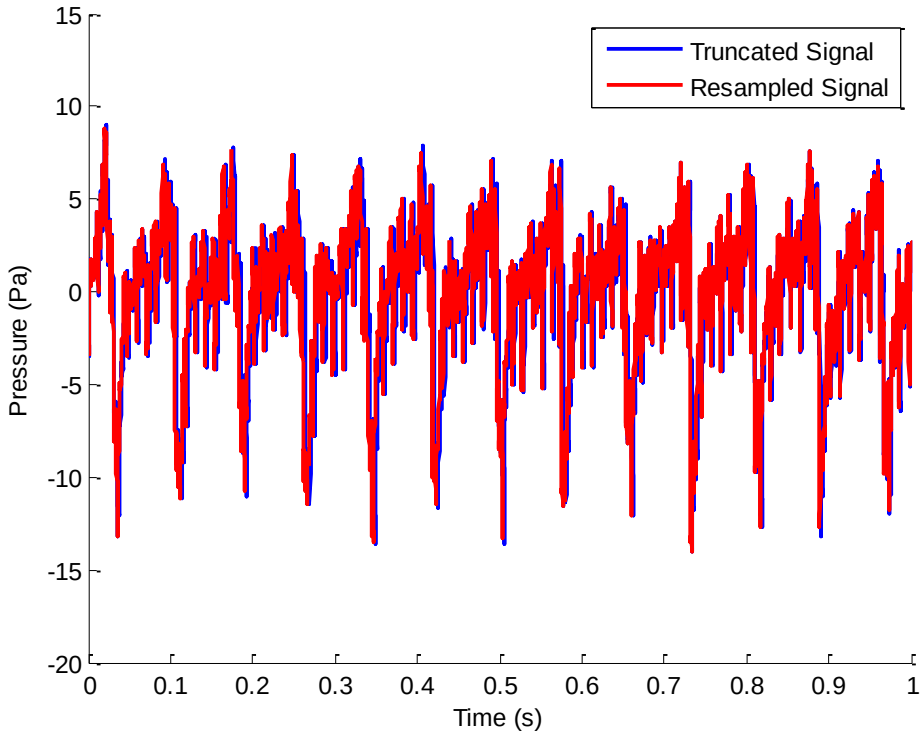

Figure 7: Comparison of the truncated back-propagated signal to the resampled blade passage windows of the main rotor for section 2.

Figure 8 shows a close-up view of three individual blade passage windows to allow for better understanding of the character of the resample individual blade passage windows.

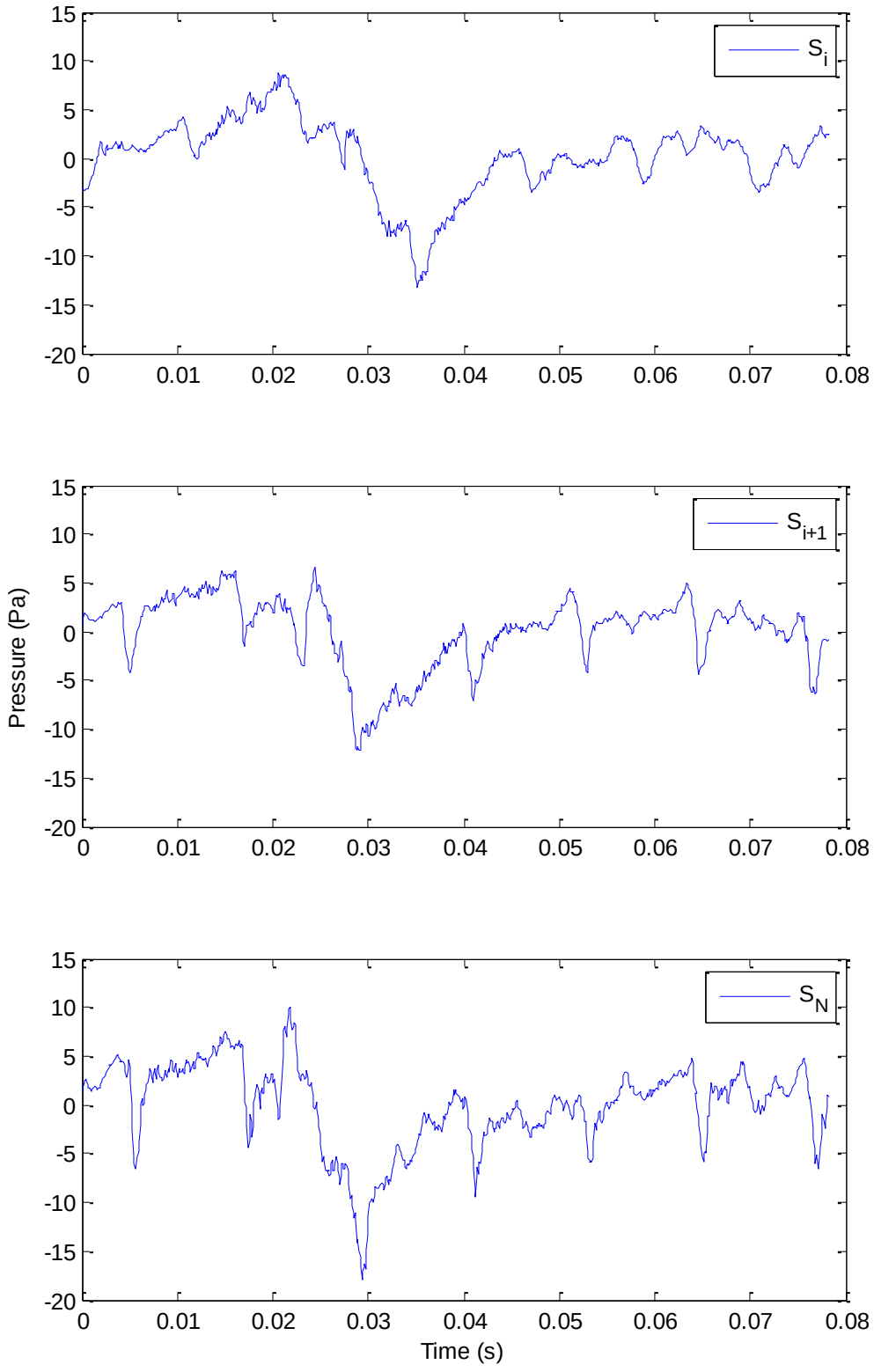

Figure 8: Individual resampled blade passages for section 2.

The synchronous time averaging process is performed by

$$\text{synchronous time-average blade passage} = \frac{1}{N}\sum_{i=1}^{N} S_i \tag{25}$$

where the number of resampled individual blade passages is denoted by N and each sample in the blade passages is denoted by S_i. The result of the synchronous time-average process is a time-averaged blade passage signal, an example of which is shown in Figure 9. The separation analysis works best when the dominant sound source is processed first. For forward radiated sound, the dominant rotor noise typically is generated by the main rotor, while the tail rotor typically is of lesser amplitude.

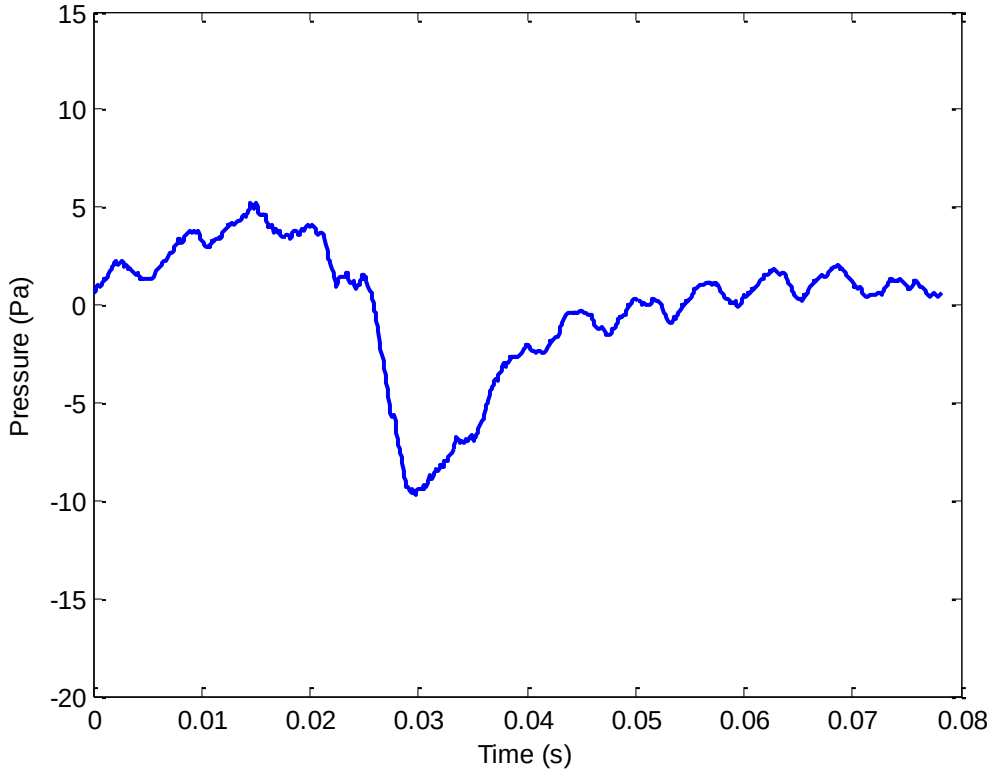

Figure 9: Time-averaged blade passage signal of the main rotor for section 2.

The concatenated time-averaged signal and the back-propagated signal (blue curve) are shown in Figure 10. Figure 10 indicates that more than just the time-averaged blade passage from the main rotor is necessary to recreate the back-propagated signal. A comparison of the auxiliary wave files for the concatenated main rotor, audiofile01.wav and audiofile02.wav (see Appendix C: Index of Supplemental Audio Files), and the

auxiliary audio files for the original back-propagated signal, audiofile25.wav and audiofile26.wav, for thickness and loading noise respectively, clearly demonstrates this. It was found that a more accurate representation of the BPF for a given section could be obtained if the time vector corresponding to the time-averaged signal is determined from the average block size and the time step present in the data, instead of the nominal BPF. This allows for an improved time-averaged signal when the actual BPF of the data being evaluated is unknown. In this case, the initial guess of the nominal BPF should still be close to the actual BPF because the blade passage periods will not be correctly detected otherwise.

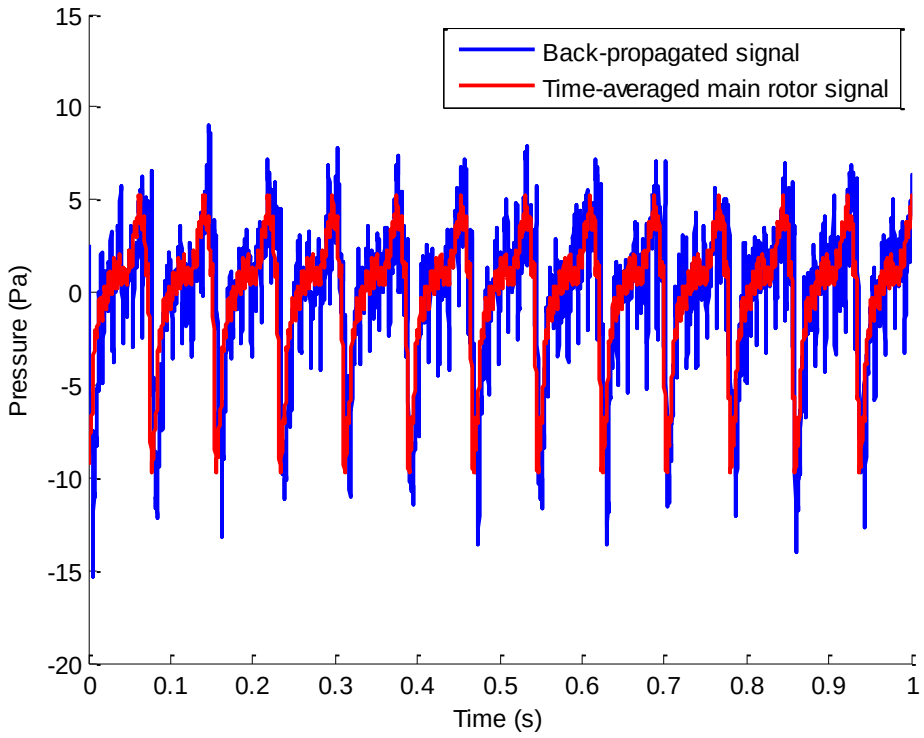

Figure 10: Comparison of the back-propagated signal to the time-averaged main rotor pulse for section 2.

3.2.1 Fidelity of Time-Averaged Main Rotor

The objective metrics used to evaluate the time-averaged main rotor are described in section 2.2. The subjective measures of fidelity will be later explored in Chapter 6.

The results of comparing the time-averaged main rotor using the synchronous time-averaged method with the original back-propagated signal are shown in Table 3.

Table 3: Objective measures of fidelity for the synchronous time-averaged main rotor signal.

Noise Type	RMS Error (%) (as compared to the reference)					
	Loudness	Roughness	Sharpness	Specific Loudness	Specific Roughness	Tonality
Thickness	8.5818	49.5704	40.7666	50.5610	53.3663	50.7225
Loading	8.0929	56.8805	37.1355	48.1371	61.5687	53.8961

The use of only the time-averaged main rotor signal produces a poor simulation of the original back-propagated signal with the exception of loudness. This seems to indicate the necessity of further exploration in order to create a high fidelity sound source simulation.

Another measure of fidelity is through a correlation analysis. Once the time-averaged main rotor signal is determined for each section, it is subtracted from each individual blade passage to create the residual. Placing the residuals of each of the individual blade passages in the original order of the corresponding blade passage windows gives the residual for the entire section of the hemisphere. The residual consists of all noise that is not correlated with the time-averaged main rotor signal. A plot of the main rotor residual for section 2 is shown in Figure 11. A correlation analysis was performed between the original back-propagated signal and the time-averaged main rotor pulse (blue curve) and between the main rotor residual and the time-averaged main rotor pulse (red curve), which are shown in Figure 12. This gives a before and after look to show how much of the time-averaged main rotor pulse is removed from the original back-propagated signal. The cross-correlation between the original back-propagated signal and the time-averaged main rotor pulse yields a maximum of 11.03. The cross-correlation of between the main rotor residual and the time-averaged main rotor pulse yields a maximum of 4.31. This shows a reduction of 60.95 percent which means that most of the time-averaged main rotor pulse is removed from the original back-propagated signal.

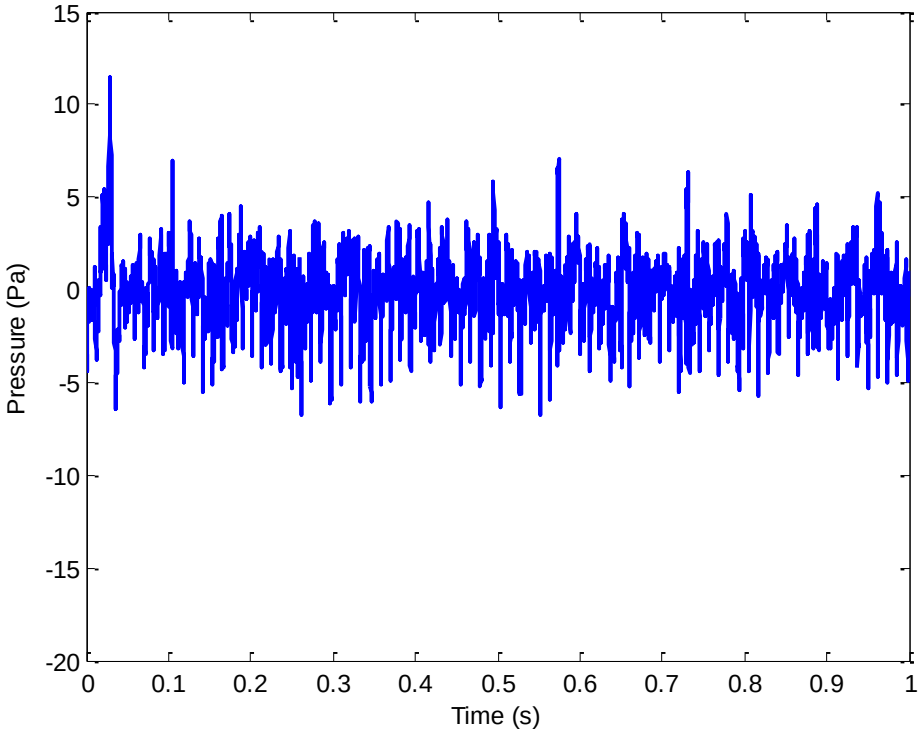

Figure 11: Residual of the main rotor for section 2.

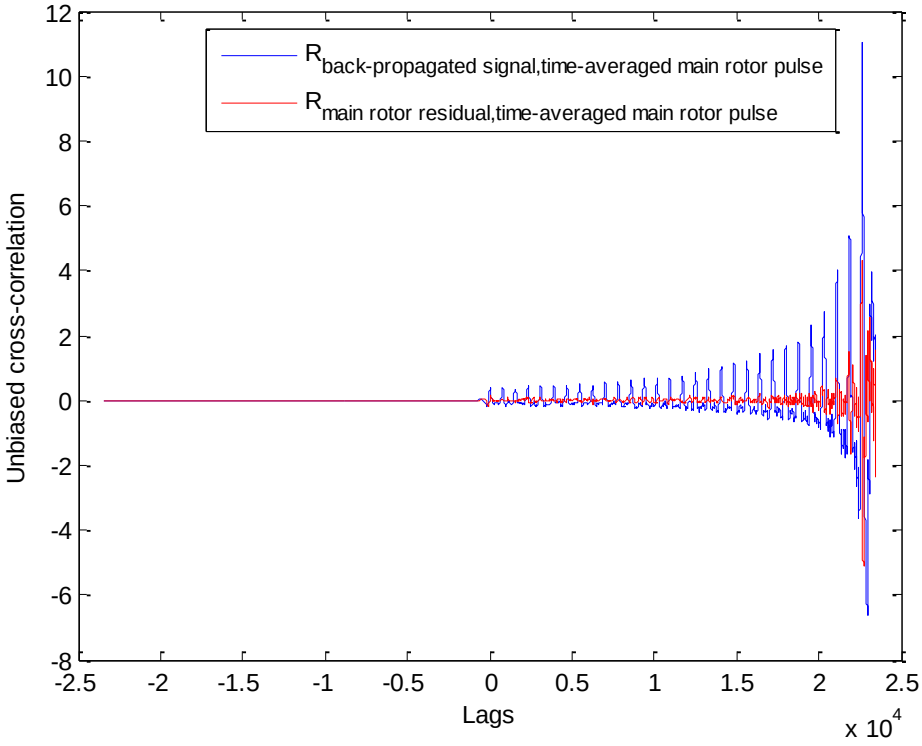

Figure 12: Main rotor cross-correlation analysis section 2.

3.3 Time-Averaged Tail Rotor Identification

The residual from the main rotor is used as the input signal for the tail rotor separation. The time-averaged tail rotor is determined through a similar process as used for the main rotor. The initial guess of the tail rotor BPF is determined by the nominal BPF. The time-averaged signal of the tail rotor noise is shown in Figure 13 for section 2. The time-averaged signal of the tail rotor is subtracted from each of the resampled blade passage windows in order to create a new residual, which is shown in Figure 14. This residual consists of all noise sources that are not correlated with either the main or tail rotor time-averaged signal. This includes amplitude and frequency modulation of the main and tail rotors, as well as gear noise, airframe and engine noise, and all of other noise sources. This technique is repeated for each section of the hemisphere.

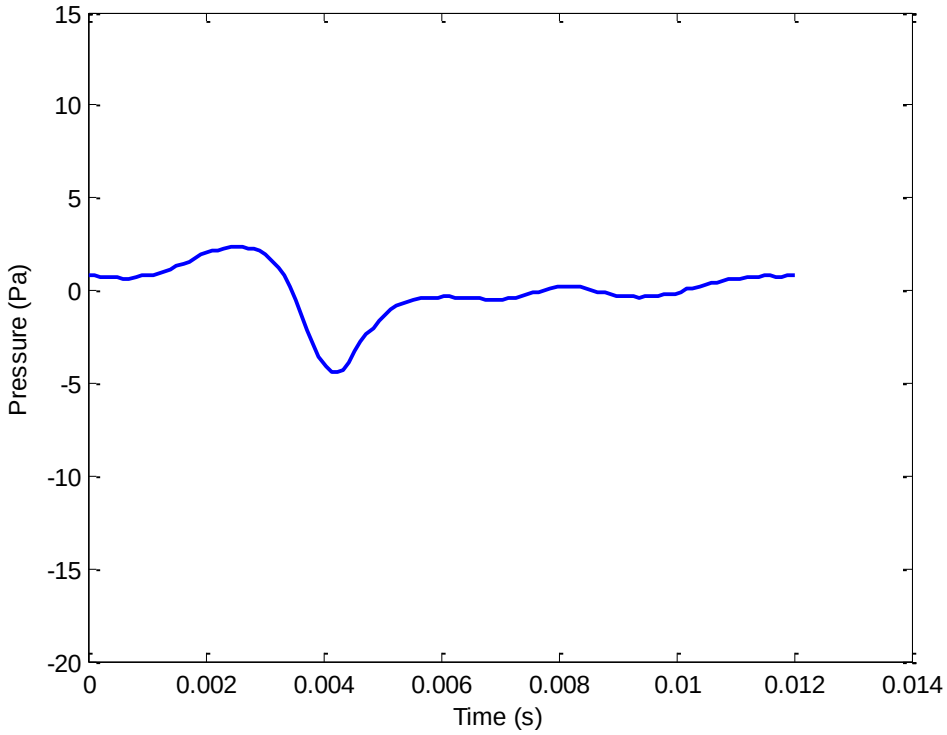

Figure 13: Time-averaged blade passage signal of the tail rotor for section 2.

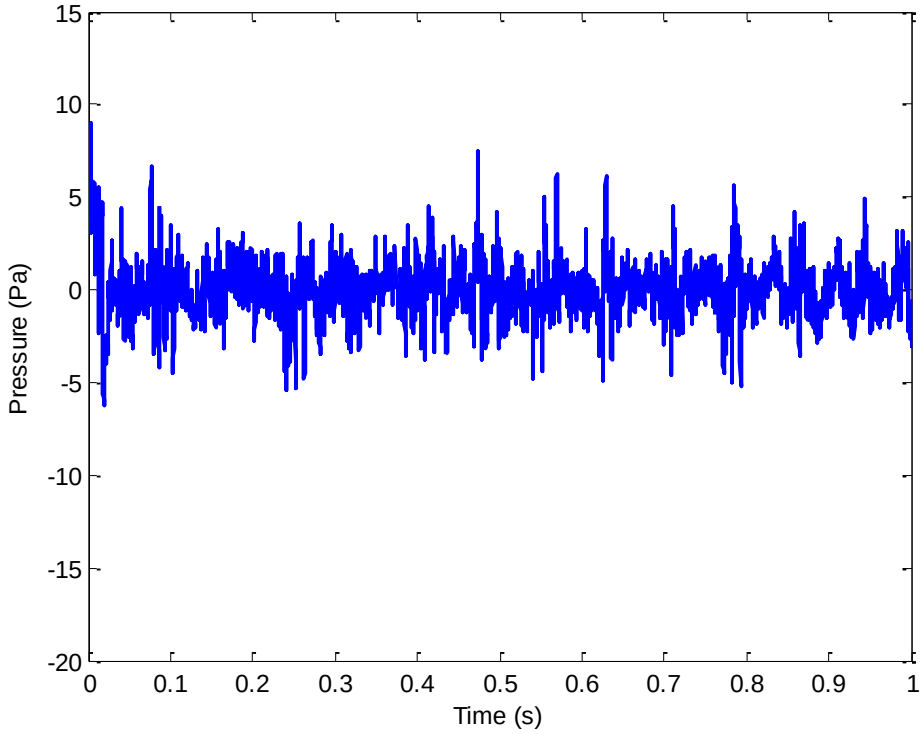

Figure 14: Residual of the tail rotor for section 2.

A plot of the combined time-averaged main and tail rotor signals with the original back-propagated input signal is shown in Figure 15. A sample of the resulting sound is available in the auxiliary wave files audiofile03.wav and audiofile04.wav (see Appendix C: Index of Supplemental Audio Files).

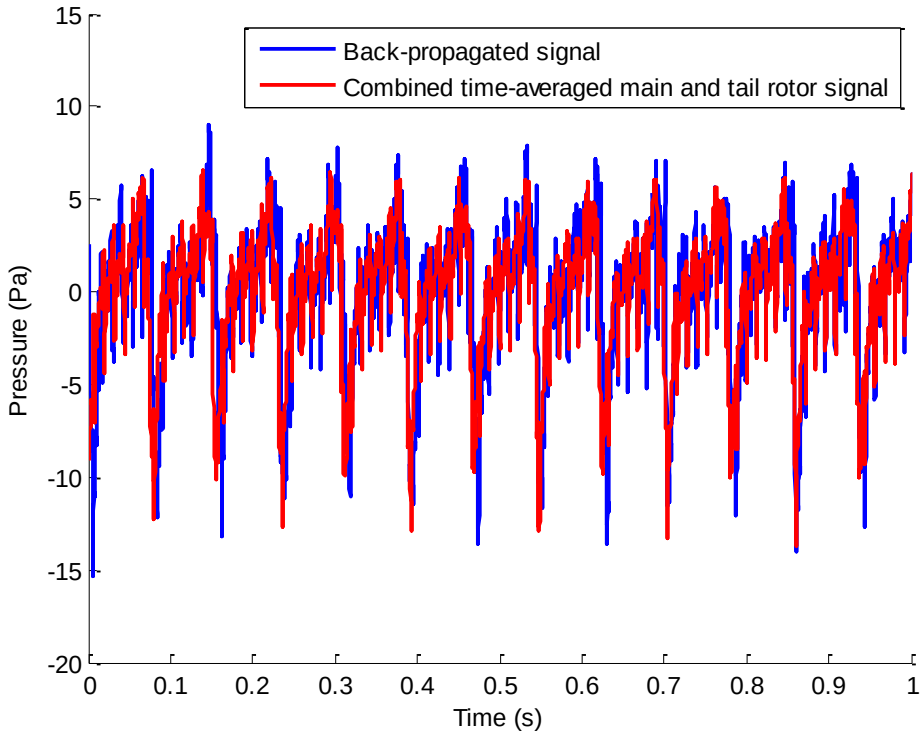

Figure 15: Comparison of the input signal to the time-averaged main rotor pulse for section 2.

The influence of the tail rotor is clearly seen. Qualitatively, the tail rotor is seen to change the peak amplitudes as a function of time. Because the main to tail rotor gear ratio is not an integer at 6.5156 (tail rotor to main rotor), the (negative) peak of the tail rotor at times aligns with the main rotor and at other times does not. The superposition of the time-averaged main and tail rotor signals thus acts to instill a time-varying quality to the resultant.

The same correlation analysis was performed for the tail rotor as for the main rotor. A cross-correlation analysis was performed between the main rotor residual, since it is the input into the tail rotor averaging process, and the time-averaged tail rotor pulse, as well as between the tail rotor residual and the time-averaged tail rotor pulse. The results are shown in Figure 16.

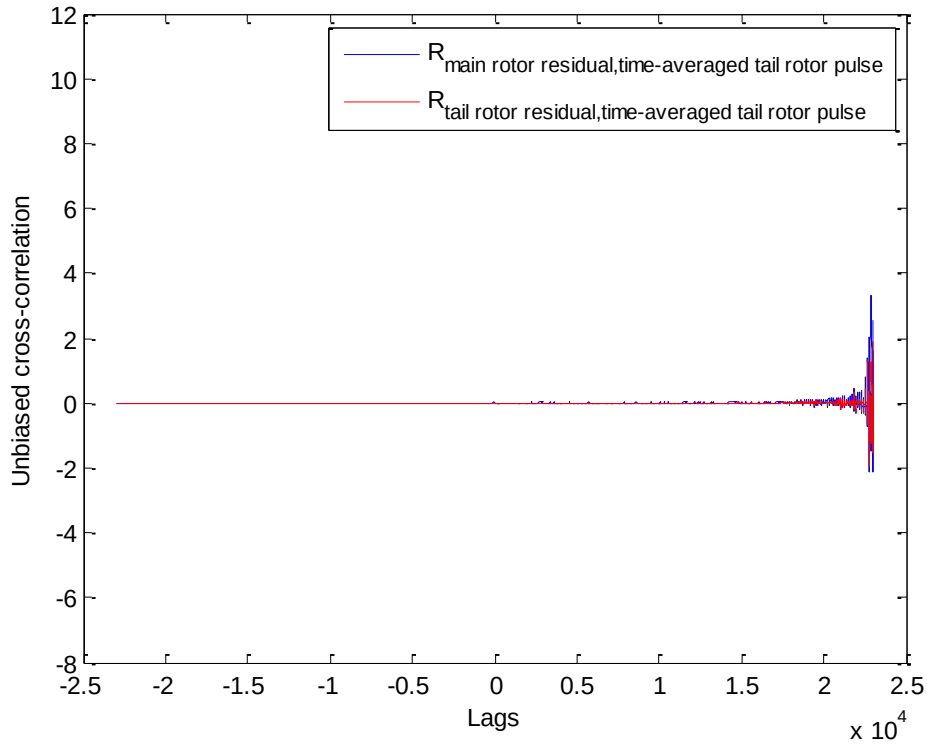

Figure 16: Tail rotor cross-correlation analysis for section 2.

The cross-correlation between the main rotor residual signal and the time-averaged tail rotor pulse yields a maximum of 3.30. The cross-correlation of between the tail rotor residual and the time-averaged tail rotor pulse yields a maximum of 1.901. This indicates a reduction of 42.15 percent, which seems to indicate that most of the time-averaged tail rotor pulse characteristics still reside in the residual of the tail rotor.

3.3.1 Fidelity of Time-Averaged Combined Main and Tail Rotors

The results of comparing the combined time-averaged main and tail rotor signal using the synchronous time-averaged method with the original back-propagated signal is shown in Table 4. A reduction in error occurs with the introduction of the time-averaged tail rotor signal with the exception of tonality. Since the time-averaged main rotor signal is misaligned with the peaks of the original back-propagated signal, shown in Figure 10, an increase in amplitude, from the addition of the time-averaged tail rotor signal, of the already misaligned peaks, seen in Figure 15, causes an increase in tonal error. Even though the error has decreased with the addition of the time-averaged tail rotor signal, the

combination of the time-averaged main and tail rotor signals is still not sufficient to accurately simulate the original back-propagated signal for the purposes of this work. The subjective measures of fidelity will be later explored in Chapter 6.

Table 4: Objective measures of fidelity for the combined synchronous time-averaged main and tail rotors signal.

Noise Type	RMS Error (%) (as compared to the reference)					
	Loudness	Roughness	Sharpness	Specific Loudness	Specific Roughness	Tonality
Thickness	4.4916	39.9857	44.1330	37.9770	47.8291	282.2505
Loading	4.8155	53.7762	38.4233	35.3723	58.8816	187.7723

3.4 Frequency Domain Representation

The BPF is equal to the inverse of the period (T) of the time-average signal for each rotor, that is,

$$BPF = \frac{1}{T} \tag{26}$$

The BPFs for each section of interest of the flying hemisphere, discussed in section 3.1, is shown in Table 5. Harmonics are integer multiples of the BPF. No effort was made to enforce a common BPF, for either the main rotor or the tail rotor, for all of the sections of the flying hemisphere. This was done in order to create a waveform that best matched the data in each section of the hemisphere.

Table 5: BPFs of the main and tail rotors for the sections of interest.

Section of the Hemisphere	Time-Averaged Main Rotor BPF (Hz)	Time-Averaged Tail Rotor BPF (Hz)
2	12.7877	83.3191
3	12.6904	82.6508
4	12.2399	80.5958

The time-averaged amplitudes ($\bar{A}$) and phases (ϕ_0) of each harmonic ($\bar{f_i}$) are determined from the FFT of the time-averaged main and tail rotor signals. This allows for the re-synthesis of the time-averaged signal using

$$p(t) = \sum_{i=1}^{N} \bar{A} \cos\left(2\pi \bar{f}_i t + \phi_{0,i}\right) \tag{27}$$

Equation (27) is recognized as Equation (5) with the time-varying amplitude and phase terms set to zero. As a practical matter, the re-synthesis of the time-averaged signal via Equation (27) is equivalent to concatenating the time-averaged signals over time.

Shown in Figure 17 and Figure 18 are the magnitude and phase of the time-averaged main rotor, respectively. Also shown in Figure 17 is the average magnitude of the original back-propagated signal, which is determined by applying a FFT to the original back-propagated time-domain signal. In general, the lower harmonics are of higher amplitude than the higher harmonics. The exception occurs at approximately 166 Hz, which is approximately twice the tail rotor BPF. This shows that the ensemble averaging process may allow some of the characteristics of the tail rotor into the time-averaged main rotor signal when the main and tail rotors harmonics are in close proximity to one another in the frequency domain. Therefore, the time-averaged main rotor signal alone may not truly represent that of an isolated main rotor. The same may be true for the tail rotor. However, the combination of the time-averaged signals of the main and tail rotors should represent the combination of the main and tail rotor together in isolation, that is, exclusive of other source noise. The energy with main and tail rotor harmonics in such cases may be misattributed to one of the other rotors, but is not lost. The magnitudes and phase were obtained from the Matlab function *fft()*. The frequency domain magnitudes of a signal, which come directly out of the Matlab FFT, must be scaled before being used in the time-domain for the synthesis process. This is accomplished by dividing the frequency domain magnitudes for 0 Hertz and the Nyquist frequency by number of points used in the FFT and dividing the frequency domain magnitudes for the frequencies in between by half of the number of points used in the FFT. For the purposes of this work, the number of points used in the FFT is equal to the length of the signal being evaluated. No scaling or correction needs to be applied to the phase measurements in preparation for use in the time domain for the synthesis process.

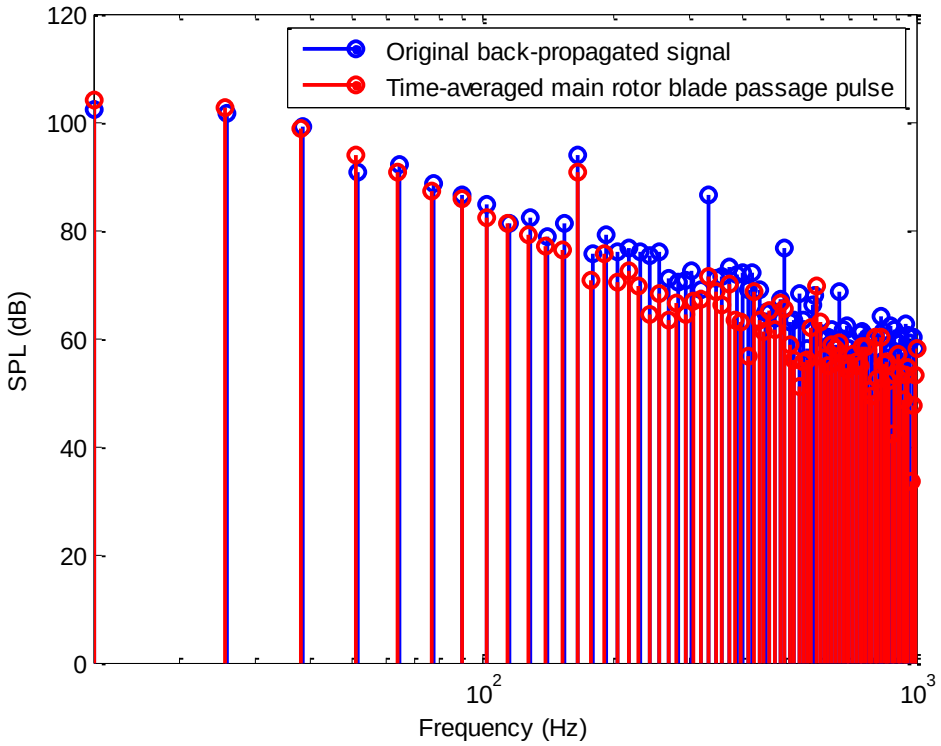

Figure 17: Main rotor magnitude of the time-averaged signal of section 2.

An apparent loss of sound pressure level (SPL) at the higher frequencies occurs when comparing the magnitudes of the time-averaged main rotor blade passage pulse and the magnitudes of the original back-propagated signal as shown in Figure 17 for section 2. However, the SPL for each of the frequencies for the time-averaged main rotor blade passage pulse corresponds well to the SPL of the original back-propagated signal for the lower frequencies. This behavior was also observed at the other sections considered.

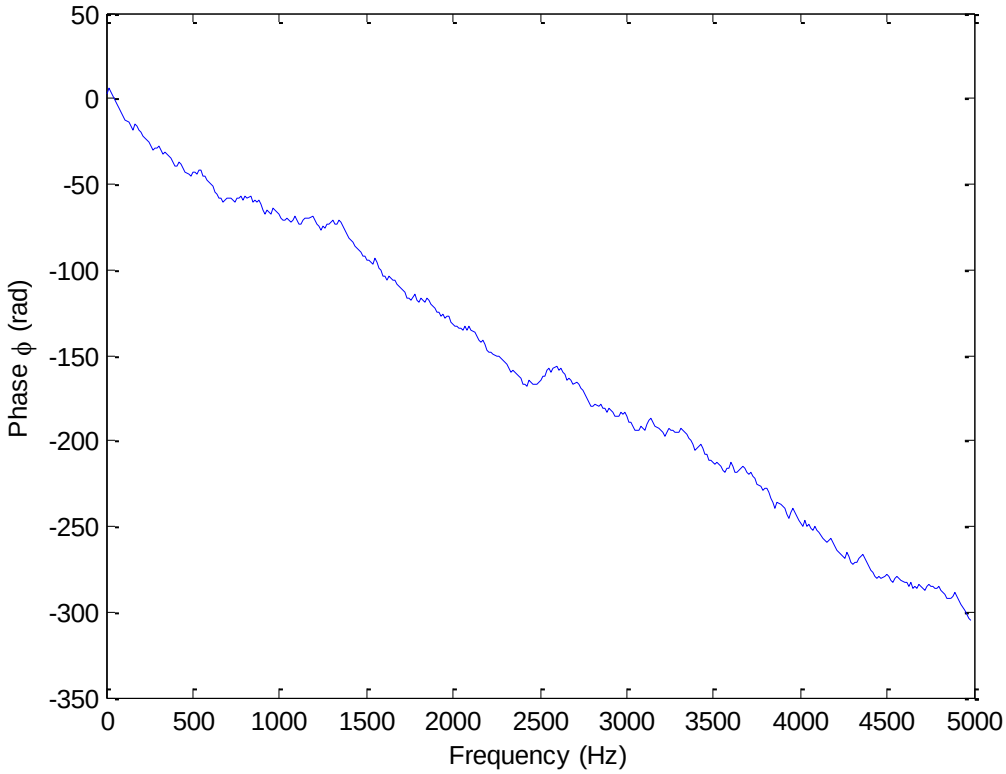

Figure 18: Main rotor phase of the time-averaged signal of section 2.

Figure 19 and Figure 20 show the magnitude and phase of the tail rotor, respectively. Figure 19 only shows the frequencies that correspond to both the time-averaged tail rotor blade passage pulse and the main rotor residual signal. Contrary to expectations, the second harmonic of the main rotor is not small. At higher frequencies, the time-averaged tail rotor SPL is consistently higher than the SPL of the main rotor residual signal. However, the time-averaged tail rotor does represent the SPL of the main rotor residual signal well for lower frequencies. The under prediction of the time-averaged main rotor pulse SPL and the over prediction of the time-averaged tail rotor pulse SPL leads to a spectral imbalance between the time-averaged main and tail rotor pulses. This spectral imbalance is not desirable because both rotors are not accurately represented individually. A synthesis process that isolates the fluctuations of each harmonic and creates time-averaged rotor pulses with a better spectral balance is desired.

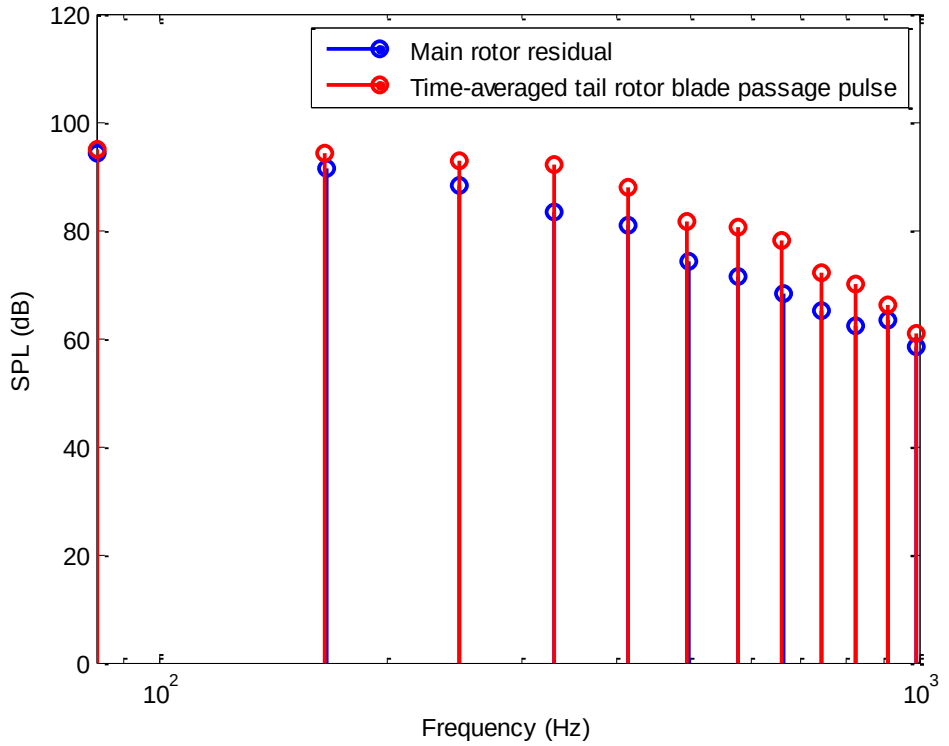

Figure 19: Tail rotor magnitude of the time-averaged signal of section 2.

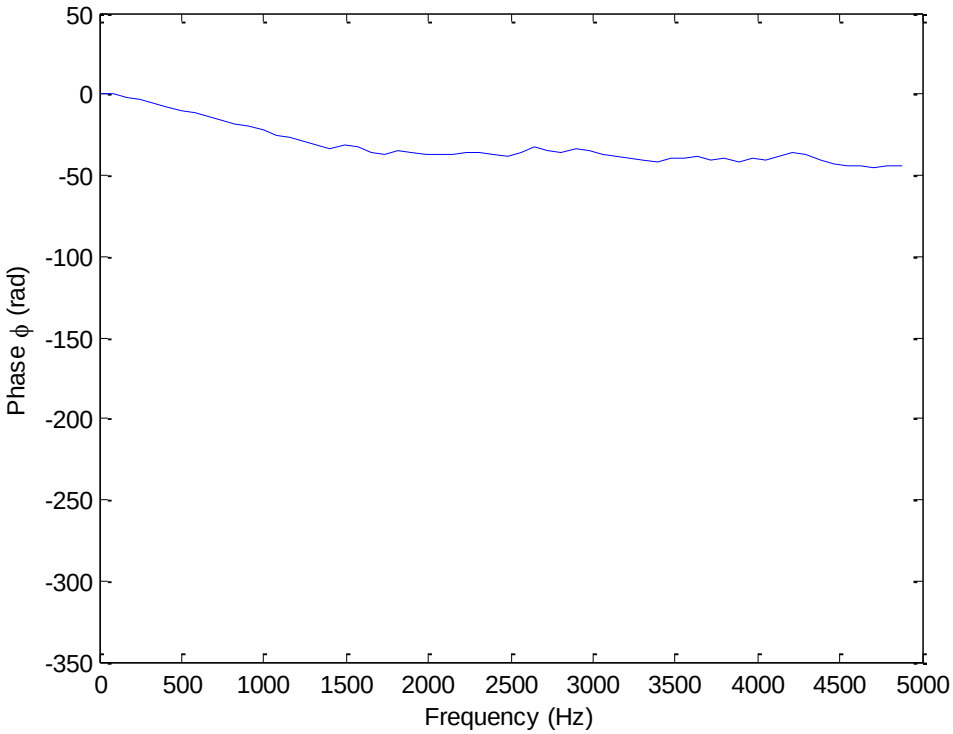

Figure 20: Tail rotor phase of the time-averaged signal of section 2.

4. Synthesis of Time-Varying Rotorcraft Noise

In this chapter, a demodulation process for extracting the fluctuations or deviations of the amplitude and frequency for the BPF and respective harmonics of the main and tail rotors is discussed. These parameters are subsequently used to synthesize time-varying rotorcraft noise.

4.1 Evaluation of Time-Varying Characteristics

There are several options when calculating the time-varying characteristics of a signal. For this particular research, the assumption was made that any phase fluctuations would be characterized as frequency fluctuations. A flowchart describing the major steps in the process is shown in Figure 21.

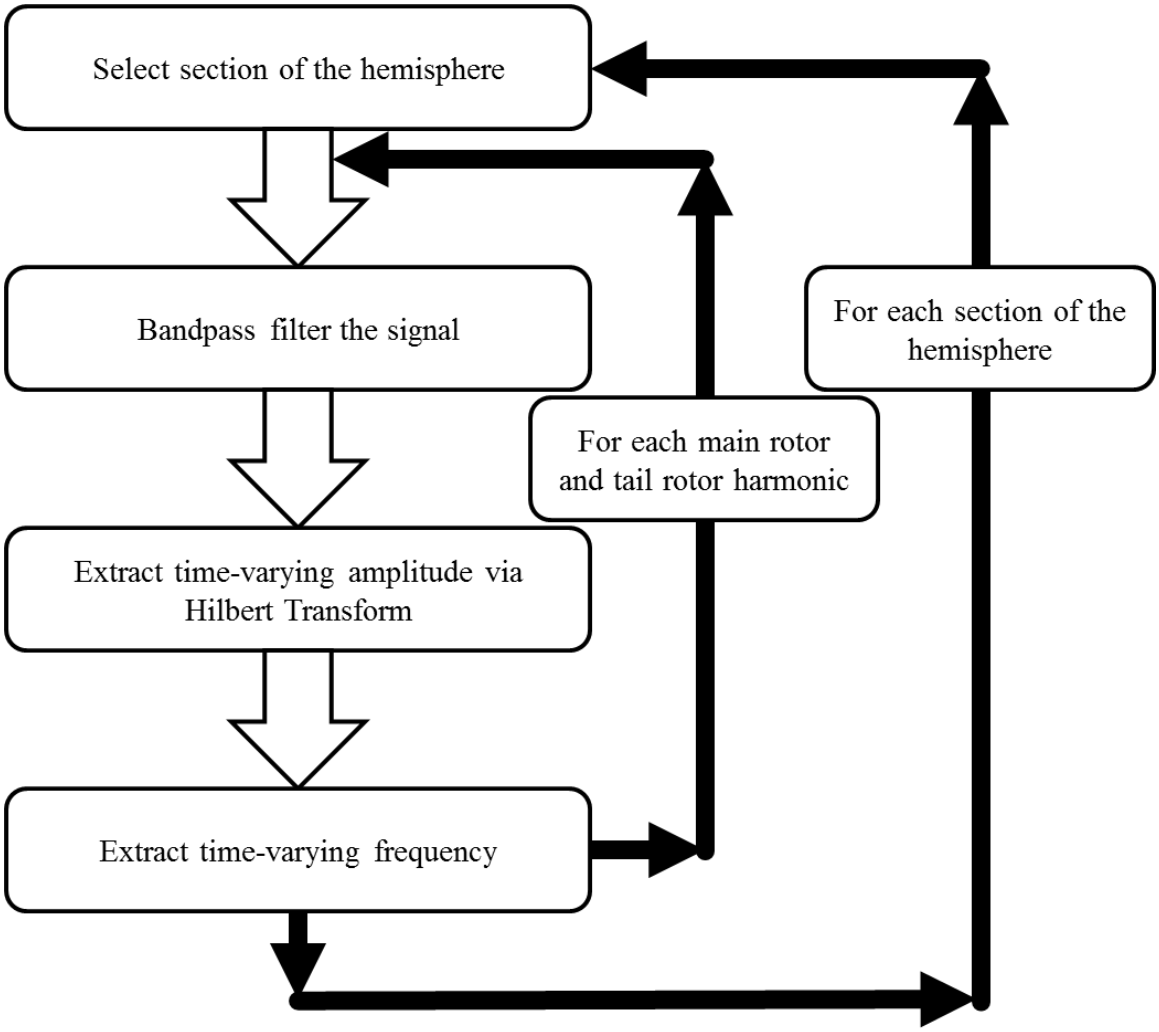

Figure 21: Extraction of time-varying quantities flowchart

The first step of demodulation is inspecting the input signal, which has been back-propagated via the method described in Chapter 3. It is often necessary to trim the processed segment in order to identify a sub-segment with an overall character that does not vary over time, as shown in Figure 22. The original pressure-time history (in blue) represents the back-propagated sound of the entire second section of the hemisphere. Over the course of the entire segment, the amplitude is seen to increase significantly. This is not desirable as that behavior will be captured in the demodulation process, and will subsequently be imparted on any synthesis utilizing that data. The sub-section identified in green exhibits less of that behavior and will serve as the waveform subsequently used.

Note that this is an artifact of the back propagation process and could possibly be eliminated through the selection of shorter duration segments.

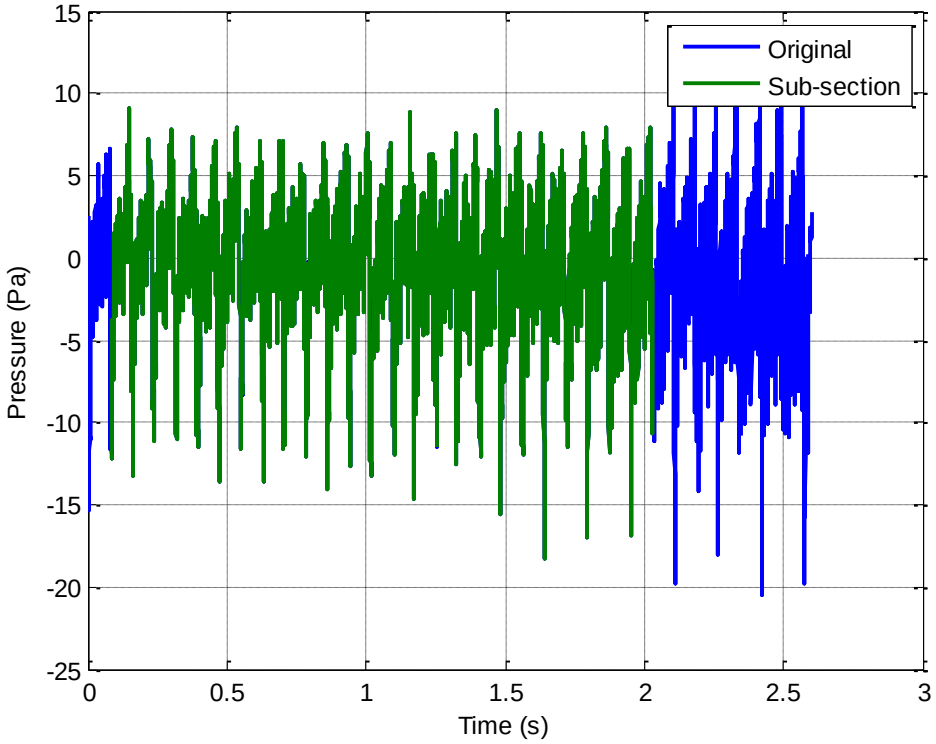

Figure 22: Choosing the sound that is most indicative of the emission angle (section 2)

The next step in this process is to isolate the main rotor and tail rotor signals from the back-propagated data. This is accomplished through the use of a Butterworth bandpass filter centered at the BPF and each harmonic of each respective rotor. The energy within the bandwidth of the Butterworth filter must be divided between the main rotor and tail rotor if any of the main rotor harmonics are within close proximity to any of the tail rotor harmonics in respect to the value of frequency. The following criterion was developed for that purpose. *If a tail rotor harmonic occurs within a band width equal to the BPF of the main rotor and centered at a main rotor harmonic, all of the energy is given to the tail rotor harmonic that resides within this band width and no energy within this band width is given to the main rotor.* The logic behind this approach is to assume that lower harmonics contain more energy than higher harmonics. Therefore the energy is given to the tail rotor harmonic since it is a lower harmonic than the main rotor harmonic within this bandwidth. When the main rotor and tail rotor are combined, the

amplitude at this specific harmonic will be equal to the respective harmonic in the original signal.

A bandpass filter keeps, or allows to pass, the frequency components between an upper and lower bound and rejects the frequency components outside these bounds. A Butterworth bandpass filter was chosen based on two of the filter's primary characteristics: maximal flatness and monotonicity. For the Butterworth filter to have a maximally flat magnitude response, the first $2N-1$ derivatives of the magnitude squared frequency response are zero at $\Omega = 0$, for a lowpass filter where N refers to the order of the filter [22]. Ω refers to the frequency, in radians per second, in the frequency domain. The same criteria hold true for a Butterworth bandpass filter where the frequency is equal to the center frequency instead of zero. The magnitude response of a Butterworth filter is monotonically increasing (the value of the derivative is always positive or zero as frequency increases), monotonically decreasing (the value of the derivative is always negative or zero as frequency increases), or both. The only instance in which the magnitude of the Butterworth filter is both monotonically increasing and decreasing is in the case of a bandpass filter. In this case, the magnitude is monotonically increasing to the right of the center frequency and monotonically decreasing to the left of the center frequency [23]. The requirements of monotonicity and maximal flatness prevent the possibility of ripple, or the occurrence of repetitive oscillations, in either the passband or the stopband (the area outside of the passband). However, the prevention of ripple does require the transition between the passband and the stopband to be larger as compared to other filters. These attributes allow for more of the frequency spectra in the passband to retain the original amplitude while reducing the occurrence of unwanted frequencies located in the stopband. This is a trade-off that is controlled through the selection of the order of the filter. The higher the order of the filter, the narrower the transition becomes [22]. The 3rd order Butterworth infinite impulse response (IIR) bandpass filter, used to isolate the BPF and harmonics for each of the rotors, was created using the *butter()* command in MATLAB. Such a filter can be seen in Figure 23 for the 1st main rotor harmonic.

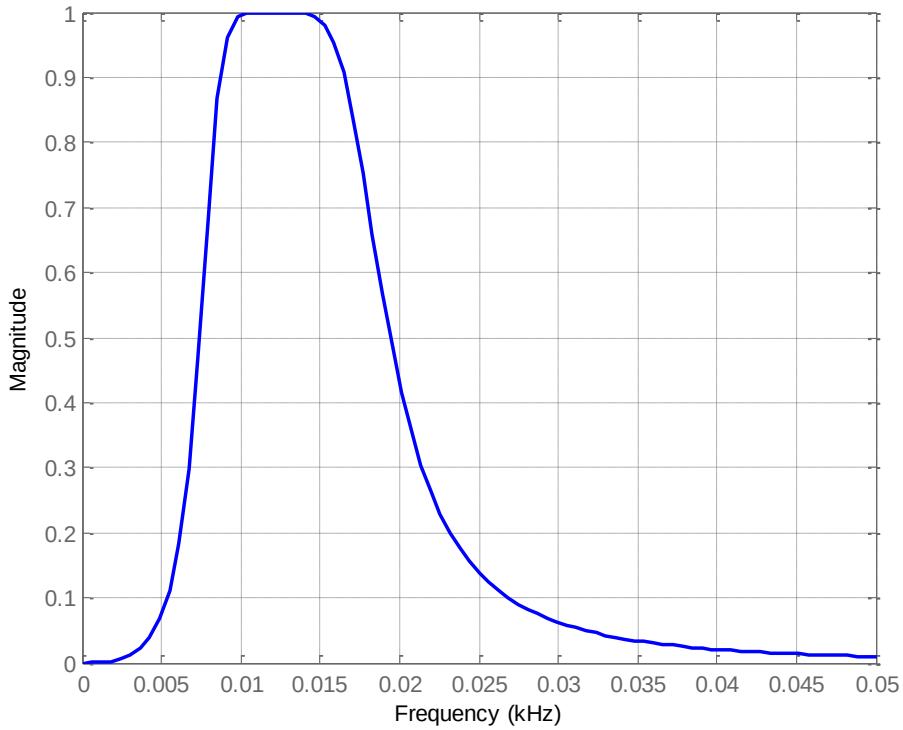

Figure 23: 3rd order Butterworth IIR band-pass filter.

Once the filter is chosen and created, it must be applied to the data. The filter is applied to the data using the *filtfilt()* command in MATLAB. The *filtfilt()* operation in MATLAB performs a zero-phase digital filter by filtering in the forward direction and then again in the reverse direction. The *filtfilt()* command also doubles the order of the original filter, therefore the data is effectively filtered using a sixth-order Butterworth bandpass filter instead of the initial third-order filter [24]. An illustration of the sixth-order Butterworth bandpass filter is shown in Figure 24, for the 1st harmonic of the main rotor.

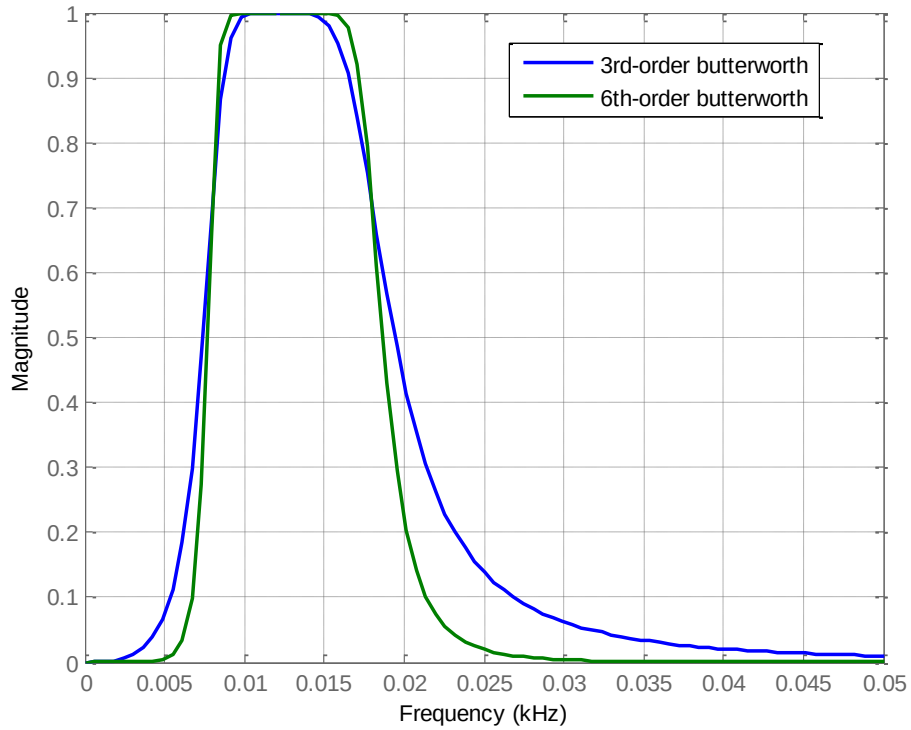

Figure 24: Comparison of frequency response of two Butterworth band-pass filters.

The higher order filter allows for more retention of the frequencies in the passband and less of those in the stopband. If the order of the filter is too high, other measures must be taken to compensate for negative side effects, such as loss of character in the signal, an increase in error, and the appearance of ripples in the passband. A loss of character occurs when the roll-off of the filter increases in steepness such that artifacts, such as "ringing" and ripple, occur in the time domain. This type of behavior is especially evident when using a sinc filter. The bounds were chosen to be defined as a center frequency, in this case the BPF or one of the harmonics, and one half the passband, both expressed in Hertz. An example would be 20Hz ± 5Hz. The filtering process is performed repeatedly on the back-propagated signal at each main and tail rotor harmonic, resulting in a set of narrowband signals from which time-varying amplitude and phase data can be extracted.

The next step is to determine the time-varying amplitude of the BPF and the harmonics for each rotor. The Hilbert transform [25] was used to extract the time-

varying amplitude of each frequency. It is helpful to define the Hilbert transform ($\tilde{x}(t)$) of a signal ($x(t)$) in terms of an analytic signal ($z(t)$) as [25]

$$z(t) = x(t) + j\tilde{x}(t). \tag{28}$$

The Hilbert transform is, essentially, the imaginary portion of the analytic signal. The analytic signal can be described using an amplitude envelope ($A(t)$) and instantaneous phase ($\theta(t)$), that is,

$$z(t) = A(t)e^{j\phi(t)}. \tag{29}$$

By combining Equation (28) and Equation (29) and rearranging the terms, the amplitude envelope and the instantaneous phase can be written as

$$A(t) = [x^2(t) + \tilde{x}^2(t)]^{\frac{1}{2}} \tag{30}$$

$$\phi(t) = \tan^{-1}\left[\frac{\tilde{x}(t)}{x(t)}\right] = 2\pi f(t)t \tag{31}$$

where $f(t)$ is the instantaneous frequency and t is the time record. The instantaneous frequency can be written in terms of the instantaneous phase as [25]

$$f(t) = \left(\frac{1}{2\pi}\right)\frac{d\phi(t)}{dt}. \tag{32}$$

4.1.1 Amplitude Variation

The Hilbert transform allows for the total amplitude of the signal to be characterized in the time-domain. This allows both the mean and fluctuations about the mean to be determined. Since the rotorcraft noise has been sub-divided into multiple narrowband signals with the BPF or one of the harmonics as the mean frequency, each narrowband signal has a time-varying amplitude envelope and phase for the duration of the time record. The amplitude envelope can be sub-divided into two parts, the mean amplitude ($\bar{A}$) and the amplitude deviations ($\tilde{A}(t)$), that is,

$$A(t) = \bar{A} + \tilde{A}(t). \tag{33}$$

The instantaneous phase can also be sub-divided into two parts, the initial phase offset (ϕ_0) and the phase deviation ($\tilde{\phi}(t)$),

$$\phi(t) = \phi_0 + \tilde{\phi}(t). \tag{34}$$

Likewise the instantaneous frequency can be separated into a mean frequency ($\bar{f}$) component and a fluctuating frequency component ($\tilde{f}(t)$).

$$f(t) = \bar{f} + \tilde{f}(t) \tag{35}$$

These sub-categories of phase and frequency will be discussed later in this chapter.

The *hilbert()* command in MATLAB was used to evaluate each narrowband data set. The Fourier transform ($\widetilde{\boldsymbol{X}}(f)$) of the Hilbert transform ($\tilde{x}(t)$) is related to the Fourier transform ($\boldsymbol{X}(f)$) of a signal ($x(t)$), with the signal phase (ϕ_x), and a phase shift (ϕ_b) expressed as

$$\widetilde{\boldsymbol{X}}(f) = |\boldsymbol{X}(f)|e^{-j[\phi_x(f)+\phi_b(f)]}. \tag{36}$$

The phase shift (ϕ_b) term changes value based on the frequency, that is,

$$\phi_b(f) = \begin{cases} \frac{\pi}{2} & \text{for } f > 0 \\ -\frac{\pi}{2} & \text{for } f < 0. \end{cases} \tag{37}$$

The Hilbert transform, as implemented in this research, effectively doubles the amplitudes of the positive frequencies while neglecting the negative frequencies, which is accomplished using a one-sided Fourier transform, in order to create an analytic signal for each data set. This is because the Hilbert transform shifts the phase of the positive frequencies by $\frac{\pi}{2}$ and the phase of the negative frequencies by $-\frac{\pi}{2}$, seen in Equation (37) [25]. The phase shifting aligns the amplitudes of the positive and negative frequencies resulting in a doubling of the amplitude and allowing the amplitudes to be denoted only using the positive frequencies. Neglecting negative frequencies is allowable since the objective is to determine the amplitudes of each frequency irrespective of the direction of the frequency or the relationship between the amplitude and the phase. However, the correct phase relationship will be determined later. *The four steps used to create the analytic signal are* [24]:

1. Perform an n-point fast Fourier Transform (FFT) of the input sequence for each harmonic, storing the result in a vector x.
2. Create a vector h whose elements h(i) have the values:
    a. 1 for i = 1, (n/2)+1
    b. 2 for i = 2, 3, …, (n/2)
    c. 0 for i = (n/2)+2, …, n
3. Calculate the element-wise product of x and h.

4. Calculate the inverse FFT of the sequence obtained in step 3 and return the first n elements of the result.

This operation is performed for each narrowband data set. The magnitude of the output from the *hilbert()* command is the amplitude envelope ($A(t)$), which is used in determining the mean amplitude and the amplitude deviation for each data set corresponding to the harmonics of interest. Figure 25 illustrates the comparison of the amplitude envelope from the Hilbert Transform to the isolated signal of the BPF for the main rotor.

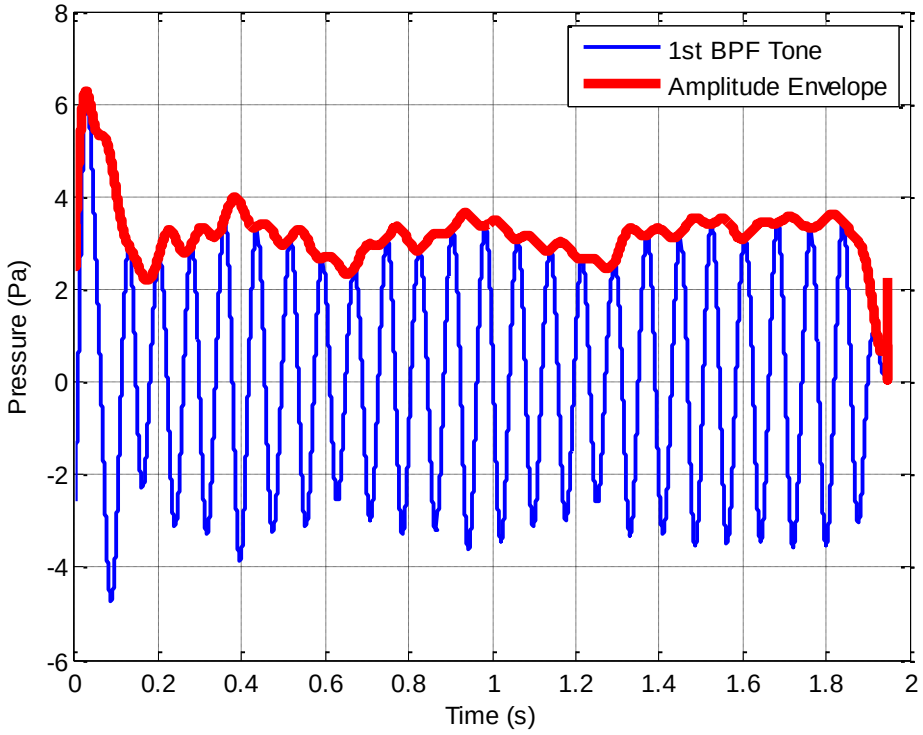

Figure 25: Amplitude envelope of main rotor BPF determined by the Hilbert transform (section 2).

The mean of the amplitude envelope ($\bar{A}$) is calculated for the BPF and each harmonic. The mean values of the amplitude envelopes are subtracted from the respective amplitude envelopes to produce the amplitude deviations ($\tilde{A}(t)$) for each harmonic individually. Now the deviation from the mean amplitude may be analyzed to determine how significant the deviation is to the overall signal. Of the three primary components of a sinusoidal wave, total amplitude, total frequency, and phase discussed in section 2.1, the

total amplitude, containing both the mean amplitude and amplitude modulation, has been successfully extracted from the BPF and harmonics.

4.1.2 Frequency Variation

The next component to be extracted is the frequency modulation. The frequency modulation, or how much the frequency deviates from an assumed mean frequency, will be shown to be important in the synthesis of rotorcraft noise. The frequency deviation is extracted from the instantaneous frequency ($f(t)$), which is obtained through a demodulation process applied to each filtered narrowband signal. This frequency demodulation process is different than the one used to determine the amplitude modulation and uses simulated annealing to determine the frequency modulation [26]. Recalling from Equation (32) that the frequency is the derivative of the phase, the time-varying phase can be expressed as:

$$\phi(t) = \int \big(f(t)\big)dt = \underbrace{\int \left(\tilde{f}(t)\right) dt}_{\tilde{\phi}} + \underbrace{2\pi\bar{f}t + \phi_0}_{line\ of\ best\ fit} \tag{38}$$

where the initial phase offset (ϕ_0) may be considered a constant of integration. Solving for the phase modulation, $\tilde{\phi}(t)$, gives

$$\tilde{\phi}(t) = \int \big(f(t)\big)dt - 2\pi\bar{f}t - \phi_0 \tag{39}$$

The solution to Equation (39) thus requires the known instantaneous frequency ($f(t)$), and the unknown mean frequency and initial phase offset which determine the line of best fit. The latter are determined from an iterative process described below which determines 1) the mean frequency in the narrowband signal containing the most energy, and 2) the corresponding initial phase. *An initial guess of the line of best fit is constructed by specifying the mean frequency $\bar{f}$ as the center frequency used in the bandpass filter operation with an initial phase offset ϕ_0 of zero. The best fit line is subtracted from first term on the right hand side of Equation (39), to determine the desired time-varying component of the phase $\tilde{\phi}(t)$.* Of course, any guess of the line of best fit will result in some value of $\tilde{\phi}(t)$, but such a guess will result in a value of $\tilde{\phi}(t)$ with a non-zero mean and that is not desired with the synthesis approach indicated by Equation (5). To obtain a value of $\tilde{\phi}(t)$ with minimum mean, an iterative approach is taken. On the second and subsequent iterations, a new guess of the line of best fit (using new values of both the

mean frequency and the initial phase) is used. The new guess is not completely random, but is guided through a process called simulated annealing [26], which uses the residual error from the prior iteration as input. The residual error is calculated as the sum of the squares between the guess of the line of best fit and the time-varying phase $\phi(t)$. This is repeated for many iterations, typically 1000, and the line with the smallest residual error is one that has a mean frequency containing the most energy. For the current application, this brute force approach was found to consistently identify the line of best fit with smallest residual error. More sophisticated approaches may however be required with other data sets. Figure 26 illustrates the components of this process.

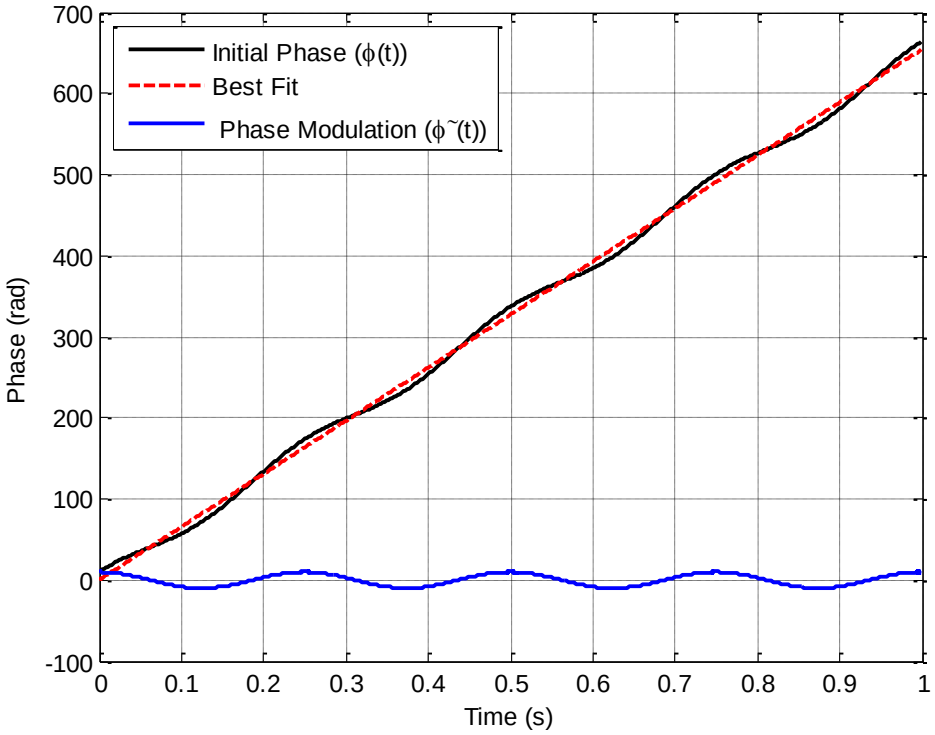

Figure 26: Extracted frequency, phase, and phase modulation from the narrow-band signal of interest.

The frequency modulation is finally determined from the phase modulation as

$$\tilde{f}(t) = \left(\frac{1}{2\pi}\right)\frac{d\tilde{\phi}(t)}{dt}. \tag{40}$$

Since Equation (40) establishes that the frequency modulation is the derivative of the phase modulation, phase modulation may be directly used to determine the pressure time history by rearranging Equation (40) and substituting it into Equation (5), that is,

$$p(t) = \sum_{i=1}^{N} \left[\bar{A}_i + \tilde{A}_i(t)\right] \cos\left(2\pi \bar{f}_i t + \tilde{\phi}(t) + \phi_{0,i}\right). \tag{41}$$

All of the components necessary to reconstruct the back-propagated signal using Equation (5) have thus been calculated. These include the mean amplitude, amplitude deviation, mean frequencies, frequency deviation, and the initial phase offset for each of the tone isolated signals. Therefore, the synthesis of the desired signals may commence.

4.2 Signal Reconstruction with Demodulation Products

Four methods for synthesis using products of the demodulation process are next discussed. These four methods of synthesis are:

(i) *Case A* is a synthesis method which only uses the unmodulated main rotor signal.

(ii) *Case B* is a synthesis method which uses the modulated main rotor signal.

(iii) *Case C* is a synthesis method which uses the unmodulated main rotor signal combined with the unmodulated tail rotor signal.

(iv) *Case D* is a synthesis method which uses modulated main rotor signal combined with the modulated tail rotor signal.

The time-averaged signal is the simplest to reconstruct and manipulate. The general equation for synthesizing a time-averaged signal is

$$p(t) = \sum_{n=1}^{N} [\bar{A}_n] cos\left(2\pi \bar{f}_n t + \phi_{0,n}\right) . \tag{42}$$

Each of the harmonics that make up the time-averaged signal is constructed using the mean amplitude ($\bar{A}$), the mean frequency ($\bar{f}$), and the initial phase offset (ϕ_0). The time-average signal is fully constructed once all of the corresponding harmonics are combined using the principle of superposition. This means that the signal is periodic for all time and does not include any fluctuations in amplitude or frequency. If the construction of the desired signal using only the time-average components is to begin, what characteristics should be considered first? Typically, the noise generated by the main

rotor contributes the most energy to rotorcraft noise in the case of unweighted data. However, that may or may not have greatest influence on human perception. Therefore, time-average signal generated by the main rotor in isolation should be considered first. A comparison of the auxiliary wave files for Case A, audiofile05.wav and audiofile06.wav (see Appendix C: Index of Supplemental Audio Files), and the auxiliary audio files for the original back-propagated signal, audiofile25.wav and audiofile26.wav, for thickness and loading noise respectively, allows further insight into this method. A comparison of the mean amplitudes from the main rotor determined from the demodulation process and the original back-propagated signal in the frequency domain is shown in Figure 27.

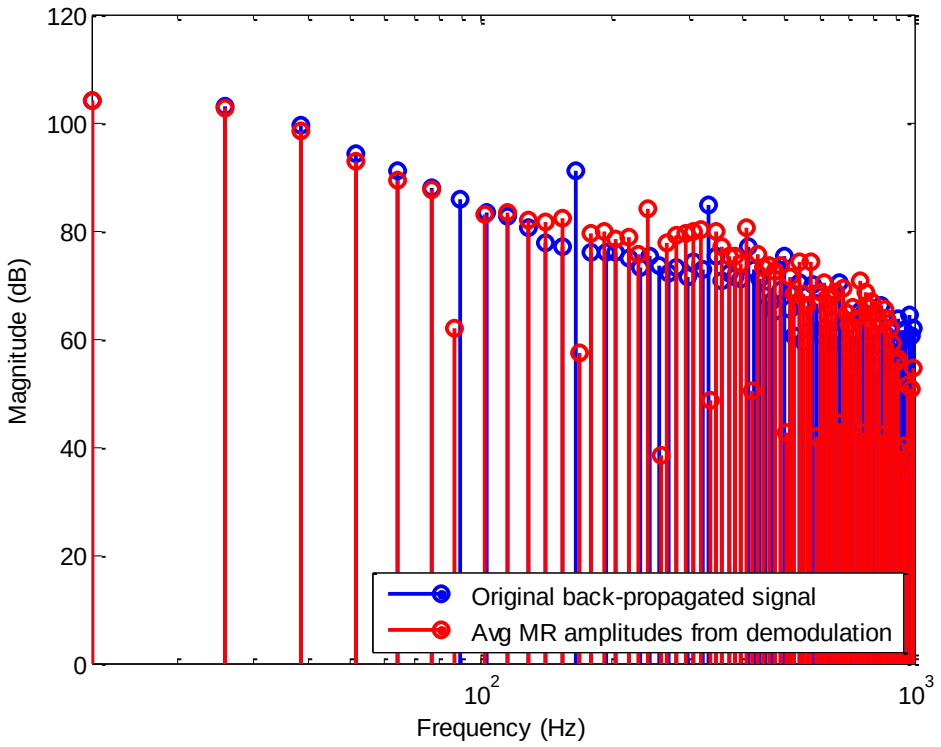

Figure 27: Average main rotor magnitudes from the demodulation process for section 2.

The amplitudes from the demodulation process correspond well to the back-propagated signal at the BPF and lower harmonics. However, the demodulation process tends to over predict the amplitudes of the higher frequency harmonics. A large amplitude difference is present at 89.81Hz (seventh harmonic from the left). This is because 89.81Hz is sufficiently close to the first tail rotor harmonic to cause the demodulation process to give a significant portion of the energy at this frequency to the tail rotor. This

phenomenon is obvious at the tail rotor harmonics as well. The pressure-time history of the signal pictured in Figure 27 is shown in Figure 28 as compared to the original signal, with are more detailed view shown in Figure 29.

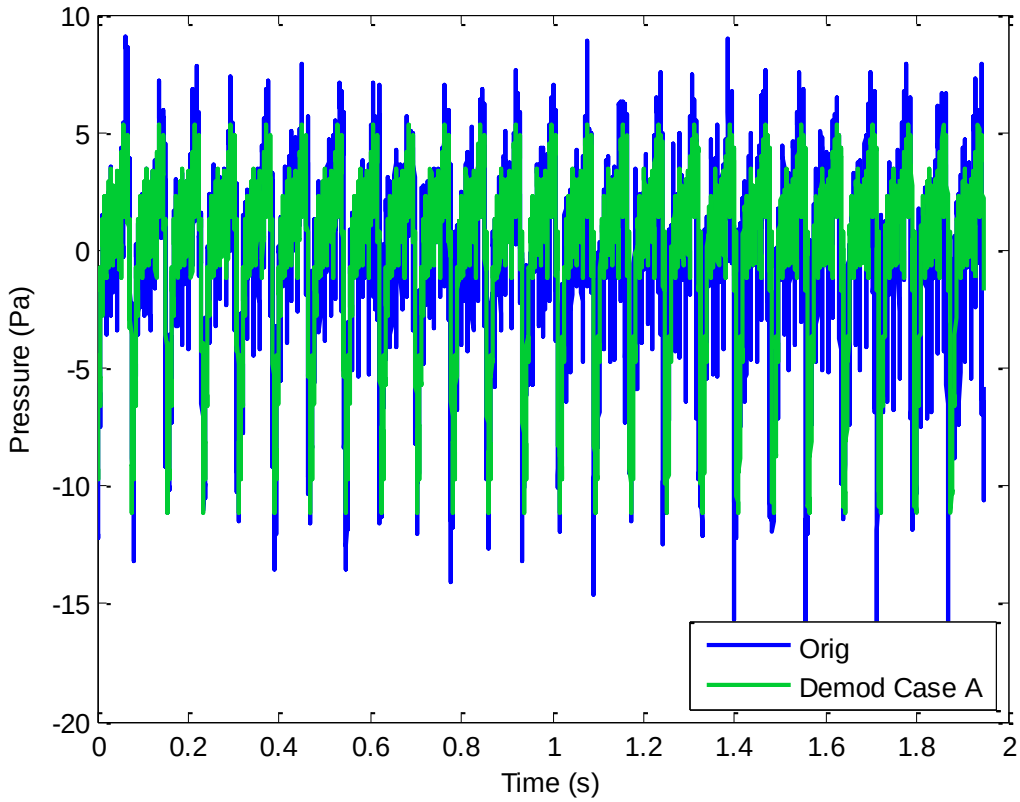

Figure 28: Time-averaged signal of the isolated main rotor from the demodulation process for section 2.

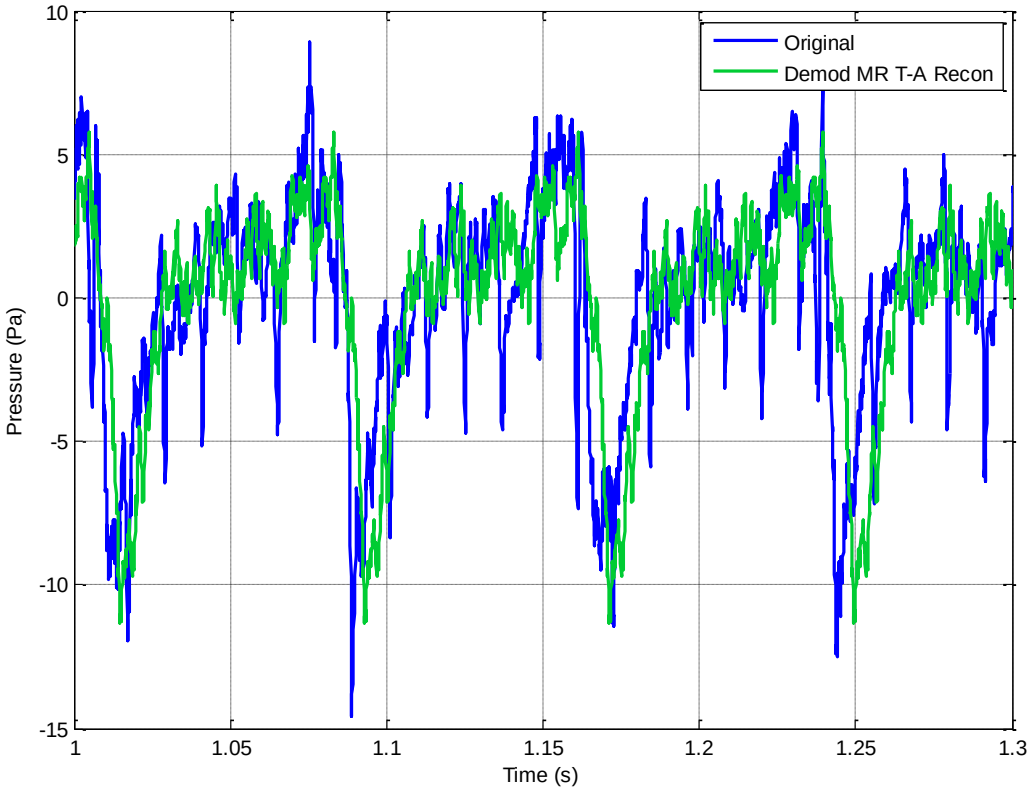

Figure 29: Detailed view of the time-averaged signal of the isolated main rotor from the demodulation process for section 2.

Figure 29 shows a small section of the time-average signal to aid in visualizing the finer structure of the signal and allows for better comparison with the original signal. The synthesized main rotor signal using only the mean amplitudes, mean frequencies, and initial phase offset (i.e. no modulation) will be subsequently referred to as Case A. The original signal and Case A are very similar in both amplitude and frequency. A frequency difference between the original signal and Case A is seen in the way the peaks of the signals do not align with each other over time. An initial phase mismatch between the peaks of Case A and the original back-propagated signal is noticeable in Figure 28 and Figure 29 since the peaks of Case A appear either in front or behind the peaks of the original back-propagated signal. Since, the two signals seem to go into and out of phase, the natural conclusion would be that an ever so slight frequency shift is occurring in the original signal over time.

The desire is to create a signal with a high fidelity, therefore the main rotor with modulation should be considered. The modulated signal is characterized by Equation (5).

This new signal will be referred to as Case B and a frequency-domain comparison is pictured in Figure 30. A comparison of the auxiliary wave files for Case B, audiofile07.wav and audiofile08.wav (see Appendix C: Index of Supplemental Audio Files), and the auxiliary audio files for Case A, audiofile05.wav and audiofile06.wav, for thickness and loading noise respectively, demonstrates the benefit of the added modulation. Here is it seen that the amplitudes of the original back-propagated signal are more accurately captured with the addition of the amplitude and frequency modulation of the main rotor. The inclusion of the main rotor amplitude and frequency modulation increases the accuracy of the main rotor harmonics that are in close proximity to frequencies of tail rotor harmonics.

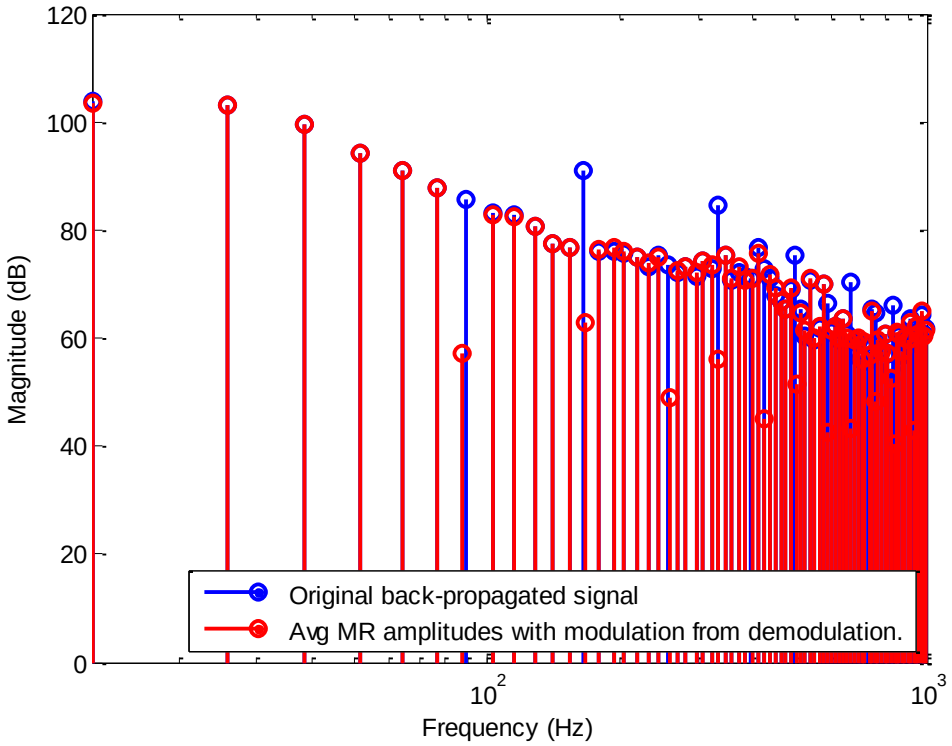

Figure 30: Average main rotor magnitudes with modulation from the demodulation process for section 2.

A time-domain comparison of the modulated main rotor and the back-propagated signal is shown in Figure 31. The addition of the modulation to the mean amplitudes and frequencies of the main rotor allow the main rotor frequency domain magnitudes to properly align, with little or no deviation, with those of the back-propagated signal. This

illustrates the importance of the modulation to properly synthesize accurate rotorcraft source noise.

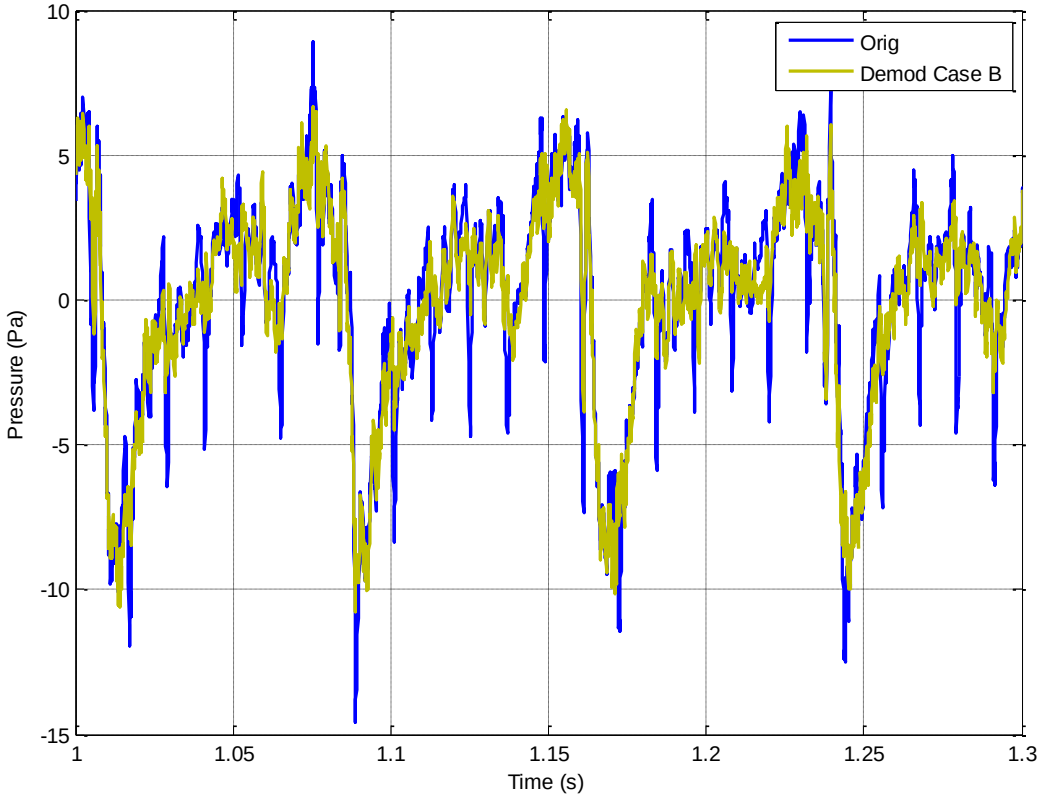

Figure 31: Average main rotor magnitudes with modulation from the demodulation process for section 2.

The addition of the modulation (in amplitude and frequency) did allow for the time-domain peaks of Case B and the original signal to align properly, however the time-domain amplitudes do not match very well. This leads to the assumption that a high fidelity model of rotorcraft noise must include both the main and tail rotor.

The next step is to test this assumption graphically. To do this, a comparison between the original signal and a signal which combines the unmodulated parts of the main and tail rotor must be made. This combination of the unmodulated parts of the main and tail rotor will be referred to as Case C, which is pictured in Figure 32 and Figure 33, in the frequency-domain and time-domain respectively. Samples of the resulting sounds are available in auxiliary wave files audiofile09.wav and audiofile10.wav, for thickness and loading noise, respectively (see Appendix C: Index of Supplemental Audio Files).

A comparison of the auxiliary wave files for Case C, audiofile09.wav and audiofile10.wav (see Appendix C: Index of Supplemental Audio Files), and the auxiliary audio files for Case A, audiofile05.wav and audiofile06.wav, for thickness and loading noise respectively, demonstrates the effect of adding the average tail rotor signal to the synthesis. The addition of the average tail rotor signal to the average main rotor signal aids in the accuracy of the magnitudes at the tail rotor harmonics and does not affect the main rotor harmonics that do not directly correspond to a tail rotor harmonic, which is expected. However, an even more accurate representation of the magnitudes is desired. Case B shows that the addition of the main rotor amplitude and frequency modulation to the average main rotor signal allows for a much more accurate calculation of the amplitudes of the main rotor frequencies in the original back-propagated signal. Therefore, the combination of the modulated main rotor and tail rotor signals should allow for accurate calculations of the amplitudes of the main rotor and tail rotor frequencies in the original back-propagated signal.

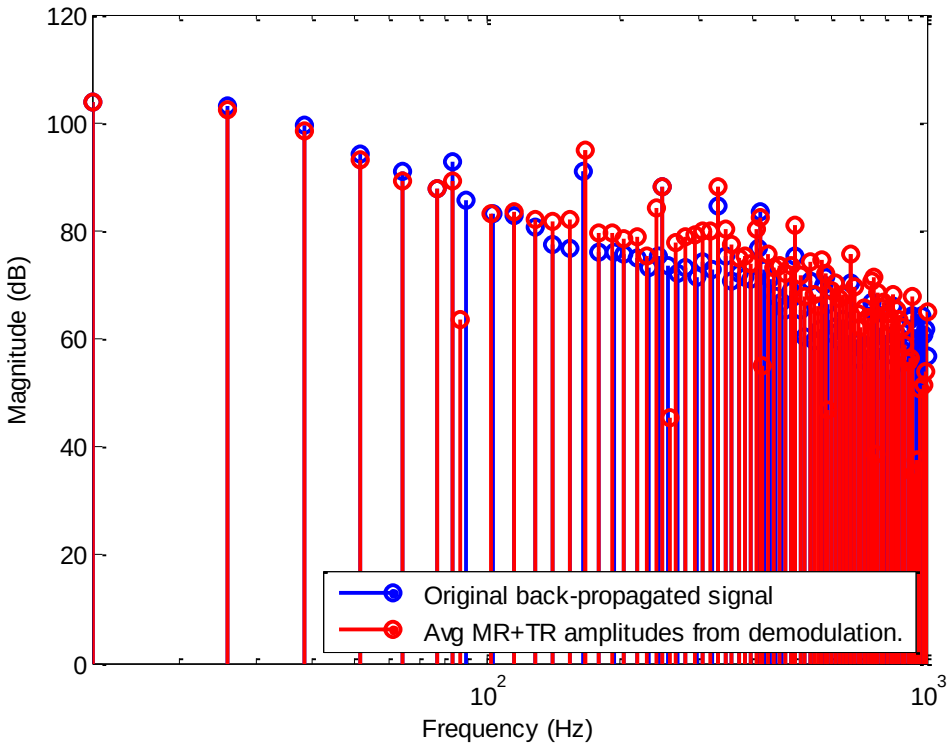

Figure 32: Combined average main rotor and tail rotor magnitudes from the demodulation process for section 2.

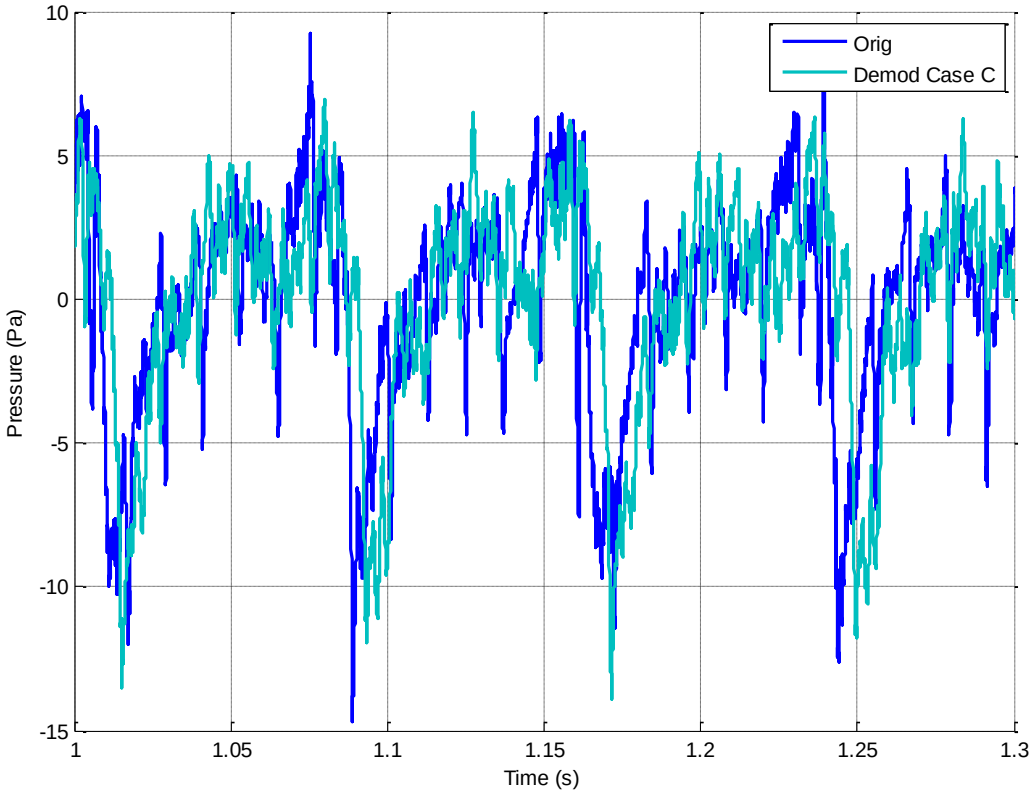

Figure 33: Combined average main rotor and tail rotor magnitudes from the demodulation process for section 2.

Figure 33 shows that peaks of Case C do not align with those of the original signal in both time and amplitude. This indicates that, not only do the unmodulated portions of main and tail rotor need to be incorporated into the synthesis, but the amplitude and frequency modulations for both rotors must also be included to gain a higher fidelity. Since the gearing ratio between the main and tail rotor is not an integer multiple, each peak of the average main rotor signal does not precisely align with a peak of the average tail rotor signal. This causes the peaks of the combined average main and tail rotor signal to vary with time, which is also evident in Figure 15. The addition of the average tail rotor signal also allows one to clearly see the average tail rotor pulses, which are most clearly visible between the larger main pulses. The use of the average main rotor and average tail rotor signals from the demodulation process allows for a more accurate representation of the original back-propagated signal as compared the time-averaged main and tail rotor signals determined by the synchronous time-averaged process, Figure

15. However, the tail rotor pulses seen in Figure 15 seem to align better with the original back-propagated signal than those seen in Figure 33.

Figure 34 and Figure 35 illustrate the comparison between the original signal and the full reconstruction, using the mean and modulation components for both the main and tail rotors, in the frequency-domain and time-domain respectively. A comparison of the auxiliary wave files for Case D, audiofile11.wav and audiofile12.wav (see Appendix C: Index of Supplemental Audio Files), and the auxiliary audio files for Case B, audiofile07.wav and audiofile08.wav, for thickness and loading noise respectively, demonstrates the effect of adding the modulated tail rotor signal to the synthesis. Figure 34 shows that the amplitudes and frequency values of the combined modulated main and tail rotor signal almost exactly match the amplitudes of the corresponding main and tail rotor frequencies in the original back-propagated signal in the frequency-domain. This is a significant improvement, in both amplitude and frequency values, over using the main rotor signal with modulation alone, Figure 30.

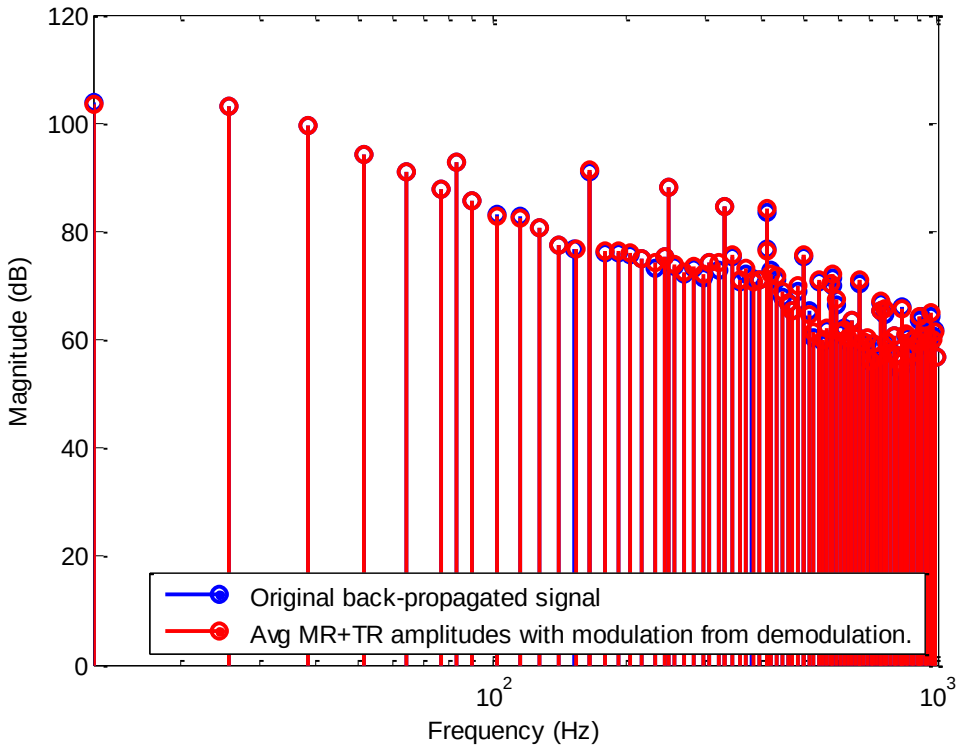

Figure 34: Combined average main rotor and tail rotor magnitudes with modulation from the demodulation process for section 2.

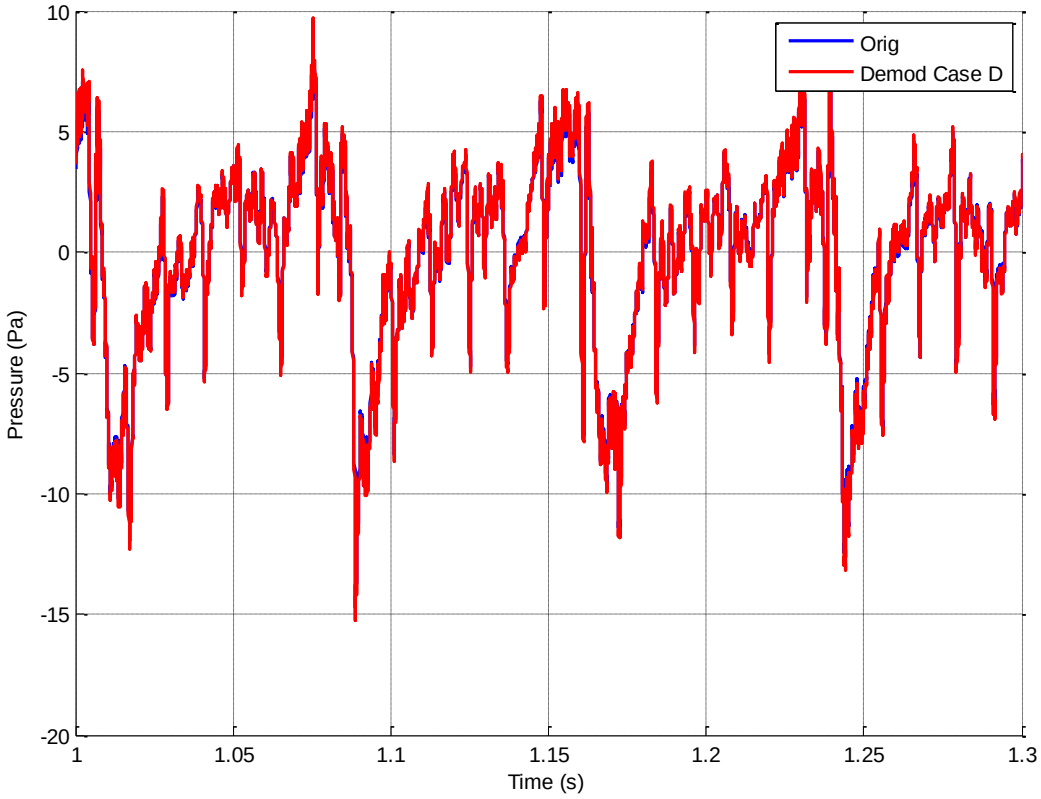

Figure 35: Full Reconstruction of the Original Signal

The full reconstruction in Figure 35 is nearly an exact match with the original back-propagated signal in the time-domain. Case D is a vast improvement over Case A, which lacks the structure of the modulated tail rotor signal apparent in the original back-propagated signal, Figure 31. The addition of the modulated tail rotor allows the peaks in Case D to match the peaks of the original back-propagated signal in both time and amplitude with the allowance of a small margin of error. The expectation is that in listening tests, Case D will represent the original back-propagated signal very well; however Case D will not exactly match the original back-propagated signal at every point. This is because this work is primarily directed toward simulating only the noise sources associated with main and tail rotor. The exclusion of other noise sources, such as engine noise and gear noise, is likely the reason for the, albeit small, error between the combined modulated main and tail rotor signal and the original back-propagated signal.

4.3 Fidelity Analyses of Reconstructed Signals

Fidelity is measured holistically, evaluating the signal as a single unit instead of analyzing the individual characteristics of the sound in isolation of one another, by

considering both objective and subjective measurements. One way of measuring the objective components of fidelity is to consider the root mean square error in the time-domain. Table 6 compares the rms error for four types of synthesis previously discussed.

Table 6: RMS error for the four methods of synthesis.

Type of noise	Case A	Case B	Case C	Case D
Thickness	87.64%	40.97%	90.00%	26.04%
Loading	87.61%	63.67%	92.17%	40.86%

The comparison of the rms error values for the various methods of synthesis using values from the demodulation process, shows that Case D best represents the original back-propagated signal, followed by Case B, Case A, and Case C, in order of lowest error to highest error respectively.

Through comparisons, in both the frequency-domain and time-domain, of the various synthesized signals from the synchronous time-averaged method and the demodulation process it seems that the demodulation process allows for the creation of higher fidelity sound source simulation. However, objective fidelity metrics must be taken into consideration. The results from the evaluation of the objective fidelity metrics are shown in Table 7.

Table 7: Objective measures of fidelity for the signals from the demodulated synthesis process.

Noise Type	Sound Type	RMS Error (%) (as compared to the reference)					
		Loudness	Roughness	Sharpness	Specific Loudness	Specific Roughness	Tonality
Thickness	Case A	2.0413	22.5131	7.6422	17.3526	32.0171	95.0544
Thickness	Case B	1.1740	6.5921	**0.9510**	13.1944	13.2303	76.4383
Thickness	Case C	0.8565	21.2731	7.4672	6.9000	26.1042	58.2659
Thickness	Case D	**0.2281**	**0.9360**	1.2520	**1.7987**	**3.7130**	**8.7649**
Loading	Case A	2.5598	42.7450	7.7559	22.2946	48.8009	97.6196
Loading	Case B	1.5585	8.0363	2.8395	17.3229	10.5312	78.9021
Loading	Case C	1.0636	40.0100	7.7158	8.6483	46.5014	**17.8556**
Loading	Case D	**0.2240**	**6.8410**	**2.6346**	**1.7441**	**3.1826**	32.2872

The bold numbers in Table 7 show which signal was the most similar to the original back-propagated signal for each of the objective fidelity metrics. A comparison of the

results in Table 3, Table 4, and Table 7 show that the synchronous time-averaged method exhibits the highest error for the majority of the categories. When comparing the signals of the synchronous time-averaged method with the corresponding sounds in the demodulation process for thickness noise, Case A and Case C, the synchronous time-averaged method incurs significantly higher error than those seen from the demodulation process, with the exception of the tonality metric. The same holds true when comparing the synchronous time-averaged method to the demodulation process for loading noise, Case A and Case C. The demodulation process produces higher fidelity signals than those produced using the synchronous time-averaged method and are better suited for this study. Therefore, for the remainder of this thesis, the mean amplitudes used will be those produced by the demodulation process.

When considering only the signals generated using the demodulation process, the data shows that the signals with only main rotor time average characteristics and no modulation (Case A for both thickness and loading noise) result in the largest error. For thickness noise, Case D has to lowest error over the majority of the metrics, with the exception of sharpness. The expectation is for Case D to have the lowest amount of error in all categories; however, Case B has the lowest error in sharpness. This suggests that the addition of the modulated tail rotor increases the error pertaining to sharpness by slightly distorting the higher frequencies. These findings agree with the hypothesis that the signals with the fewest components of the original back-propagated signal (Case A for both thickness and loading noise) are least representative of the original back-propagated signal; and the signals with the most components of the original signal (Case D for both thickness and loading noise) best represent the original back-propagated signal while the other signals will fall between these two extremes.

For the purposes of this study, a high fidelity signal is required. However, this may not be the case for all studies. If a lower level of fidelity is sufficient to fulfill the goals of a study, the synchronous time-averaged method may be sufficient. In the case where the original mean amplitudes are unavailable, using the mean amplitudes from the synchronous time-averaged method may be an acceptable alternative.

5. Practical Considerations for Synthesizing Flyover Noise

The time-varying synthesis technique developed in chapter 4 was successful in closely replicating the original signal for the original time record when modulated main and tail rotor were present. The signals considered there were synthesized at a fixed emission angle and had a time record length between one and two seconds. A longer term objective of this research effort is the synthesis of an entire flyover. In order to accomplish this, two additional developments are needed. The first is a means of morphing the synthesized sound from one emission angle to another during the course of a flyover event. This development is outside the scope of this research, but will be discussed in the context of future work in Chapter 7.

The second development necessary for synthesizing flyover noise is that synthesized pressure-time histories must be of arbitrary length. Extending the synthesis of unmodulated signals is easily accomplished by simply summing longer duration harmonics. The crux of synthesizing high fidelity signals of arbitrary length thus amounts to how best to extend limited duration amplitude and frequency modulation data. A desired approach is the development of a fluctuation model capable of generating fluctuation data for as long as is needed. Such a modeling effort is, however, also beyond the scope of this thesis. Instead, a simpler option is explored herein to extend the modulation data by various wrapping methods. Three methods of wrapping the modulation[1] data are subsequently discussed which allow the modulation data to be extended to any desired length. Random application implies that there is a loss of absolute modulation phase and amplitude information across the frequency spectrum. This process of wrapping the modulation, or randomly applied modulation, is a separate process from the unwrapped coherent application of modulation which is used in Case B

[1] The term wrapped may be interchanged with the term random. This is because the wrapping process randomly shifts the modulation of each harmonic to induce a random relative phase between the harmonics.

and Case D from Chapter 4. Coherent application implies that an attempt is made to line up the absolute phase and amplitude of the modulation signal with that which is being replaced.

Thus far, the synthesis methods described in Chapter 4 only utilize the modulation specific to the emission angle of interest. Another possible way to simulate the modulation of the original back-propagated signal, which is utilized in jet noise synthesis, is to apply the modulation from an arbitrary emission angle to all other emission angles. This would aid in morphing the synthesized sound from one emission angle to another since the modulation is the same for each individual emission angle.

5.1 Wrapping

5.1.1 Wrapping Method 1 – Linear Transition

In the first method, a short linear transition is made in each harmonic's amplitude modulation data to connect the last point in the series with the first. The resulting circular buffer retains all the characteristics of the original amplitude modulation. An example of this process is shown in Figure 36 where the amplitude modulation of the BPF (shown in blue) is transitioned from the end value to the starting value with a short, 20-sample linear transition (shown in red). Since the back-propagated signal is sampled at 10 kHz, the 20-sample linear transition adds only 2 milliseconds to the time record of the modulation. This short transition allows the modulation pressure-time history to be extended for many periods without significant misalignment relative to the original back-propagated signal. Due to the compressed time scale in Figure 36, it is difficult to see that the end point of the transition does properly coincide with the first point in the modulation pressure-time history. The compressed time scale causes the transition to appear vertical which is not the case.

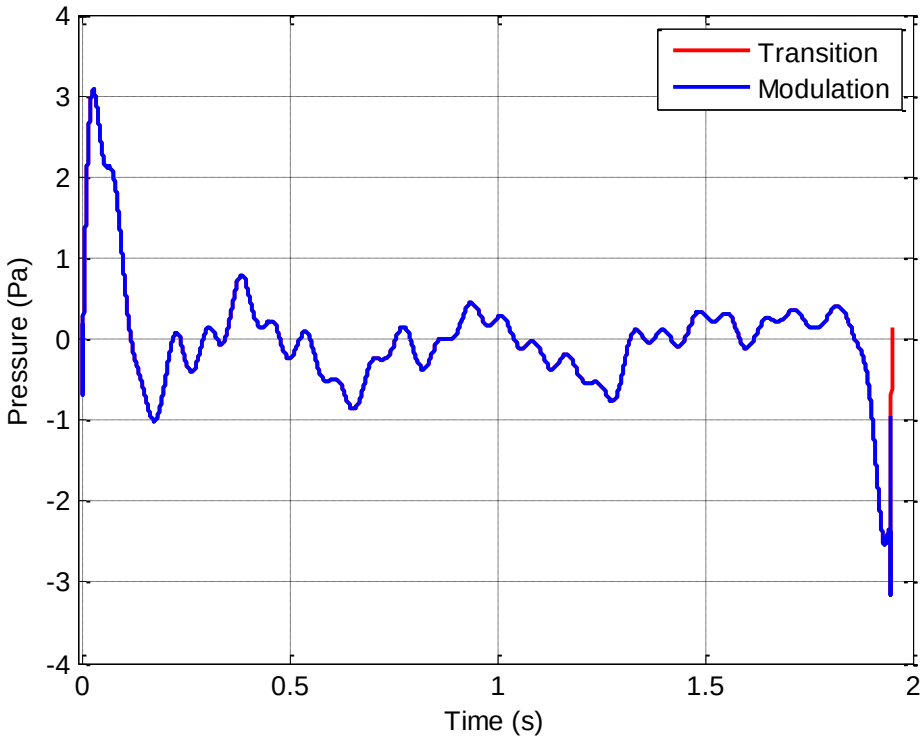

Figure 36: Wrap Method 1 Stage 1: Adding transition to the amplitude modulation.

The frequency modulation is handled slightly differently than the amplitude modulation. Since the simulated annealing process determines the phase modulation for each filtered narrowband signal, the same modulation methods used to extend the amplitude modulation were applied to the phase modulation. This means that the initial phase modulation is modified, such as shortening the modulation pressure-time history, adding a transition, and/or performing a circular shift on the modulation, according to each individual wrapping process. Equation (40) establishes that the frequency modulation is merely the derivative of the phase modulation. Therefore the frequency modulation was determined by taking the derivative of the modified phase modulation. This frequency modulation is then concatenated for the desired time length to create the wrapped frequency modulation, as seen in Figure 37. This process does not affect the mean frequency or initial phase for the BPF and corresponding harmonics.

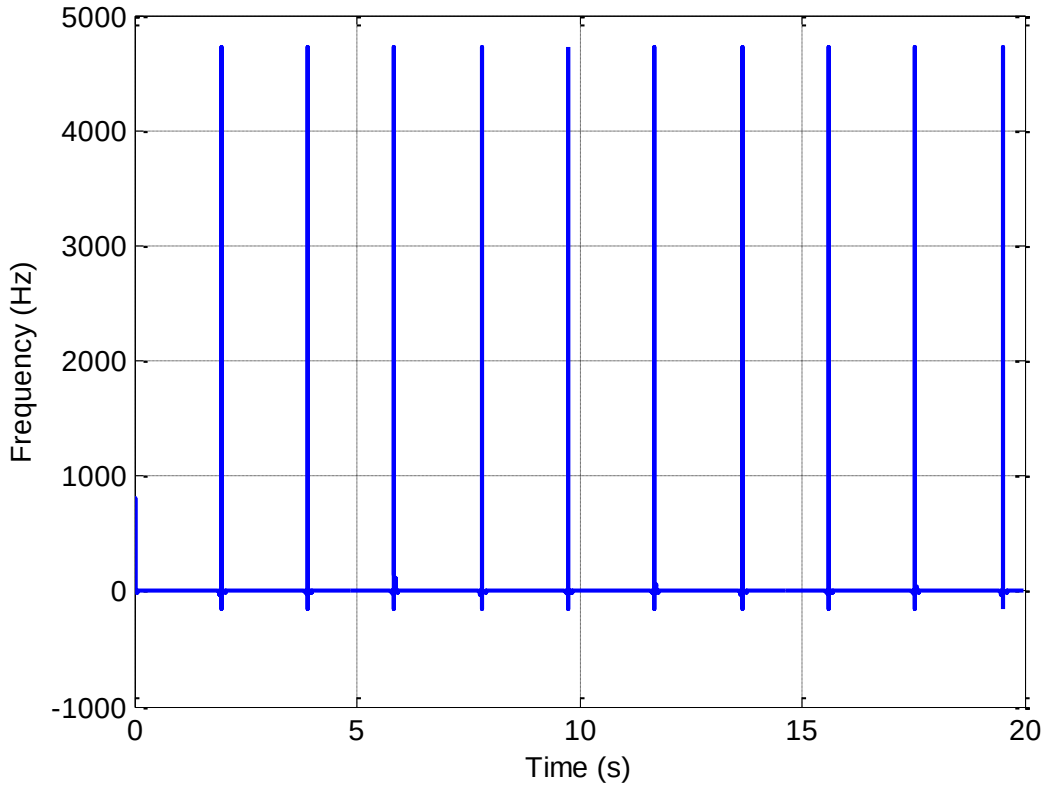

Figure 37: Wrap Method 1 Stage 2: Concatenating the new frequency modulation.

The combination of concatenated modifications of amplitude (Figure 38) and phase modulations, as with the mean amplitudes and frequencies allows a record of arbitrary length to be synthesized; Method 1 creates a very rhythmic sound since the modulation of each harmonic has the same period, which is seen by the transition points at the beginning, middle, and end of Figure 39 (shown by the red brackets). These transition points are also referred to as "wrap boundaries." A "wrap boundary" is the location in the pressure-time history where two consecutive modulation periods are connected in order to extend the pressure-time history for a longer period of time than is represented by the original back-propagated signal. Figure 39 illustrates the fully synthesized signal using wrapping method 1. The rhythmic character overshadows the finer structure of the modulation. Samples of the resulting sounds are available in auxiliary wave files audiofile13.wav and audiofile14.wav, for thickness and loading noise, respectively (see Appendix C: Index of Supplemental Audio Files). The elimination, or at least reduction, of this rhythmic character was the motivation behind the creation of method 2.

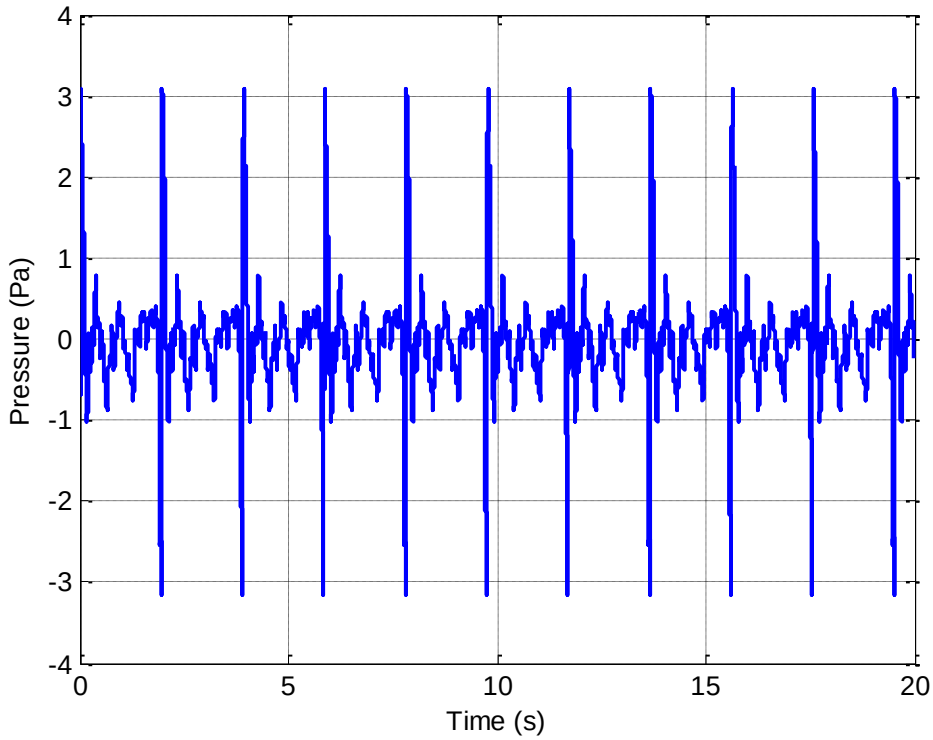

Figure 38: Wrap Method 1 Stage 2: Concatenating the new modulation.

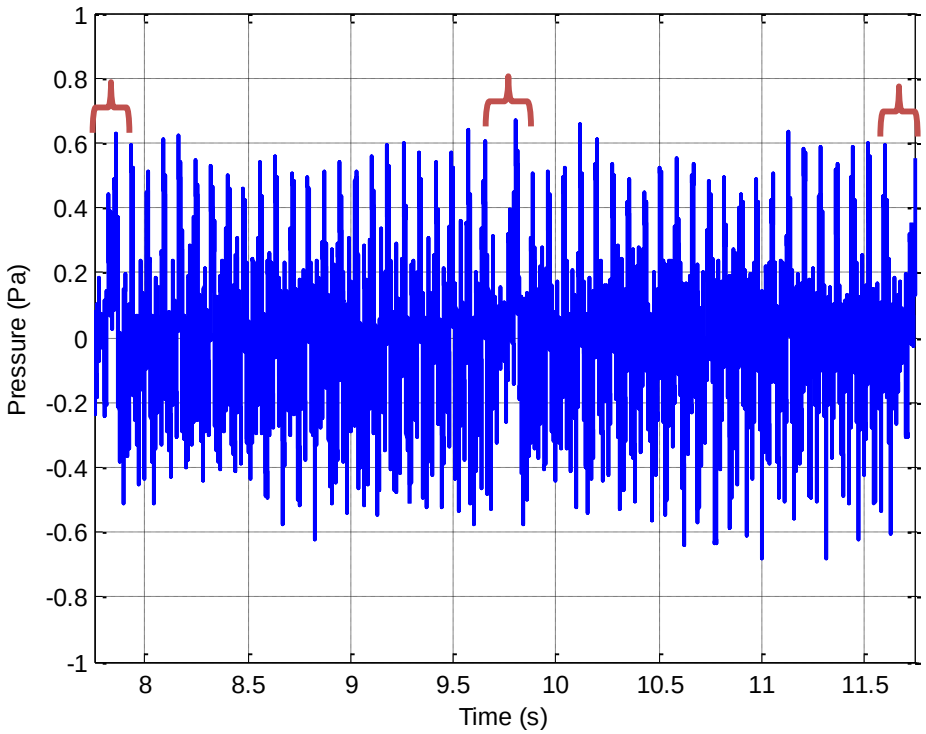

Figure 39: Full synthesis using wrapping method 1.

5.1.2 Wrapping Method 2 – Random Truncation with Linear Transition

Method 2 is a modified version of method 1. A random portion of each amplitude modulation is first removed, as illustrated in Figure 40. The original signal is shown in blue and the portion remaining after truncation is shown in green. Next, a short linear transition is applied to join the last point of the truncated modulation with the (original) first point. The result is shown in Figure 41 for the first harmonic of the main rotor of section 2.

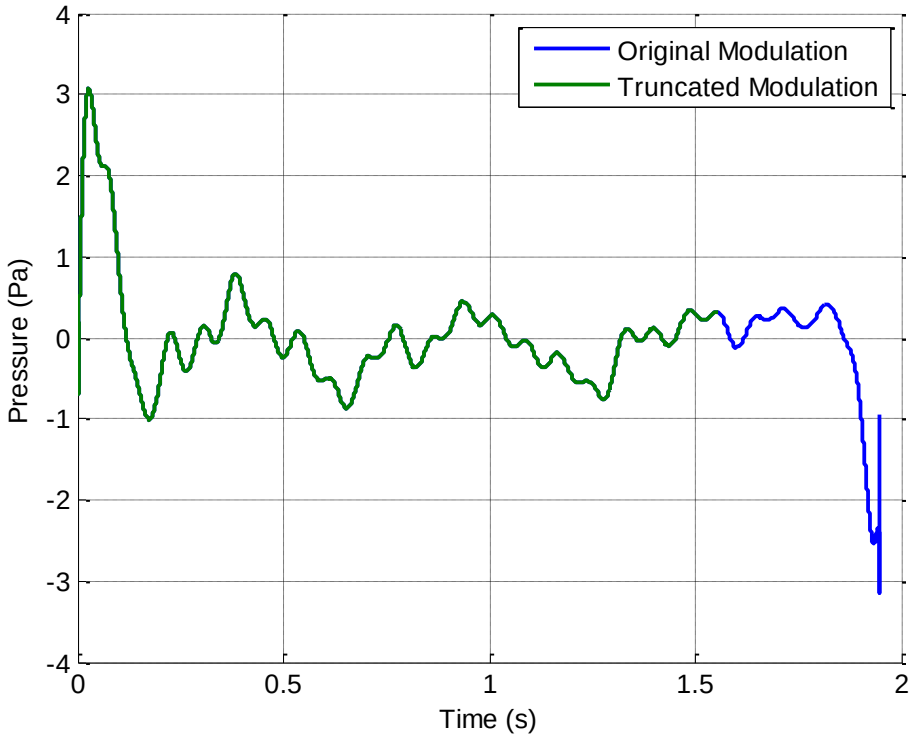

Figure 40: Wrap Method 2 Stage 1: Trimming the modulation to a random length.

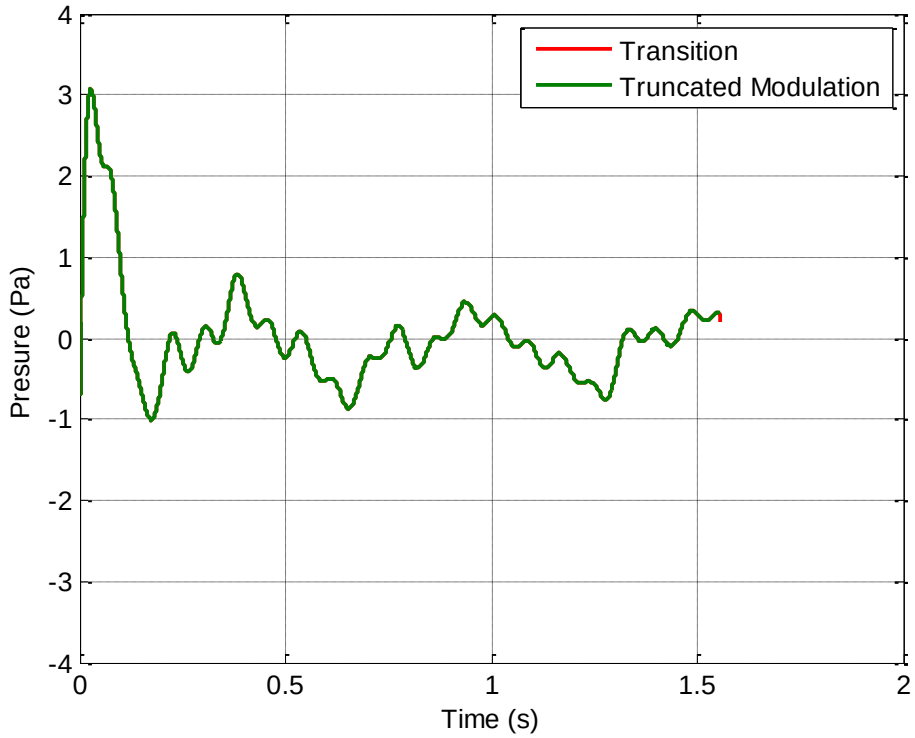

Figure 41: Wrap Method 2 Stage 2: Adding a transition to the truncated amplitude modulation.

What breaks up the rhythmic character associated with method 1 is not the truncation itself, but the fact that it is applied differently for each harmonic. In particular, an arbitrary amount of a 10-period section, based on the BPF of the rotor being evaluated, is truncated from the end of each amplitude deviation history. The arbitrary amount is determined by using the *rand()* command within MATLAB to create a random set of numbers between zero and one. The random numbers are multiplied by the 10 periods, where the period is determined by the BPF of each rotor. One random length segment is removed from the amplitude deviation history of each harmonic. The amount removed for each amplitude deviation history is different.

As in method 1, the linear interpolation joining the end points extends over 20 samples. The concatenated modification of the amplitude is shown in Figure 42. The temporal character is clearly different than that shown in Figure 38 for method 1. This technique does succeed in reducing the rhythmic nature, but still allows this characteristic to dominate the finer structure of the modulation, as heard in auxiliary wave files audiofile15.wav and audiofile16.wav, for thickness and loading noise, respectively (see

Appendix C: Index of Supplemental Audio Files). This reduction in rhythmic nature is visually evident in Figure 43 because the wrap boundaries are much more difficult to see as compared to Figure 39. Finally, note that this method actually removes some portion of the already limited modulation data in an effort to extend the record.

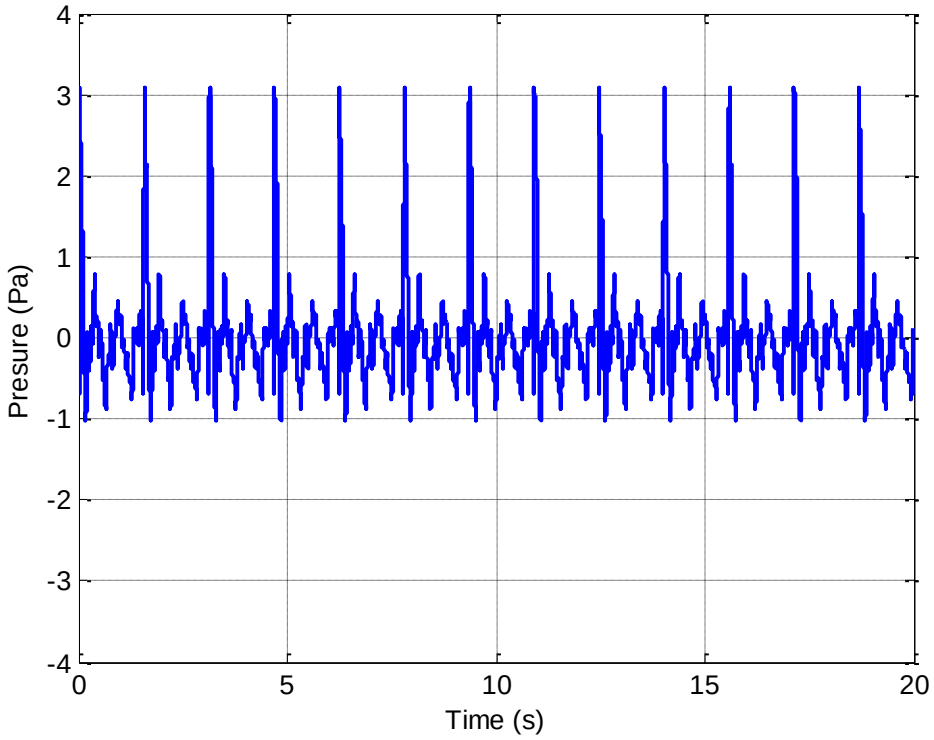

Figure 42: Wrap Method 2 Stage 3: Synthesized with the wrapped modulation.

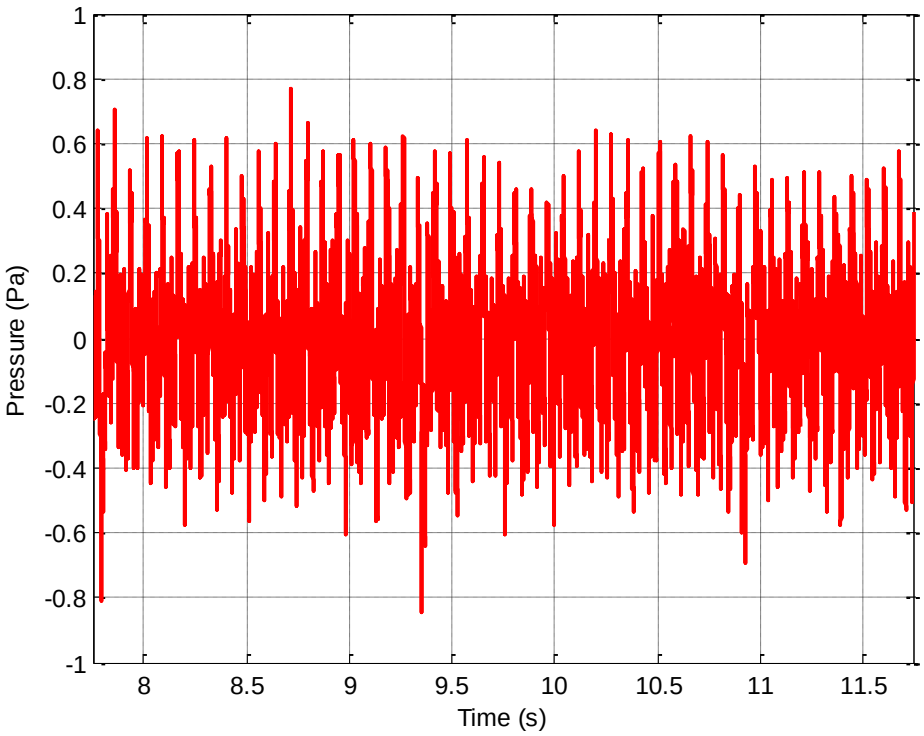

Figure 43: Full synthesis using wrapping method 2.

An objective fidelity metrics analysis was performed on the signals created by wrapping method 2. Since wrapping method 1 retains all the characteristics of the original amplitude modulation and the pressure-time history only differs from the original back-propagated signal by a phase shift induced by the linear transition, the objective fidelity metrics analysis represents the extent to which wrapping method 2 differs from wrapping method 1, specifically at a "wrap boundary." The results from this analysis are shown in Table 8.

Table 8: Objective measures of fidelity for wrapping method 2.

Noise Type	RMS Error (%) (as compared to the wrapping method 1)					
	Loudness	Roughness	Sharpness	Specific Loudness	Specific Roughness	Tonality
Thickness	1.4096	6.1894	4.8510	7.7279	9.7815	47.6226
Loading	1.1481	6.0102	5.4676	4.4181	7.4366	49.6044

Wrapping method 2 does not significantly differ from wrapping method 1 in regard to the objective metrics, with the exception to tonality. The large error in tonality is due to the random phasing of wrapping method 2.

5.1.3 Wrapping Method 3 – Linear Transition with Random Starting Index

The third and final method, method 3, is further modification of method 1. This approach is also meant to remove periodicity that may be perceived in the synthesis of the rotorcraft noise. This method starts as method 1 by adding a short transition to the amplitude modulation, as seen in Figure 36. The rhythmic character associated with method 1 is destroyed by allowing the starting index of each harmonic to be random. This is achieved with the circular shift function, *circshift()*, within MATLAB. Figure 44 compares the circularly shifted amplitude modulation (green curve) obtained using method 3 with the unshifted version (blue curve) obtained using method 1.

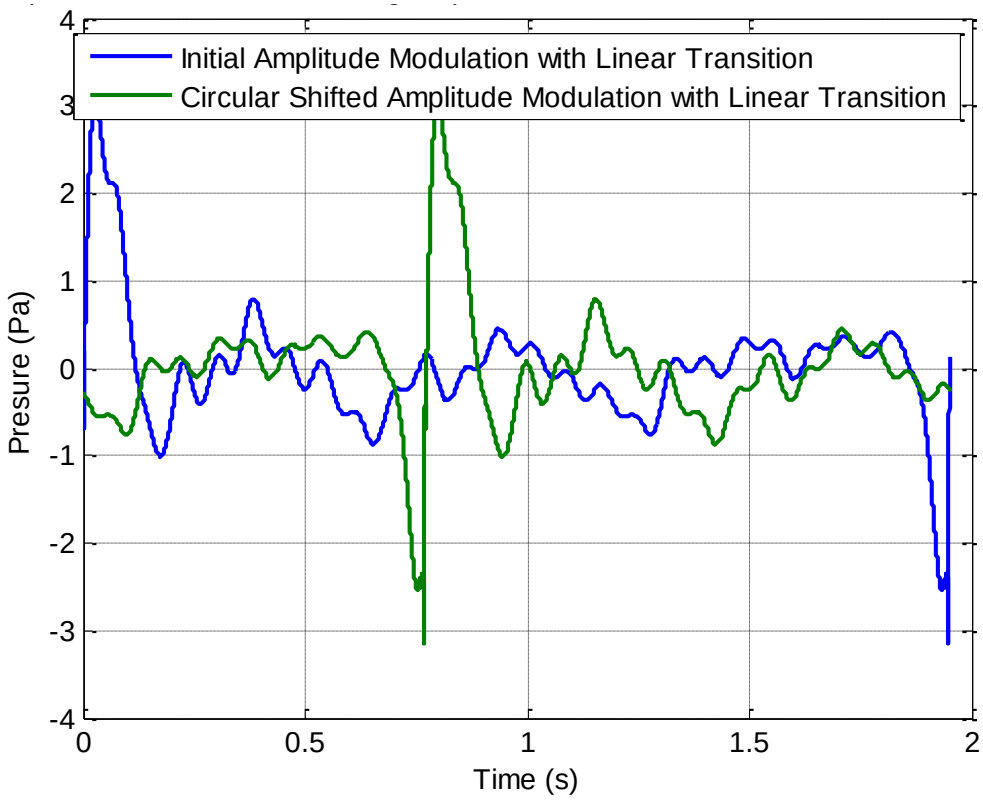

Figure 44: Wrap Method 3 Stage 2: Circular shifting of the new amplitude modulation.

Figure 45 shows the concatenated version of the amplitude modulation. Note that this is identical to that shown in Figure 38 except for an initial time delay. Further, the

operation is performed without eliminating limited modulation data. The fact that each harmonic is delayed differently accounts for the disruption in the rhythmic nature associated with method 1. The rhythmic disruption is visually evident in Figure 46 with any obvious "wrap boundary" being completely indistinguishable. The auxiliary wave files, audiofile17.wav and audiofile18.wav, for thickness and loading noise, respectively (see Appendix C: Index of Supplemental Audio Files), clearly demonstrate this. Method 3 reduces the rhythmic nature sufficiently to allow the finer structure of the modulation to be heard, but distorts the phase of the signal.

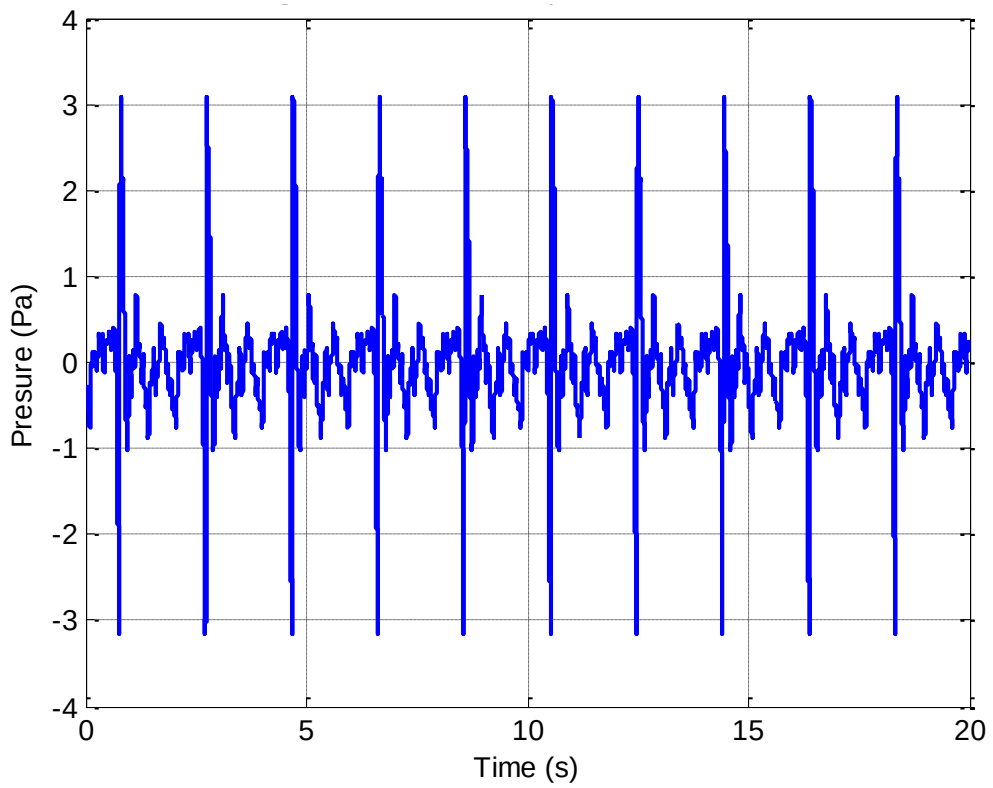

Figure 45: Wrap Method 3 Stage 2: Concatenating the new modulation to the length of the desired time record.

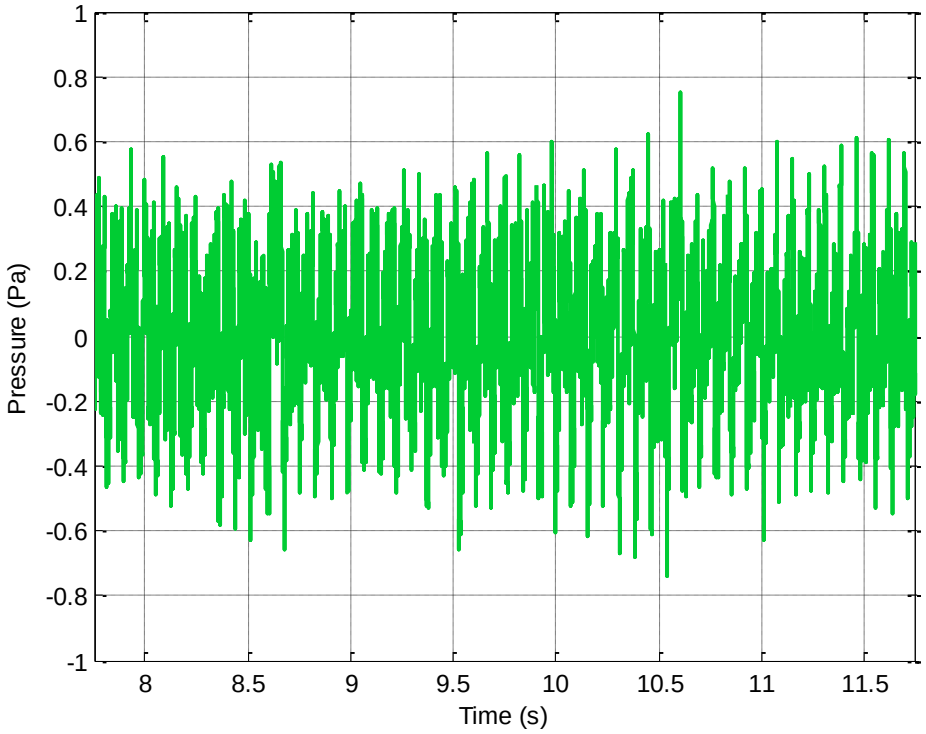

Figure 46: Full synthesis using wrapping method 3.

An objective fidelity metrics analysis was performed on the signals created by wrapping method 3 to allow for a better understanding of how well this method compares to wrapping method 1. The results from this analysis are shown in Table 9.

Table 9: Objective measures of fidelity for wrapping method 3.

Noise Type	RMS Error (%) (as compared to wrapping method 1)					
	Loudness	Roughness	Sharpness	Specific Loudness	Specific Roughness	Tonality
Thickness	1.7531	5.0574	4.4361	9.7866	12.0168	47.2415
Loading	1.6344	8.0227	4.9275	4.1493	10.2689	43.8779

A comparison between the error values of wrapping method 2 and wrapping method 3 shows that wrapping method 3 decreases error for the metrics of roughness, sharpness, and tonality for thickness noise, and the metrics of sharpness, specific loudness, and tonality for loading noise. The comparison indicates an increase in error for the metrics of loudness, specific loudness, and specific roughness for thickness noise, and the metrics of loudness, roughness, and specific roughness for loading noise. The maximum

difference in error between wrapping method 2 and wrapping method 3 is less than three percent error. Therefore, the objective fidelity analysis does not obviously show which of the wrapping methods best represents the original back-propagated signal, but the analysis does reveal that the two methods are similar in accuracy.

A flow chart depicting each of the wrapping methods is shown in Figure 47 to allow for a direct comparison between the wrapping methods for amplitude deviation. The frequency modulation for each step of the three wrapping methods is shown in Figure 48 to also allow for a direct comparison between each of the wrapping methods. The spikes in Figure 48 denote where the phase has a particularly a large slope in the time record.

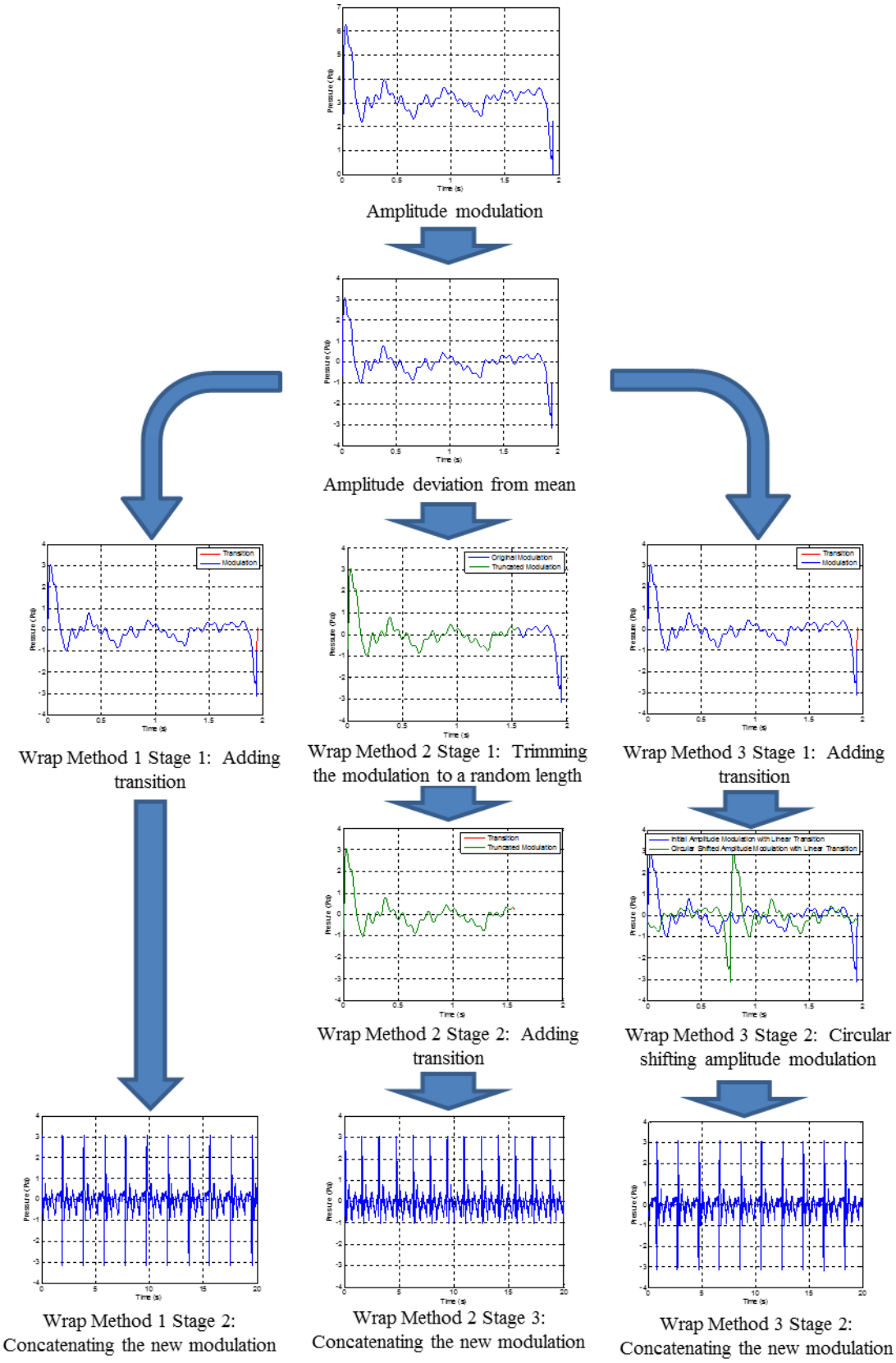

Figure 47: Amplitude modulation wrapping process.

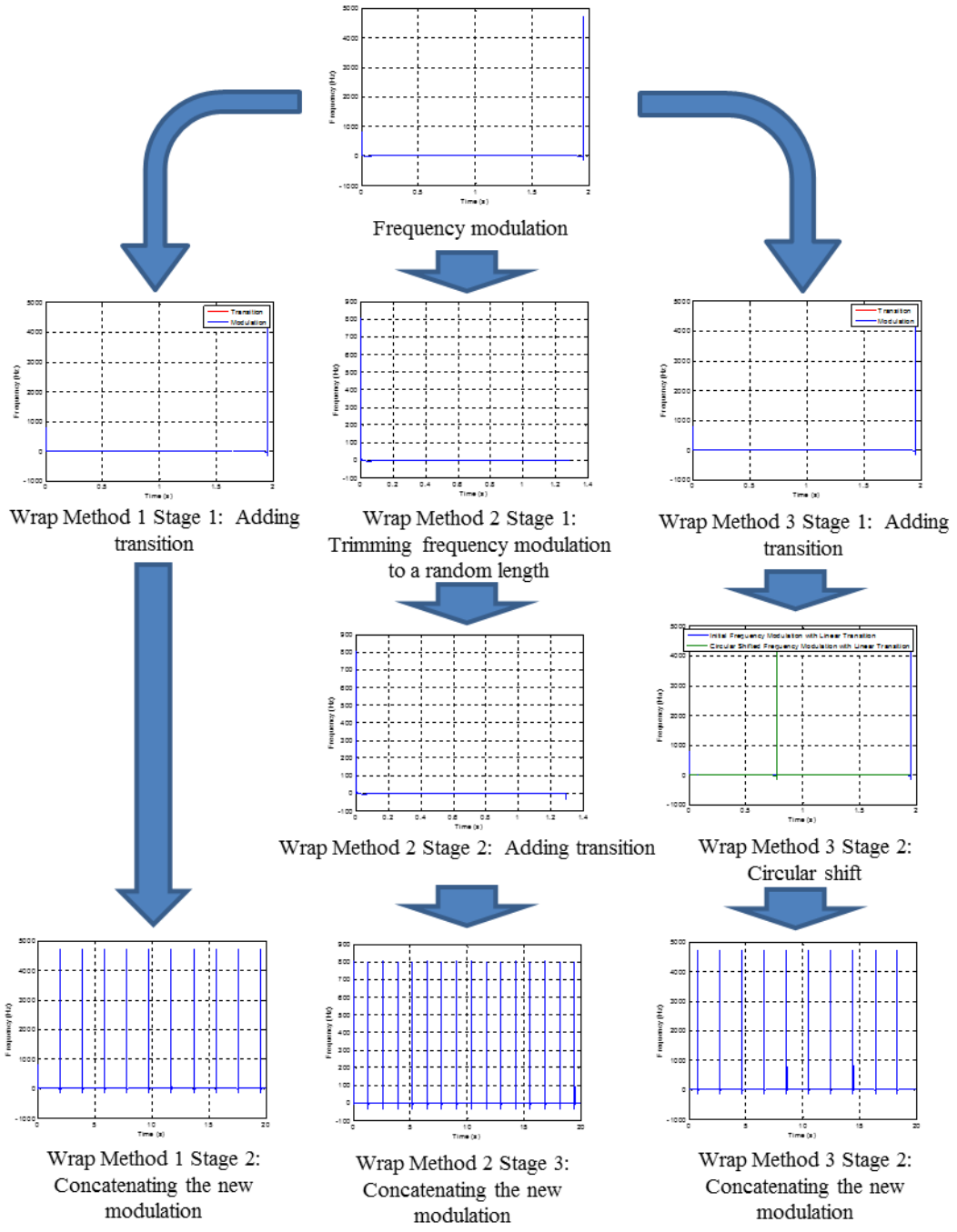

Figure 48: Frequency modulation wrapping process.

Even though the objective fidelity analysis does not indicate which of the wrapping methods is best suited for extending the time record of the original back-propagated signal, an initial subjective listening test of the three methods revealed that wrapping method 3 allows listeners to focus on the finer structure of the signal instead of the rhythmic nature induced by wrapping methods 1 and 2. Therefore method 3 will be

added to the unmodulated main and tail rotor and used in the subsequent human subject testing. Now that all of the signals have been created, the next step is to perform a human subject test to determine the subjective fidelity of the different types of synthesis and modulation.

5.2 Transitioning Between Adjacent Emission Angles

The capability to transition the sound between adjacent emission angles is necessary in order to create a high fidelity sound source simulation for a flyover scenario. This is possible when a model of the modulation as a function of emission angle is available. Such a model was developed for tonal fan noise [27]. Development of that model was facilitated as long pressure time histories were available from ground test data. Lack of such a data set precludes that approach at this time. In lieu of that, an alternative approach is application of modulation data from a single angle to all angles. For jet noise, this approach was successfully demonstrated by applying modulation from an arbitrary emission angle to all other emission angles [28]. This modulation approach will be referred to as generic modulation. Generic modulation data is derived from a section of the source recording which is different than the section to which it is applied. For the purposes of this study, it is from a different section of the source recording which is not clearly dominated by either thickness or loading noise characteristics, but still displays long-term modulation. So far the primary focus has been directed toward thickness and loading, the modulation from an emission located between these two types of noise was chosen as the generic modulation. This is in contrast with specific modulation which is the modulation from the original back-propagated signal for a particular emission angle. Specific modulation is synthesized in Chapter 4.

To better understand how well the use of generic modulation simulates the original back-propagated, an objective fidelity analysis was performed and the results are shown in Table 10. Samples of theses generically modulated synthesized sounds are available in the auxiliary wave files audiofile19.wav through audiofile24.wav, for thickness and loading noise, respectively (see Appendix C: Index of Supplemental Audio Files).

Table 10: Objective measures of fidelity for generic modulation applied coherently (without wrapping).

Noise Type	Process Method	RMS Error (%) (as compared to the reference)					
		Loudness	Roughness	Sharpness	Specific Loudness	Specific Roughness	Tonality
Thickness	Case D w/ specific modulation	0.2281	0.9360	1.2520	1.7987	3.7130	8.7649
Thickness	Case D w/ generic modulation	1.2902	13.5115	5.6852	12.2414	20.9853	64.3744
Loading	Case D w/ specific modulation	0.2240	6.8410	2.6346	1.7441	3.1826	32.2872
Loading	Case D w/ generic modulation	0.3942	33.9043	6.6704	6.4692	38.6165	26.4529

"Case D w/ generic modulation", in Table 10, uses generic modulation instead of specific modulation, which is used in Chapter 4. The use of generic modulation has a detrimental effect on the fidelity of the synthesized signal, as seen in Table 10. The use of generic modulation causes the error to increase in each objective metric category as compared to the use of specific modulation. This increase in error may be caused by the application of generic modulation, which has a characteristic BPF of 12.6904 Hz, to an average signal with a different characteristic BPF. As seen in sections 5.1.1, 5.1.2, and 5.1.3, the addition of generic modulation into the wrapping methods is not expected to improve the comparison of Table 10.

6. Human Response

The overall goal of this experiment is to gauge the relative fidelity of the different synthesis methods using an alternative measure based on subjective response. This will aid in determining if the objective measures of fidelity discussed in Chapter 4 and Chapter 5 reflect human perception. Once the time-varying signals are synthesized, fidelity can be evaluated using subjective measures. This is done by performing an experiment using human test subjects, also known as a psychoacoustic test. This is accomplished by asking three targeted research questions.

6.1 Research Questions

The first research question investigates the hierarchy of fidelity of the four methods of synthesis discussed in Chapter 4, which are pictured in Figure 29 through Figure 35. These four methods of synthesis are:

(a) Unmodulated main rotor

(b) Modulated main rotor

(c) Unmodulated main rotor combined with the unmodulated tail rotor

(d) Modulated main rotor combined with the modulated tail rotor

The second research question aims to determine the hierarchy of fidelity between various types of modulation. The types of modulation included in the second research question are as follows:

(a) No modulation

(b) Generic modulation, applied randomly

a. Generic modulation is from a different section of the source recording which is not clearly dominated by either thickness or loading noise characteristics, but still displays long-term modulation.

b. Random application implies that there is a loss of absolute modulation phase and amplitude information across the frequency

spectrum. This was introduced as wrapping method 3 in chapter 5.1.3.

(c) Generic modulation, coherently applied

a. Coherent application implies that an attempt is made to line up the absolute phase and amplitude of the modulation signal with that which is being replaced (i.e. that which was stripped from the original recording and expanding or contracting to fit the signal to which it is applied).

(d) Specific modulation, applied randomly

a. Specific modulation source is the recording which is being reconstructed, again using wrapping method 3.

(e) Specific modulation, applied coherently

The final research question is aimed to determine whether the wrapping process introduces any undesirable artifacts into the modulation that is audibly perceptible to the human ear but is not indicated when the data is displayed graphically. An undesirable artifact is any perceptual queue that the test subjects may use to distinguish between different segments of the same randomly modulated signal. This research question is meant to determine if the results of research questions 2b and 2d are dependent on the particular segment(s) used. This will be accomplished by selecting two segments from each of the randomly modulated signals. One section ("x") will be taken near the beginning of each signal and the other section ("y") will be taken at a later time in each of the signals. Each of the "x" sections will be compared to one another and each of the "y" sections will be compared to one another. The results of the third research question are derived from those asked in question 2 parts b and d for both thickness and loading noise. The expectation is that the subjects will not be able to distinguish between different segments of the same randomly modulated signal. These sounds correspond to auxiliary wave files audiofile27.wav through audiofile30.wav.

Each of the research questions will be posed toward an emission angle which is indicative of the characteristics of thickness noise and toward an emission angle which is indicative of the characteristics of loading noise separately.

6.2 Testing Procedure

Each of the research questions will be answered using a two alternative forced choice (2AFC) test. This type of test asks the participants to compare two noise samples ("A" and "B") to a reference noise ("R") and select which noise sounds most like the reference. The reference sounds are found in auxiliary wave files audiofile25.wav and audiofile26.wav, for thickness and loading noise, respectively. The combination of the reference noise and the two noises which are being compared are called a triad. Each time a participant is asked to make a comparison, the triad of interest will be presented twice. Each session begins with the following graphic.

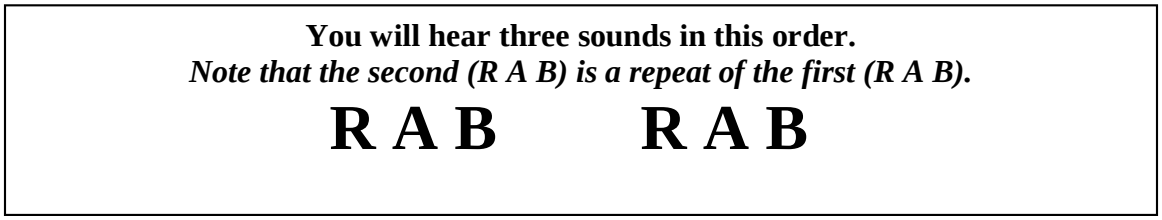

Figure 49: Note telling the subject the number of times each triad will be played and the order in which they are played.

Figure 49 explains to the participants that each triad will be presented twice and that the order will not change. When each of the sounds are played for the participant the corresponding letter will be highlighted red to remind the listener which sound is currently being played. This is illustrated in Figure 50, Figure 51, and Figure 52 for the reference noise, "A", and "B", respectively.

Figure 50: Screenshot of image to be displayed to listeners during playback of the reference signal "R".

Figure 51: Screenshot of image to be displayed to listeners during playback of the test signal "A".

Figure 52: Screenshot of image to be displayed to listeners during playback of the test signal "B".

Once each sound has been presented twice the participant is instructed to choose the sound that best represents the reference, which is displayed in Figure 53.

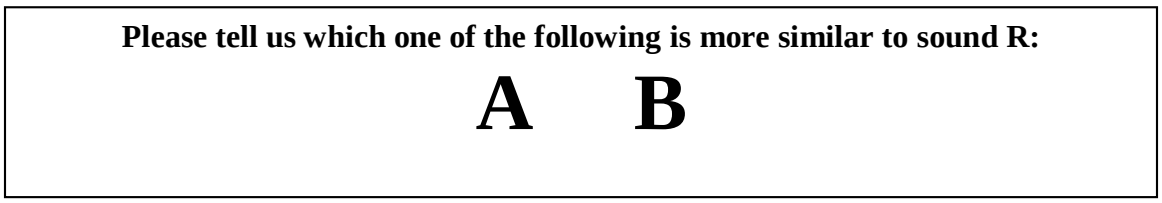

Figure 53: Screenshot of image to be displayed to listeners during their evaluation.

Once each participant has answered the current question, the next question starts and the process repeats. The participants are not allowed to proceed to the next question until all participants have selected an answer for the current question. This allows all participants to answer without inducing anxiety due to a specified time limit. The test is administered using tablet computers. The test is divided into multiple sections or sessions to allow the participants a break between sessions. Each session consists of multiple questions.

The heart of the test consists of 64 comparisons or questions. Half of the comparisons pertain to thickness noise and the other half pertain to loading noise. A chart of all of the comparisons is shown in Table 24 in Appendix A: Noise Comparisons. A shorthand notation used to designate the particular waveforms used is provided in Table 23 and the naming convention is shown in Figure 54. The first letter of the shorthand notation denotes the type of noise used for the time-averaged components of the signal, which will either be T for thickness or L for loading. The second letter of the shorthand notation denotes the type of modulation applied to the time-averaged components, which will be T for thickness noise modulation, L for loading noise modulation, G for generic modulation, or N for no modulation. The third letter of the shorthand notation denotes the modulation application process, which will be M for main rotor signal only, C for coherently applied modulation, or R for randomly applied

modulation. The notation of TN and LN denote the use of the time-averaged components of both main and tail rotor without modulation, for thickness and loading noise respectively.

$$\underbrace{T}_{\substack{base\ signal\ or \\ time-average\ components \\ (T\ or\ L)}} \qquad \underbrace{G}_{\substack{type\ of\ modultion \\ (T,\ L,\ G,\ or\ N)}} \qquad \underbrace{R}_{\substack{modulation\ application \\ process \\ (M,\ R,\ C,\ or\ blank)}}$$

Figure 54: Shorthand notation for the synthesized waveforms.

The 64 comparisons are randomized and divided into four sessions containing 16 questions each, as shown in Table 26 in Appendix B: Order of the Presentation of Signals. These four sessions, along with two other sessions which allow the subjects to acclimate to the testing environment and equipment, make up the entirety of the test. One of the additional sessions, the familiarization session, plays 10 miscellaneous sounds that would be played during the test to introduce the participants to the different types of sounds. The second session added was the practice session. This is where the participants are asked 10 practice questions that resemble the questions that will be asked later in the test to allow the participants to become acclimated to the hardware and how each question will be asked. The data from these first two sessions are not used in the analysis.

The human subject test consists of 32 participants which were divided into eight groups. This means that four participants were tested at one time. The comparison sessions were randomized for each group of test subjects based on a Latin square array as seen in Table 27 in Appendix B: Order of the Presentation of Signals. Each of the sounds played were normalized to a loudness of 90 phon in order that test subjects not select similarity of "A" and "B" signals to the reference "R" signal based on loudness. A window was applied to each of the sounds to allow for the sounds to fade-in for 0.1 seconds at the start of the playback and fade-out for 0.1 seconds at the end of the playback to prevent the speakers from emitting a "snap" or "pop." Each of the sounds played for the test participants lasted 0.8 seconds. The participants were isolated from one another through the use of partitions to reduce likelihood of interaction between the subjects during the test. The sounds were played through the overhead speakers in the External Effects Room (EER) at NASA Langley Research Center. The EER resembles a movie theater, which is seen in Figure 55.

Figure 55: Placement of test subjects in the External Effects Room (EER) at the NASA Langley Research Center.

The EER is equipped with 27 monitor speakers and four subwoofers [29]. A limiter system was active during each of the testing sessions to protect the wellbeing of participants by shutting off the power to all of the speakers if the sound pressure level (SPL) exceeded 95 decibels (dB). Human subject response data were acquired under the auspices of the "Synthesized Engine Noise Test 2 (SENT-2)" study during the period of March 31, 2014 through April 3, 2014.

6.3 Statistical Methods

A two-tailed binomial test, with a five percent confidence interval, was performed to determine the p-value for each comparison. One of the drawbacks of the binomial test is that this test cannot distinguish between a random distribution, seen in Figure 56, and a bi-modal distribution, seen in Figure 57, since both are represented by a p-value of, or close to, 0.5. This means that a deeper look at the data may be necessary, such as plotting the actual data on a graph. A unimodal distribution is a distribution that exhibits a single

peak or one of the categories, or choices, has a greater amplitude than any of the other categories. Therefore, a random distribution is a type of unimodal distribution.

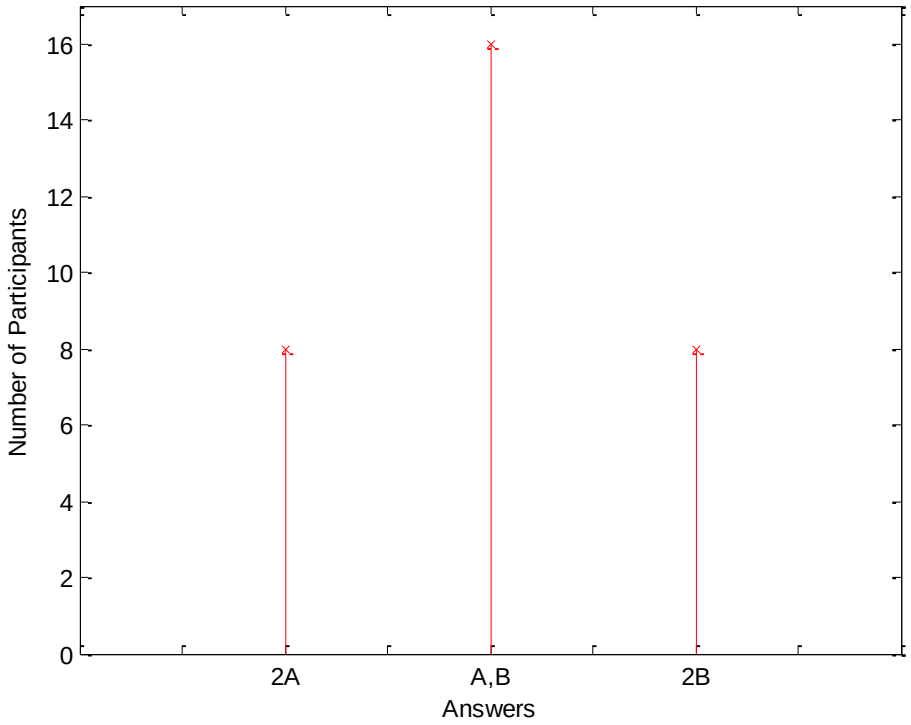

Figure 56: Random distribution.

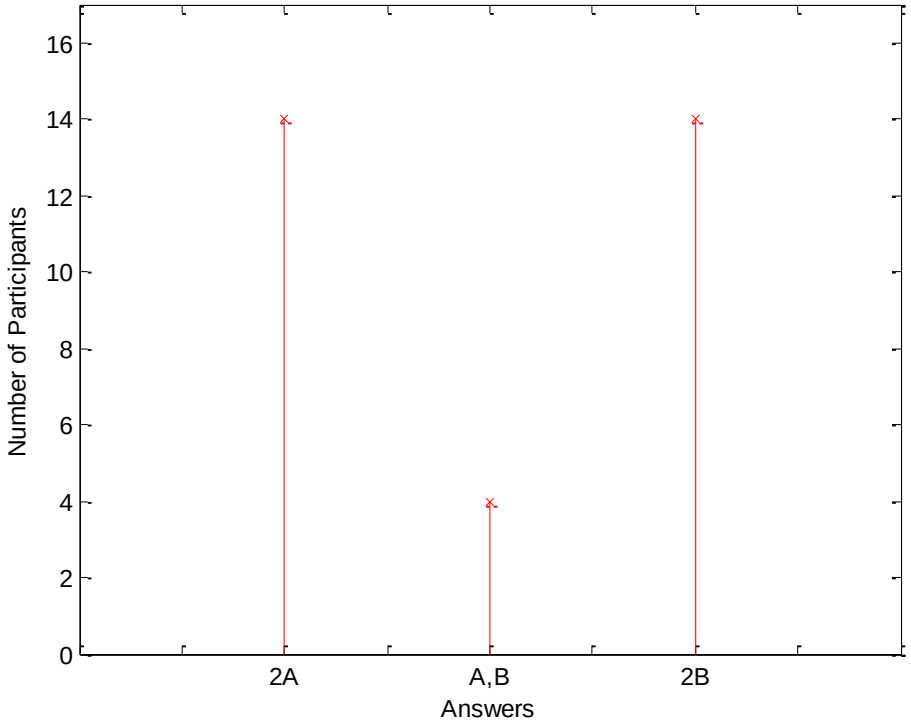

Figure 57: Bi-modal response (a.k.a. "Split Decision").

The subjective responses during the test of signal “A” or signal “B” were converted into numerical responses, which allows for easier analysis of the test subjects’ responses. A subject response was awarded zero points for choosing signal “A” and one point for choosing signal “B” for each comparison. Since each question is asked twice, with the exception of the comparison of question 2 parts b and d, each participant can gather zero points, one point, or two points depending on how the questions are answered. Therefore, zero points (or 2A on the graphs above) denotes a person who chose signal “A” both times; one point denotes a person who chose signal “A” then signal “B” or vice versa (or A,B in the graphs above); and two points denotes a person who chose signal “B” both times (or 2B in the graphs above). The bi-modal distribution occurs when the majority of participants note a perceptible difference between signal “A” and signal “B.” Of this majority, approximately half show a preference for signal “A” (zero points) while the remaining portion of the majority show a preference for signal “B” (two points). This may also be referred to as a split decision. In order to distinguish between the two distributions, the χ^2 test was implemented to determine how well the data fits a normal

distribution and if the fit was poor what was the representative p-value of the most likely distribution (p_{ML}). The χ^2 value represents the complement of the cumulative distribution function (cdf) value of the χ^2 distribution. This value is an indicator of goodness of fit or how well the distribution fits the data. If the χ^2 value is large, the expected values based on the distribution indicated by p_{ML} are close to the observed values from the experiment thus supporting the null hypothesis. The null hypothesis for this test is that both sounds being compared have an equal chance of being chosen as the sound that best represents the reference. If the χ^2 value is low, the expected values are not close to the observed values therefore the null hypothesis is not supported. If the p-value conflicts with the χ^2 value, such as the case of a high p-value but a low χ^2 value, the distribution of the data is not unimodal and may indicate a bi-modal character. However, if both the p-value and the χ^2 value are high, the data has a unimodal character.

6.4 Results

Once the subject tests were completed and all of the responses were recorded, the data was grouped with respect to each of the research questions and analyzed. The results for each of the research questions are discussed in the following sections.

6.4.1 Research Question 1

The first research question investigates the hierarchy of different synthesis methods to determine which is most representative of the reference sound. The reference sound is a portion of the original back-propagated signal. The four sounds, each representing a method of synthesis, being compared to the reference are listed as follows:

(a) Unmodulated main rotor

(b) Modulated main rotor

(c) Unmodulated main rotor combined with the unmodulated tail rotor

(d) Modulated main rotor combined with the modulated tail rotor

In each case, signals were synthesized according to the method discussed in Chapter 4, as these were found to have improved objective fidelity measures compared to those synthesized using the method in Chapter 3. Samples of the test signals used are provided in the auxiliary wave files audiofile05.wav through audiofile12.wav (see Appendix C:

Index of Supplemental Audio Files). When viewing the results tables, the first letter in the Part column denotes signal "A" and the second letter denotes signal "B." N refers the number of times the question was answered by all participants. The third column, %B, shows the percentage of times that signal "B" was chosen over signal "A." The last column displays the p-value for each question. The green cells, in Table 11 and Table 12, indicate results that agree with initial expectations. The initial expectation was that the synthesized signals would increase in fidelity from (a) to (d). The yellow cells denote which questions have "% B" values near 50 percent. These cells indicate no preference as to which signal best represents the reference. For the majority of the comparisons the participants displayed a distinct choice for which of the two signals better resembled the reference. Overall the results definitively show that the test subjects could tell the difference between each sound and showed an obvious preference in each comparison. Looking at Table 11 and Table 12, one can see that (a), the main rotor without modulation, is the least representative of the reference sound. Also, (d), the combination of the modulated main rotor combined with the modulated tail rotor, seems to best represent the reference sound. This was found to be the case for both thickness and loading noise.

Table 11: Results for research question 1 for thickness noise.

Part	N	% B	p-value[2]
a, b	64	89.06%	< 0.0001
a, c	64	82.81%	< 0.0001
a, d	64	95.31%	< 0.0001
b, c	64	45.31%	0.3817
b, d	64	89.06%	< 0.0001
c, d	64	89.06%	< 0.0001

[2] If the p-value was very small the value was replaced with "<0.0001." A p-value this small refers to a high significance.

Table 12: Results for research question 1 for loading noise.

Part	N	% B	p-value
a, b	64	89.06%	< 0.0001
a, c	64	90.63%	< 0.0001
a, d	64	92.19%	< 0.0001
b, c	64	75.00%	< 0.0001
b, d	64	87.50%	< 0.0001
c, d	64	76.56%	< 0.0001

A further look at the comparison, for thickness noise, of research question 1 part b and c is needed. This is the comparison of the main rotor with modulation to the combination of the main rotor without modulation and the tail rotor without modulation. When the data is evaluated using the χ^2 test based on a random distribution, the result was 70.91 percent. This means that the data is not purely random but is a random distribution skewed toward one of the two signals. When the data is evaluated to determine the most likely p-value (p_{ML}), the result is a value of 0.45. The corresponding χ^2 test value is 95.41 percent. The p_{ML} and χ^2 value supports the conclusion that the data is random but skewed toward signal "A" or the main rotor with modulation. A plot of the data for this comparison is shown in Figure 58.

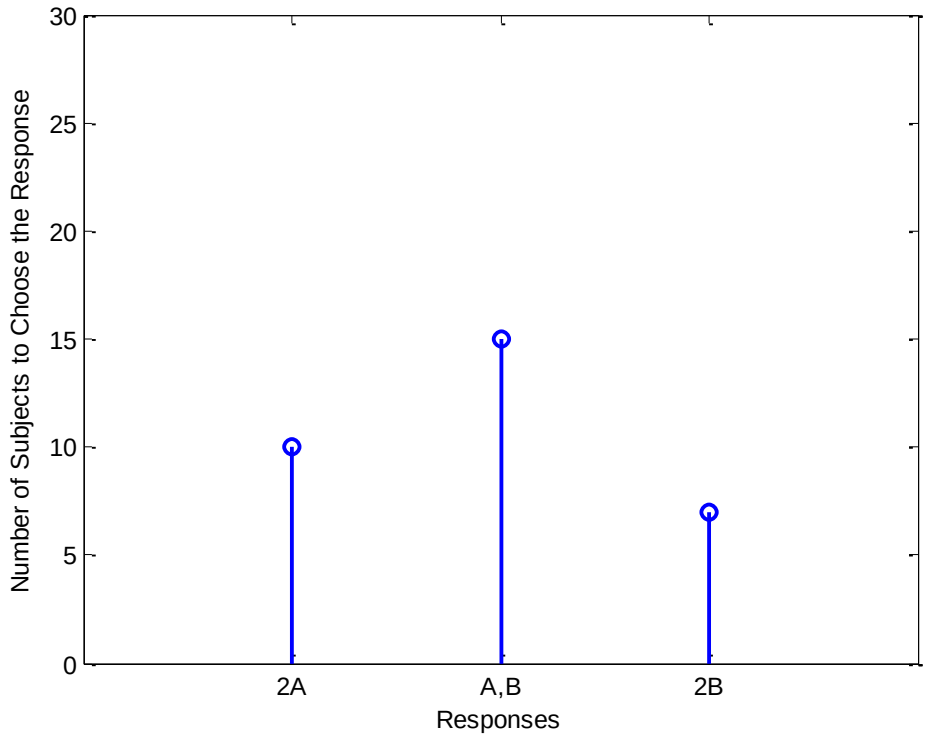

Figure 58: Responses for research question 1 parts b and c for thickness noise.

Now that the data for each of the comparisons has been evaluated, the hierarchy can be determined. The hierarchy is determined using a probabilistic ranking scheme based on the Perron-Frobenius Theorem [30]. The assumption is made that the probability of choosing signal "A" or signal "B" is defined by the following equation.

$$P(A > B) = \frac{Rank(A)}{Rank(A) + Rank(B)} \tag{43}$$

The rank of signal "A" and signal "B" may be replaced with the respective scores or the percentage of times the subjects chose each signal. By substituting the rank of each signal by the score of each signal in Equation (43), Equation (43) becomes

$$P(A > B) = \frac{S_A}{S_A + S_B} \tag{44}$$

where S_A and S_B are the respective scores of signal "A" and signal "B." This process eventually allows the of ranking of the different types of synthesis to be represented as the Eigenvector solution of an Eigenvalue problem, which satisfies equation (4.7) in [30], which is shown in the following matrix equation.

$$B\boldsymbol{r} = \mu\boldsymbol{r} \tag{45}$$

where the matrix B has entries b_{ij}, given by [30], as

$$b_{ii} = \sum_j S_{ij}^2, \quad b_{ij} = -S_{ij}S_{ji}, \quad i \neq j" \tag{46}$$

From the above equation, S is the percentage each signal was chosen during the human subject test. The S matrices are shown below in Table 13 and Table 14.

Table 13: S matrix for thickness noise for research question 1.

	a	b	c	d
a	0	0.109375	0.171875	0.046875
b	0.890625	0	0.546875	0.109375
c	0.828125	0.453125	0	0.109375
d	0.953125	0.890625	0.890625	0

Table 14: S matrix for loading noise for research question 1.

	a	b	c	d
a	0	0.109375	0.093750	0.078125
b	0.890625	0	0.250000	0.125000
c	0.90625	0.750000	0	0.234375
d	0.921875	0.875000	0.765625	0

The way to read the above tables is the left hand vertical column ((a) through (d)) beats the top row ((a) through (d)). As an example, (b) beats (a) 89.06 percent of the time. Once the B matrices are complete, the inverse power method is used to solve for the Eigenvector. The first step of this method is to invert the B matrices. The inverted B matrix is multiplied by a weighting matrix (r). Since this process is iterative, the first iteration of the weighting matrix uses equal weights for each of the sounds. The first set of values for the weighting matrix are arbitrary, thus for the purposes of this experiment the values were kept simple by using unity divided by the number of sounds (i.e. (a), (b), (c), and (d)), or 4. The weighing matrix is updated with the values of this matrix multiplication. Before the completion of the update the new values are normalized by

$$r_i = \frac{B^{-1} r_{i-1}}{sum(B^{-1} r_{i-1})}. \tag{47}$$

This process is repeated until the values stabilize or no longer fluctuate. Once, this occurs the Eigenvector solution has been reached. The signal ranking is the most recent update to the weighting matrix (r_N). Solving the Eigenvector problem yields the ranking shown in Table 15. The ranking values for the different types of modulation were normalized so that the signal that had the highest ranks is represented by unity. This process of ranking allows Equation (43) to use these ranking values to approximate the probability (Table 13 and Table 14) of each of these sounds being chosen to represent the reference.

Table 15: Ranking for research question 1.

	Thickness Noise	Loading Noise
a	0.0311	0.0453
b	0.1287	0.1295
c	0.1193	0.3169
d	1.0000	1.0000

An example calculation is shown below.

$$P(a > d) = \frac{Rank(a)}{Rank(a) + Rank(d)} = \frac{0.0311}{0.0311 + 1.0000} = 0.0302$$

The ranking is verbose in showing Case D, or the full reconstruction using the combination of the main rotor with modulation and tail rotor with modulation, as having the highest fidelity with a value of 1.0000 when considering both thickness noise and loading noise. Also, the census seems to be consistent in denoting that (a), or the main rotor only without modulation, displaying the lowest fidelity for both types of noise. These two types of noise seem to disagree when evaluating (b), or main rotor with modulation, and (c), or the combination of the unmodulated main rotor and unmodulated tail rotor. For thickness noise, main rotor with modulation barely outshines the combination of the unmodulated main and tail rotor. The close proximity of the values for these two signals seems to indicate that the participants of the human subject test felt that these signals are very similar to one another, possibly having the same level of

fidelity. The same is not true when considering loading noise. A significant difference in the ranking shows that the main rotor with modulation is of a lower level of fidelity than the combination of the unmodulated main and tail rotors. The type of noise determines which method of synthesis is used to reconstruct the original signal depending on the desired level of fidelity.

The type of application dictates the necessary level of fidelity. The above results indicate that when considering the level of fidelity, the angle of emission or type of noise must be taken into consideration. The type of noise and the level of fidelity will determine the components necessary for creating the most appropriate synthesized signal.

6.4.2 Research Question 2

The second research question investigates the effect of the different types of modulation on the subjective fidelity. The five types of modulation are:

(a) no modulation
(b) randomly applied generic modulation
(c) coherently applied generic modulation
(d) randomly applied specific modulation
(e) coherently applied specific modulation.

For further explanation refer to section 6.1. In the case of (b) and (d), signals were synthesized according to wrapping method 3 (see 5.1.3). Samples of the test signals used are provided in auxiliary wave files audiofile11.wav, audiofile12.wav, audiofile19.wav through audiofile24.wav, and audiofile27.wav through audiofile30.wav (see Appendix C: Index of Supplemental Audio Files). The results of the human subject test for the comparisons pertaining to the second research question are shown in Table 16 and Table 17, for thickness and loading noise respectively. The green cells indicate results that agree with initial expectations. The initial expectation was that the synthesized signals would increase in fidelity from (a) to (e), according the list above. The yellow cells denote which questions have "% B" values near 50 percent. These cells indicate no preference as to which signal best represents the reference. The red cells indicate the results that are contrary to expectations. The original assumption was that the subjects

would prefer sounds that included some form of modulation (b-e) over a signal without modulation (a). However, the data seems to contradict the previous assumption to a degree. Looking at the thickness noise, the subjects preferred no modulation (a) over both forms of generic modulation (b-c), see first two rows of Table 16. For loading noise, the subjects indicated that no modulation (a) is equivalent or slightly better than generic modulation (b-c), see first two rows of Table 17. This shows that using modulation from an emission angle that includes both thickness noise and loading noise is no better and may even be worse than no modulation when compared to the reference. The best representation of the reference signal is the signal with coherently applied specific modulation (e), see rows 4, 7, 9-10 of both tables.

Table 16: Results for research question 2 for thickness noise.

Part	N	% B	p-value
a, b	64	32.81%	0.0037
a, c	64	32.81%	0.0037
a, d	64	40.63%	0.1034
a, e	64	89.06%	< 0.0001
b, c	64	57.81%	0.1686
b, d	128	63.28%	0.0019
b, e	64	92.19%	< 0.0001
c, d	64	68.75%	0.0016
c, e	64	87.50%	< 0.0001
d, e	64	87.50%	< 0.0001

Table 17: Results for research question 2 for loading noise.

Part	N	% B	p-value
a, b	64	50.00%	0.9007
a, c	64	54.69%	0.3817
a, d	64	62.50%	0.0328
a, e	64	76.56%	< 0.0001
b, c	64	46.88%	0.5323
b, d	128	53.91%	0.3309
b, e	64	84.38%	< 0.0001
c, d	64	53.13%	0.5323
c, e	64	82.81%	< 0.0001
d, e	64	81.25%	< 0.0001

Further analysis is necessary to determine the ranking of the various types of modulation. A deeper look will start with investigating the comparisons with "% B" values near 50 percent to better understand the distribution of the data. The results whose "% B" values are close to 50 percent are shown in Table 18 and Table 19, for thickness and loading noise respectively.

Table 18: χ^2 results for thickness noise.

Part	N	% B	p-value	χ^2 (p = 0.5)	p_{ML} (% B)	χ^2 (p_{ML})
a, d	64	40.63%	0.1034	11.94%	0.41	45.34%
b, c	64	57.81%	0.1686	26.09%	0.57	47.10%
b, d	128	63.28%	0.0019	5.61%	0.62	78.68%
c, d	64	68.75%	0.0016	0.41%	0.68	77.26%

Table 19: χ^2 results for loading noise.

Part	N	% B	p-value	χ^2 (p = 0.5)	p_{ML} (% B)	χ^2 (p_{ML})
a, b	64	50.00%	0.9007	10.54%	0.50	10.54%
a, c	64	54.69%	0.3817	15.82%	0.54	22.31%
a, d	64	62.50%	0.0328	13.53%	0.62	93.14%
b, c	64	46.88%	0.5323	68.73%	0.47	76.50%
b, d	128	53.91%	0.3309	60.78%	0.53	70.00%
c, d	64	53.13%	0.5323	68.73%	0.53	76.50%

In Table 18, all of the comparisons show that the data does not precisely fit a normal distribution (p-value = 0.5) well, as seen by the χ^2values in column 5. The first three rows of Table 19 show, again, that a normal distribution does not adequately represent the data. However, this is not the case for the last three rows of Table 19, which show χ^2values in excess of 60%. Since the results vary significantly, the data was used to determine the most likely p-value (p_{ML}) to better understand the type of distribution that best represents the data. The p-values in column 6 differ from 0.5 but not significantly. In further investigation, the data was evaluated to determine how well the p_{ML} value describes the data through the use of a chi-squared (χ^2) test. The results are shown in the "χ^2 (p_{ML})" column. For thickness noise, the comparison of question 2 parts (b) and (d), and question 2 parts (c) and (d) are close to random distributions, which is indicated by a low "χ^2 (p = 0.5)" value, a high "χ^2 (p_{ML})" value, and a p_{ML} near 0.5. These two distributions are random but skewed toward signal "B."

Table 18 indicates that, for thickness noise, the comparison of question 2 parts (a) and (d) is skewed toward signal "A" with the p_{ML} value of 0.41. However, when evaluated with the χ^2 method, the data for this p_{ML} value yields a value of 45.34 percent. A simple plot may allow for a better understanding of the nature of this data, which is shown in Figure 59.

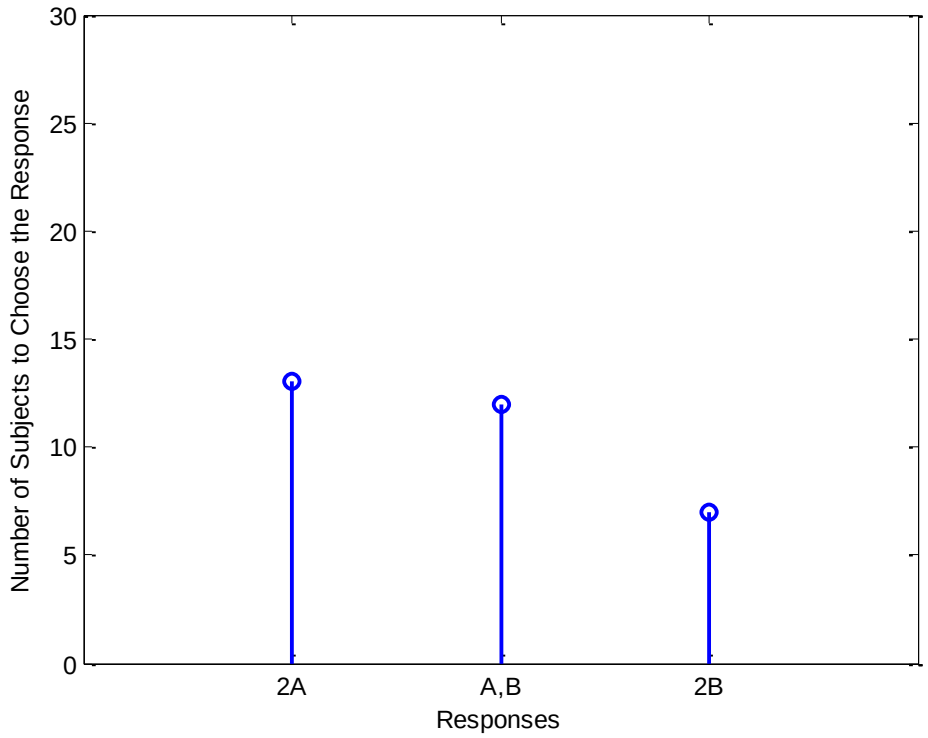

Figure 59: Results from question 2 a,d for thickness noise.

Figure 59 seems to display a random distribution which is skewed toward signal "A" or no modulation (a). The above figure displays characteristics of multiple distributions. Figure 59 is a combination of a random distribution and a distribution that prefers signal "A." When data displays characteristics of multiple distributions, the χ^2value is a poor measure of the data and thus a plot allows a better understanding of the data. A similar occurrence is seen, for thickness noise, with the comparison of question 2 parts (b) and (c), where the result of the χ^2 method in regard to the new p-value, of 0.57, yields only 47.10 percent. This means that distribution with a p-value of 0.57 is 47.10% as likely to yield a value as extreme in a chi-squared distribution. Again, a plot of the data is necessary to properly determine the true nature of this data, as seen in Figure 60.

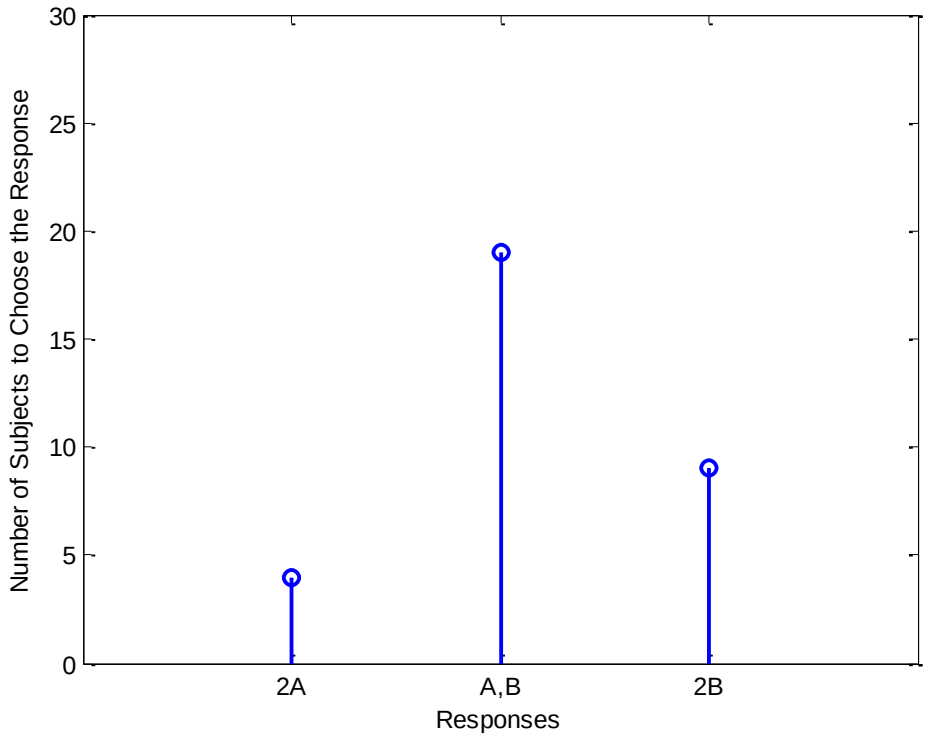

Figure 60: Results from question 2 b,c for thickness noise.

Figure 60 displays data which is indicative of a random data with a slight skew toward signal "B" or, in this case, coherently applied generic modulation. Looking at loading noise, an example of a split decision is seen with the comparison of question 2 parts (a) and (b), as seen in Figure 61.

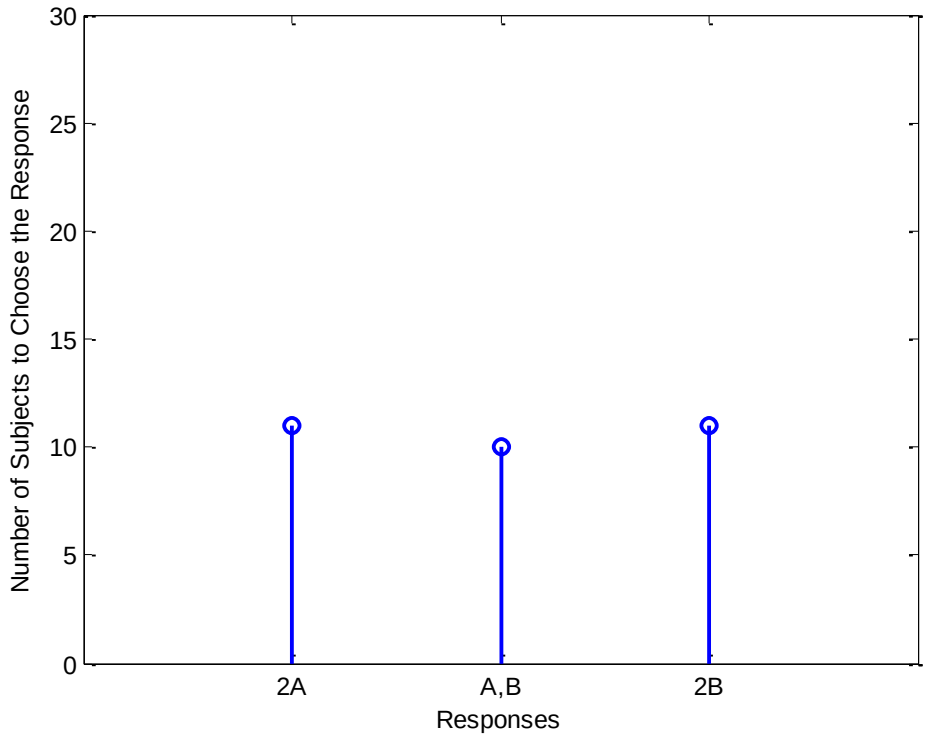

Figure 61: Results of question 2 a,b for loading noise.

This shows that most of the participants could distinguish between the no modulation condition and the randomly applied generic modulation condition. Of that majority, half preferred the no modulation and the other half preferred the randomly applied generic modulation. This also shows how a p-value of 0.50 does not directly indicate a random distribution and that further inquiry is necessary to determine the type of distribution.

Now that the comparisons with "% B" values near 50 percent have been investigated, the journey of ranking the various types of modulation begins. The matrices used in the Perron-Frobenius analysis are shown in Table 20 and Table 21 for thickness and loading noise, respectively. These tables indicated the percentage that each signal was chosen. Again, the way to read the tables is the left hand vertical column ((a) through (e)) beats the top row ((a) through (e)). As an example, (b) beats (a) 32.8125 percent of the time.

Table 20: *S* matrix for thickness noise for research question 2.

	a	b	c	d	e
a	0	0.6718750	0.6718750	0.5937500	0.1093750
b	0.3281250	0	0.4218750	0.3671875	0.0781250
c	0.3281250	0.5781250	0	0.3125	0.1250000
d	0.4062500	0.6328125	0.6875000	0	0.1250000
e	0.8906250	0.9218750	0.8750000	0.8750000	0

Table 21: *S* matrix for loading noise for research question 2.

	a	b	c	d	e
a	0	0.5000000	0.4531250	0.3750000	0.2343750
b	0.5000000	0	0.5312500	0.4609375	0.1562500
c	0.5468750	0.4687500	0	0.4687500	0.1718750
d	0.6250000	0.5390625	0.5312500	0	0.1875000
e	0.7656250	0.8437500	0.8281250	0.8125000	0

These tables are used to solve the Eigenvalue problem, in same manner described in section 6.4.1, which results in the ranking shown in Table 22. Again, the ranking values have been normalized so that the highest rank (signal most similar to the reference) has a value of unity. The full reconstruction, or coherently applied specific modulation (e), best represents the reference. In looking at the ranking for both thickness noise and loading noise, (e) has a much higher rank than any of the other signals. The other signals appear to be clustered together on the lower end of the ranking scale. This seems to indicate that these signals only differ slightly in fidelity and may be equivalent according to the ranking alone. This also indicates that the use of generic modulation (randomly or coherently applied) and randomly applied specific modulation is ineffective in representing the reference sound. Therefore, rotorcraft noise modulation is specific to each emission angle. To produce the highest fidelity synthesis, the full reconstruction must be performed for each emission angle. These results demonstrate that the shortcut methods proposed for wrapping (see section 5.1) and applying a single generic

modulation (see section 5.2) are ineffective and that a more sophisticated approach is needed for production of a high fidelity flyover event with time-varying emission angle.

Table 22: Ranking for research question 2.

	Thickness Noise	Loading Noise
a	0.1456	0.2268
b	0.0792	0.2084
c	0.1020	0.2164
d	0.1372	0.2537
e	1.0000	1.0000

6.4.3 Research Question 3

Next considered is whether multiple parts of the same extended synthesized signal (using the wrapping method 3) sound similar. Specifically, two segments of the combined modulated main and tail rotor with wrapped (randomly applied) generic modulation (signal "A"), and two segments of the combined modulated main and tail rotor with wrapped (randomly applied) specific modulation (signal "B") were used. These comparisons were performed for both thickness and loading noise. This means that four different segments will be used for each type of noise, e.g. TGR-x, TTR-x, TGR-y, TTR-y (see comparison numbers 21-24 in Table 24 for thickness noise and comparison numbers 53-56 in Table 25 for loading noise). For this type of analysis, the point distribution is as follows:

- 0 points (4A): Participants choose the generic modulation for each question.
- 1 point (3A, 1B): Participants choose the generic modulation for three questions and the specific modulation for one question.
- 2 points (2B, 2A): Participants choose the generic modulation for half of the questions and the specific modulation for the other half.
- 3 points (1A, 3B): Participants choose the specific modulation for three questions and the generic modulation for one question (the inverse of the case of 1 point).
- 4 points (4B): Participants choose the specific modulation for each question.

The distributions of subject responses are shown below in Figure 62 and Figure 63, for thickness and loading noise, respectively.

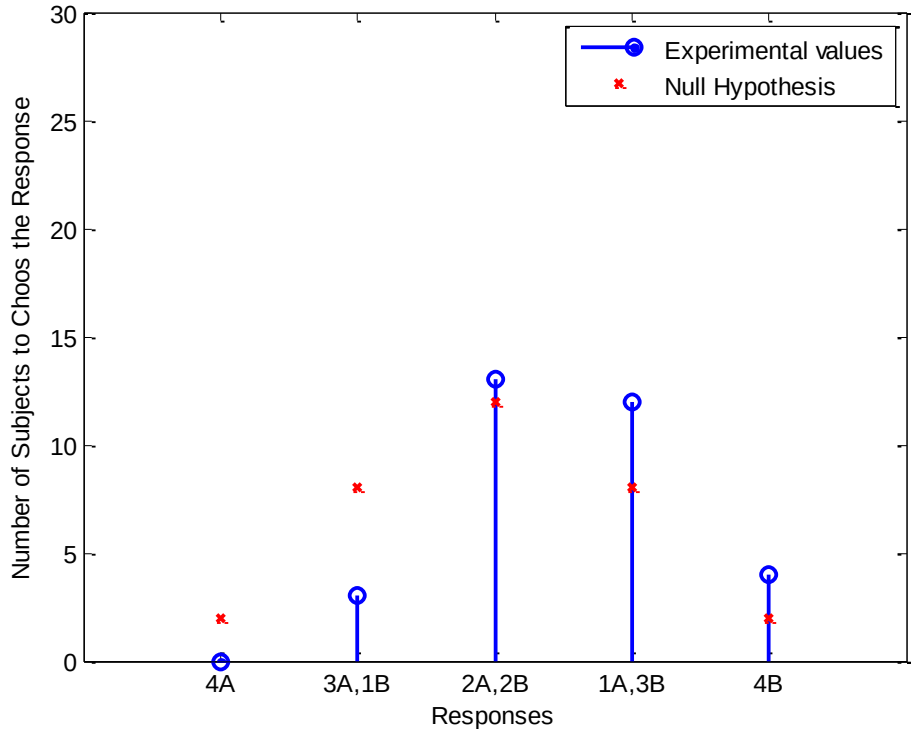

Figure 62: Responses for question 3 part a for thickness noise.

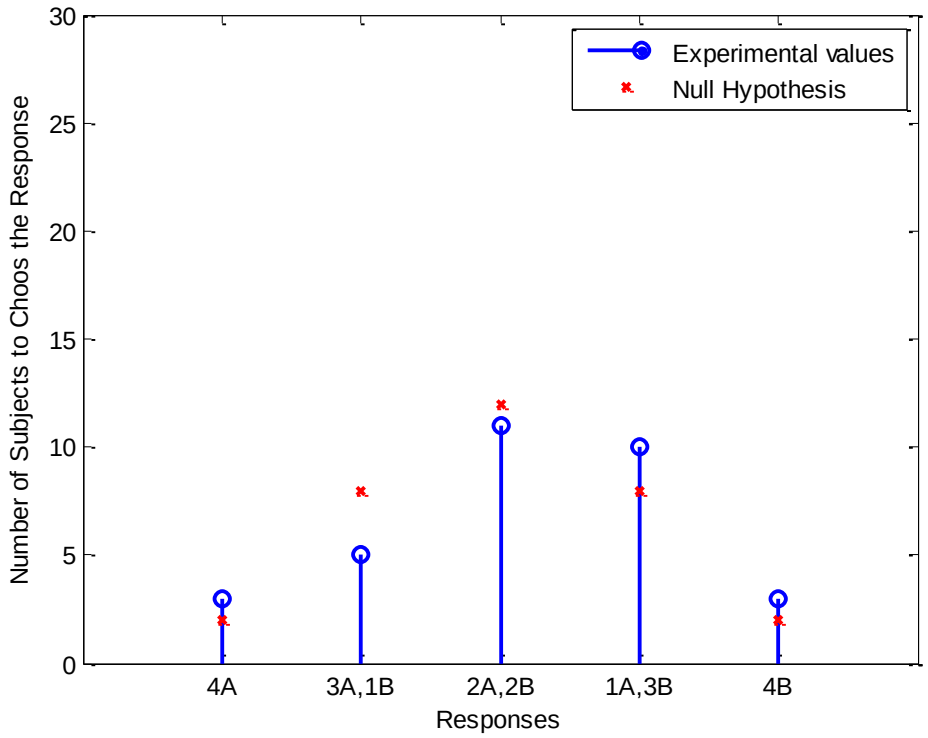

Figure 63: Responses for question 3 part a for loading noise.

The blue lines represent the values from the subjective test and the red x's represent values according to the null hypothesis in Figure 62 and Figure 63. The distribution generated by the null hypothesis is a random or Gaussian distribution. The experimental distributions resemble random distributions, which indicate that the participants cannot distinguish between the randomly applied generic modulation and the randomly applied specific modulation, in general. This may be due to the wrapping process which distorts the relative phase between each harmonic within each sound. However, the participants seem to favor signal "B" slightly more than signal "A", since more participants are to the right of 2A,2B than to the left. This means that the participants seem to favor the randomly applied specific modulation slightly more than the randomly applied generic modulation which is supported by the ranking in Table 22. This implies that the modulation of the helicopter noise is specific to each emission angle and a generic modulation is insufficient to characterize the modulation for all emission angles. This seems to be the case for the thickness noise slightly more so than the loading noise, when comparing the distributions of Figure 62 and Figure 63. Even though the thickness noise distribution is skewed toward randomly applied specific modulation, the distribution still

supports the null hypothesis that both signals have an equal chance of being chosen as the sound that best represents the reference sound. The chi-squared statistic was determined to be 9.2083 for the thickness noise. The threshold to support the null hypothesis for a distribution with four degrees of freedom and five percent significance is 9.488. Recall that the null hypothesis states that each signal has an equal chance (50 %) of being picked during each comparison, which is represented by a random or Gaussian distribution. Even though the χ^2 statistic for the thickness noise does not exceed the threshold for supporting the null hypothesis, the null hypothesis does not represent the data well since the distributions are skewed toward the randomly applied specific modulation.

6.4.4 Correlation of the Objective Fidelity Metrics and Subjective Ranking

A correlation of the objective fidelity metrics and subjective ranking is a logical next step in this process. A cursory look was taken to determine if a useful correlation could be found between the objective fidelity metrics and the subjective ranking. A comparison between Table 7 and Table 15, for research question 1, and Table 7 and Table 22, for research question 2, does not reveal a clear trend between the objective fidelity metrics and subjective ranking for either research question. This is due to the close grouping of the signals, excluding the combination of the modulated main rotor and modulated tail rotor signals, near the lower end of the ranking scale. Since the distribution of the subjective ranking only reveals data points at the two extremes, very little information, if any, is known of the signals that would fall between these extremes. Therefore, it is unlikely that performing a statistical analysis on such data would reveal a useful trend that would be applicable for data beyond the scope of this work.

One should not be surprised that the data would not be expected to make for a good statistical correlation given that the test was not designed for this purpose. This test was designed to aid in determining a method for synthesizing high fidelity rotorcraft noise. The ability to create a correlation between the objective metrics and subjective ranking was a secondary goal of this work. A new testing method, which focuses on the relationship between the objective metrics and subjective ranking, is needed to develop such a correlation. New sounds will need to be synthesized to validate this correlation. These sounds should be tailored in such a way to create a more even distribution across the subjective ranking scale.

7. Conclusion

The objective of this thesis was to determine a method by which high fidelity rotorcraft source noise could be synthesized. Several approaches were investigated to accomplish this goal. Two processes, a synchronous time-averaged process (Chapter 3) and a demodulation process (Chapter 4), were implemented to determine the time-invariant (periodic) harmonic signals of the main and tail rotors. The synchronous time-averaged process produced lower fidelity signals when compared to the demodulation process. The demodulation process was also used to isolate the modulation for each harmonic of the main and tail rotors. The demodulation process was successful in closely replicating the original signal for the original time record when modulated main and tail rotor were present.

A longer term objective of this research effort is the synthesis of an entire flyover. A necessary development for synthesizing flyover noise is that synthesized pressure time histories must be of arbitrary length. This was addressed through the implementation of the wrapping methods in section 5.1. Wrapping method 3 proved to be best suited for extending the time record of the original back-propagated signal. The capability to transition the sound between adjacent emission angles is necessary in order to create a high fidelity sound source simulation for a flyover scenario. Due to the lack of long pressure-time histories, this capability was addressed through the use of generic modulation.

Fidelity includes objective and subjective measures to aid in the determination of what is to be considered realistic [11]. The objective fidelity metrics, discussed in section 2.2, are used to evaluate the various synthesized signal throughout this work. The human subject test, also known as the second Synthesized Engine Noise Test (SENT2), described in Chapter 6 was performed to access the subjective fidelity of the synthesized signals. This test revealed that the full reconstruction of the intended sound produced a significantly higher fidelity signal than any of the other synthesized signals. The fully reconstructed sound combines the coherently modulated main rotor with the coherently modulated tail rotor ((d) in section 6.4.1 and (e) in section 6.4.2). A high fidelity rotorcraft sound source simulation was successfully achieved, thus fulfilling the overall

goal of this thesis. Several other conclusions may also be determined from this work, such as:

(i) Care must be taken when considering methods to extend the time record of the original back-propagated signal in order to prevent the introduction of artifacts in the synthesized signal.

(ii) The use of randomly applied specific modulation was insufficient in representing the true character of the original signal, which suggests that the noise of a rotorcraft is dependent upon time and the phase relationship between harmonics of a single rotor.

(iii) The use of generic modulation was insufficient in representing the true character of the original signal. This means that the noise of a rotorcraft is dependent on the emission angle of the sound.

(iv) The test subjects were unable to significantly differentiate between the randomly applied generic modulation and the randomly applied specific modulation. This suggests that wrapping method 3 sufficiently distorts the character of the original back-propagated signal and creates a signal significantly dissimilar to the original back-propagated signal.

(v) A model of the specific modulation, as well as the phase relationship between adjacent emission angles, is necessary to produce a complete high fidelity flyover scenario.

The methods outlined in this thesis are ideal for creating a synthetic version of the original signal but still lack the necessary components to produce a full flyover scenario. Synthesized aircraft noise is essential when creating a flyover scenario for aircraft that are a mere concept and where physically recording the sound of the aircraft is not a possibility.

8. Future Work

In order to create a proper flyover scenario, a model of the modulation is required. This model not only depends on the emission angle but also on time and the flight conditions during the flyover. This model will allow the observer to pass seamlessly from one emission angle to the next during a flyover simulation. More flight data is needed in order to properly characterize rotorcraft modulation in order to accurately represent all of the necessary flyover scenarios. This model must accurately characterize the phase and emission angle dependence of the rotorcraft noise for each of the many flight conditions, such as ascending flight, descending flight, or whether interactions between the rotor and the vortices exist in the case of BVI. A model for each rotorcraft will need to be created to properly capture the nuances of the various types and models of rotorcraft. The data for which this model is to be derived from should ideally be recorded in isolation, such as in a wind tunnel. The data from NASA's HART-II test may aid in the development of a model of rotorcraft modulation. Even though the amount of fluctuation may be reduced in a wind tunnel environment, such an environment would aid by facilitating long rotorcraft noise pressure-time histories. If wind tunnel data is not available, using discrete sections of flyover data, like the sounds used in this thesis, from multiple flyovers would be necessary to develop an adequate model of the modulation of the rotorcraft. Another possible way to gather the necessary data is to use in-flight microphones to record the aircraft of interest. In-flight microphones are microphones that are either attached to an apparatus, which is attached the aircraft of interest, or microphones attached to a separate aircraft, which flies with the aircraft of interest [6, 10]. The use of an interpolation scheme will be necessary to smoothly transition from one emission angle to the next. This smooth transition will allow for a truly immersive flyover environment. This immersive flyover environment will allow future researchers to evaluate the entire flyover or simply a small section of the flyover. In the future, a correlation between the objective metrics and subjective ranking may be desired. Such a correlation would allow the fidelity of a signal to be determined without the need for a psychoacoustic test. This topic is discussed in section 6.4.4. This ability would allow engineers to determine the fidelity of signals efficiently.

A better understanding of the relationship between human perception of aircraft noise and annoyance will allow for the manufacturing of quieter aircraft. Future researchers may eventually evaluate human perception of aircraft noise in a fully immersive virtual reality simulation, which will allow the test subjects to evaluate aircraft noise in various environments, such as inside an office building, in an open field, etc., without leaving the testing room.

Bibliography

[1] Lopes, L.V. and Burley, C.L., "Design of the Next Generation Aircraft Noise Prediction Program: ANOPP2," *17th AIAA/CEAS Aeroacoustics Conference*, Portland, OR; United States, 6-8 June, 2011.

[2] Shirey, J.S., Brentner, K.S., and Chen, H.-n., "A Validation Study of the PSU-WOPWOP Rotor Noise Prediction System," *45th AIAA Aerospace Sciences Meeting and Exhibit*, AIAA 2007-1240, Reno, Nevada, 8-11 January, 2007.

[3] David, C., Bryan, E., Peter, K., William, D., and Michael, M., "NASA/Army/Bell XV-15 tiltrotor low noise terminal area operations flight research program," *6th Aeroacoustics Conference and Exhibit*, American Institute of Aeronautics and Astronautics, AIAA-2000-1923, Lahaina, HI, 12-14 June, 2000.

[4] JanakiRam, R.D. and Khan, H., "Prediction and Validation of Helicopter Descent Flyover Noise," *American Helicopter Society 56th Annual Forum*, Virginia Beach, Virginia, May 2-4, 2000.

[5] Brentner, K.S. and Farassat, F., "Modeling aerodynamically generated sound of helicopter rotors," *Progress in Aerospace Sciences*, Vol. 39, pp. 83-120, 2003.

[6] Schmitz, F.H., Greenwood, E., Sickenberger, R.D., Gopalan, G., Sim, B.W.-C., Conner, D., III, E.M., and Decker, W.A., "Measurement and Characterization of Helicopter Noise in Steady-State and Maneuvering Flight," *American Helicopter Society 63rd Annual Forum*, Virginia Beach, VA., May, 2007.

[7] Harris, F.D., "2.7 NOISE," In *Introduction To Autogyros, Helicopters, and Other V/STOL Aircraft*, vol. Volume II: Helicopters, *Introduction To Autogyros, Helicopters, and Other V/STOL Aircraft*, Catherine Dow, D.T.S., Ed., NASA Center for AeroSpace Information and National Technical Information Service, pp. 437-538, 2012.

[8] Sickenberger, R., Gopalan, G., and Schmitz, F.H., "Helicopter Near-Horizon Harmonic Noise Radiation due to Cyclic Pitch Transient Control," *American Helicopter Socienty 67th Annual Forum*, Virginia Beach, Virginia, 03-05 May, 2011.

[9] Magliozzi, B., Hanson, D.B., and Amiet, R.K., "1. Propeller and Propfan Noise," NASA Langley Research Center, Reference Publication NASA RP-1258, Vol. 1 WRDC Tech Rep 90-3052, August 1991.

[10] Splettstoesser, W.R., Schultz, K.J., Boxwell, D.A., and Schmitz, F.H., "Helicopter Model Rotor-Blade Vortex Interaction Impulsive Noise: Scalability and Parametric Variation," NASA, Ed., 1984.

[11] "Fidelity," *Modeling & Simulation Coordination Office*, 2011.

[12] O'Neil, P.V., "Chapter 13: Fourier Series," In *Advanced Engineering Mathematics*, Adams, R., Ed., Seventh Edition ed, Global Engineering, pp. 427-464, 2007.

[13] Bendat, J.S. and Piersol, A.G., "Chapter 13: The Hilbert Transform," In *Random Data: Analysis and Measurement Procedures*, Vic Barnett, N.A.C.C., Nicholas I. Fisher, Iain M. Johnstone, J. B. Kadane, David G. Kendall, David W. Scott, Bernard W. Silverman, Adrian F. M. Smith, Jozef L. Teugles; Ralph A. Bradley,

Emeritus, J. Stuart Hunter, Emeritus, Ed., 3rd ed, Wiley-Interscience Publication, pp. 518-549, 2000.

[14] Allen, M.P., Rizzi, S.A., Burdisso, R., and Okcu, S., "Analysis and Synthesis of Tonal Aircraft Noise Sources," *18th AIAA/CEAS Aeroacoustics Conference (33rd AIAA Aeroacoustics Conference)*, AIAA 2012-2078, Colorado Springs, CO, 04-06 June, 2012.

[15] Greenwood, E. and Schmitz, F.H., "Separation of Main and Tail Rotor Noise Sources from Ground-Based Acoustic Measurements in the Time-Domain," *Journal of Aircraft*, Vol. 51, No. 2, pp. 464-472, 2014.

[16] Page, J.A., Wilmer, C., and Plotkin, K.J., "Rotorcraft Noise Model Technical Reference and User Manual (Version 7.1)," Wyle Laboratories, Inc, 241 18th Street S., Suite 701, Arlington VA 22202 WR 08-04, 2008.

[17] Kinsler, L.E., Frey, A.R., Coppens, A.B., and Sanders, J.V., *Fundamentals of Acoustics*, 4th Edition ed, John Wiley & Sons, Inc, 2000.

[18] "Psychoacoustic Analyses in the ArtemiS SUITE," HEAD Acoustics, Application Notes 2014.

[19] "Loudness and Sharpness Calculation," HEAD Acoustics, Application Notes 2013.

[20] Pierce, A.D., "Chapter 4: Radiation from Vibrating Bodies," In *Acoustics: An Introduction to Its Physical Principles and Applications*, Acoustical Society of America1991.

[21] Turkdogru, N., "Validity of the Point Source Assumption of a Rotor for Farfield Acoustic measurements with and without Sheilding," *Doctoral Dissertation*, Aerospace Engineering, Georgia Institute of Techonology, 2010.

[22] Oppenheim, A.V. and Shafer, R.W., "Appendix B: Continuous-Time Filters," In *Discrete-Time Signal Processing 3rd Ed.*, Disanno, S., Ed., Pearson Higher Education, Inc., pp. 1056-1058, 2010.

[23] Lacanette, K., "A Basic Introduction to Filters--Active, Passive, and Switched-Capacitor," National Semiconductor Corporation, 1991.

[24] MathWorks, "Signal Processing Toolbox," The MathWorks, Inc., 2013.

[25] Bendat, J.S. and Piersol, A.G., "Chapter 13: The Hilbert Transform " In *Random Data: Analysis and Measurement Procedures*, David J. Balding, N.A.C.C., Garrett M. Fitzmaurice, Iain M. Johnstone, Geert Molenberghs, David W. Scott, Adrian F. M. Smith, Ruey S. Tsay, Sanford Weisburg; Vic Barnett, Emeriti; J. Stuart Hunter, Emeriti; Jozef L. Teugels, Emeriti, Ed., 4th ed, John Wiley & Sons, pp. 473-504, 2010.

[26] Kirkpatrick, S., Gelatt, C.D., and Vecchi, M.P., "Optimization by Simulated Annealing," *Science* Vol. 220, No. 4598, pp. 671-680, http://links.jstor.org/sici?sici=0036-8075%2819830513%293%3A220%3A4598%3C671%3AOBSA%3E2.0.CO%3B2-8, 1983.

[27] Allen, M.P., "Analysis and Synthesis of Aircraft Engine Fan Noise for Use in Psychoacoustic Studies," Mechancial Engineering, Virginia Polytechnic Institute and State University, 2012.

[28] Okcu, S., Allen, M.P., and Rizzi, S.A., "Psychoacoustic assessment of a new aircraft engine fan noise synthesis method," *164th Meeting of the Acoustical*

Society of America, Vol. 132, pp. 1926-1926, Kansas City, Missouri, 22-26 October, 2012.

[29] Faller, K.J., Rizzi, S.A., and Aumann, A.R., "Acoustic Performance of a Real-Time Three-Dimensional Sound-Reproduction System," National Aeronautics and Space Administration NASA/TM-2013-218004, June 2013.

[30] Keener, J.P., "The Perron-Frobenius Theorem and the Ranking of Football Teams," *Society for Industrial and Applied Mathematics*, Vol. 35, No. 1, pp. 80-93, http://links.jstor.org/sici?sici=0036-1445%28199303%2935%3A1%3C80%3ATPTATR%3E2.0.CO%3B2-O, 1993.

Appendix A: Noise Comparisons

Table 23: Test sounds naming convention.

Number	Name	Recorded or Synthesized	Included Rotors	Noise Source	Modulation Source	Modulation Application	Length [s]	Chunks Needed	Question 1	Question 2	Question 3
1	RT	Recorded	Main and Tail	2			2.4	Ref.	All		
2	RL	Recorded	Main and Tail	4			1.1	Ref.			
3	TNM	Synthesized	Main Only	2	None		20	X	a		
4	TTM	Synthesized	Main Only	2	2	Coherent	2.4	X	b		
5	TN	Synthesized	Main and Tail	2	None		20	X	c	a	
6	TTC	Synthesized	Main and Tail	2	2	Coherent	2.4	X	d	e	
7	LNM	Synthesized	Main Only	4	None		20	X	a		
8	LLM	Synthesized	Main Only	4	4	Coherent	1.1	X	b		
9	LN	Synthesized	Main and Tail	4	None		20	X	c	a	
10	LLC	Synthesized	Main and Tail	4	4	Coherent	1.1	X	d	e	
11	TGR	Synthesized	Main and Tail	2	3	Random	20	X,Y		b	x
12	TGC	Synthesized	Main and Tail	2	3	Coherent	1.3	X		c	
13	TTR	Synthesized	Main and Tail	2	2	Random	20	X,Y		d	x
14	LGR	Synthesized	Main and Tail	4	3	Random	20	X,Y		b	x
15	LGC	Synthesized	Main and Tail	4	3	Coherent	1.3	X		c	
16	LLR	Synthesized	Main and Tail	4	4	Random	20	X,Y		d	x

Table 24: SENT 2 thickness noise comparisons.

Number	Question 1	Question 2	Question 3	Reference	A Sample	A Chunk	B Sample	B Chunk
1	a, b			RT	TNM		TTM	
2	a, b			RT	TTM		TNM	
3	a, c			RT	TNM		TN	
4	a, c			RT	TN		TNM	
5	a, d			RT	TNM		TTC	
6	a, d			RT	TTC		TNM	
7	b, c			RT	TTM		TN	
8	b, c			RT	TN		TTM	
9	b, d			RT	TTM		TTC	
10	b, d			RT	TTC		TTM	
11	c, d	a, e		RT	TN		TTC	
12	c, d	a, e		RT	TTC		TN	
13		a, b		RT	TN		TGR	x
14		a, b		RT	TGR	x	TN	
15		a, c		RT	TN		TGC	
16		a, c		RT	TGC		TN	
17		a, d		RT	TN		TTR	x
18		a, d		RT	TTR	x	TN	
19		b, c		RT	TGR	x	TGC	
20		b, c		RT	TGC		TGR	x
21		b, d	a	RT	TGR	x	TTR	x
22		b, d	a	RT	TTR	x	TGR	x
23		b, d	a	RT	TGR	y	TTR	y
24		b, d	a	RT	TTR	y	TGR	y
25		b, e		RT	TGR	x	TTC	
26		b, e		RT	TTC		TGR	x
27		c, d		RT	TGC		TTR	x
28		c, d		RT	TTR	x	TGC	
29		c, e		RT	TGC		TTC	
30		c, e		RT	TTC		TGC	
31		d, e		RT	TTR	x	TTC	
32		d, e		RT	TTC		TTR	x

Table 25: SENT 2 loading noise comparisons.

Number	Question 1	Question 2	Question 3	Reference	A Sample	A Chunk	B Sample	B Chunk	Comments
33	a, b			RL	LNM		LLM		
34	a, b			RL	LLM		LNM		
35	a, c			RL	LNM		LN		
36	a, c			RL	LN		LNM		
37	a, d			RL	LNM		LLC		
38	a, d			RL	LLC		LNM		
39	b, c			RL	LLM		LN		
40	b, c			RL	LN		LLM		
41	b, d			RL	LLM		LLC		
42	b, d			RL	LLC		LLM		
43	c, d	a, e		RL	LN		LLC		
44	c, d	a, e		RL	LLC		LN		
45		a, b		RL	LN		LGR	x	
46		a, b		RL	LGR	x	LN		
47		a, c		RL	LN		LGC		
48		a, c		RL	LGC		LN		
49		a, d		RL	LN		LLR	x	
50		a, d		RL	LLR	x	LN		
51		b, c		RL	LGR	x	LGC		
52		b, c		RL	LGC		LGR	x	
53		b, d	a	RL	LGR	x	LLR	x	
54		b, d	a	RL	LLR	x	LGR	x	
55		b, d	a	RL	LGR	y	LLR	y	
56		b, d	a	RL	LLR	y	LGR	y	
57		b, e		RL	LGR	x	LLC		
58		b, e		RL	LLC		LGR	x	
59		c, d		RL	LGC		LLR	x	
60		c, d		RL	LLR	x	LGC		
61		c, e		RL	LGC		LLC		
62		c, e		RL	LLC		LGC		
63		d, e		RL	LLR	x	LLC		
64		d, e		RL	LLC		LLR	x	

Appendix B: Order of the Presentation of Signals

Table 26: Question order for each comparison session.

	Order			
Forward Order #	a	b	c	d
1	59	40	50	49
2	6	16	13	19
3	41	43	55	54
4	56	60	46	58
5	9	18	11	3
6	38	34	57	61
7	21	23	7	27
8	31	14	12	15
9	52	62	63	37
10	20	4	10	8
11	29	32	1	17
12	48	64	47	39
13	25	26	24	30
14	42	36	53	44
15	22	5	28	2
16	51	35	33	45

Table 27: Order of the comparison session for each test group (prime designation indicates order reversal).

	Session			
Subject Group #	1	2	3	4
1	a	b	c	d
2	b	d	a	c
3	c	a	d	b
4	d	c	b	a
5	a'	b'	c'	d'
6	b'	d'	a'	c'
7	c'	a'	d'	b'
8	d'	c'	b'	a'

Appendix C: Index of Supplemental Audio Files

Table 28: Auxiliary audio files.

Audio File Name	Description
audiofile01.wav	Synchronous time-averaged main rotor signal only for thickness noise
audiofile02.wav	Synchronous time-averaged main rotor signal only for loading noise
audiofile03.wav	Synchronous time-averaged main rotor and tail rotor signal for thickness noise
audiofile04.wav	Synchronous time-averaged main rotor and tail rotor signal for loading noise
audiofile05.wav	Demodulation method Case A for thickness noise (TNM)
audiofile06.wav	Demodulation method Case A for loading noise (LNM)
audiofile07.wav	Demodulation method Case B for thickness noise (TTM)
audiofile08.wav	Demodulation method Case B for loading noise (LLM)
audiofile09.wav	Demodulation method Case C for thickness noise (TN)
audiofile10.wav	Demodulation method Case C for loading noise (LN)
audiofile11.wav	Demodulation method Case D for thickness noise (TTC)
audiofile12.wav	Demodulation method Case D for loading noise (LLC)
audiofile13.wav	Sample of wrapping method 1 signal to showcase the periodicity of this method for thickness noise
audiofile14.wav	Sample of wrapping method 1 signal to showcase the periodicity of this method for loading noise
audiofile15.wav	Sample of wrapping method 2 signal to showcase the periodicity of this method for thickness noise
audiofile16.wav	Sample of wrapping method 2 signal to showcase the periodicity of this method for loading noise
audiofile17.wav	Sample of wrapping method 3 signal to showcase the lack of periodicity of this method for thickness noise
audiofile18.wav	Sample of wrapping method 3 signal to showcase the lack of periodicity of this method for loading noise
audiofile19.wav	Section x of the randomly applied, generically modulated signal for thickness noise
audiofile20.wav	Section x of the randomly applied, generically modulated signal for loading noise
audiofile21.wav	Section y of the randomly applied, generically modulated signal for thickness noise
audiofile22.wav	Section y of the randomly applied, generically modulated signal for loading noise
audiofile23.wav	Coherently applied, generically modulated signal for thickness noise
audiofile24.wav	Coherently applied, generically modulated signal for loading noise

audiofile25.wav	Reference signal for thickness noise
audiofile26.wav	Reference signal for loading noise
audiofile27.wav	Section x of the randomly applied, specifically modulated signal for thickness noise (TTR-x)
audiofile28.wav	Section y of the randomly applied, specifically modulated signal for thickness noise (TTR-y)
audiofile29.wav	Section x of the randomly applied, specifically modulated signal for loading noise (LLR-x)
audiofile30.wav	Section y of the randomly applied, specifically modulated signal for loading noise (LLR-y)

Appendix D: List of Attachments

Table 29: Attached files.

Filename	Description
Auxiliary_Audio_Files.zip	Contains all of the auxiliary audio files listed in Appendix C: Index of Supplemental Audio Files.
dedop_bandpass_sect2only_mainrotor.m	Performs all of the calculations to produce sounds used in this work for the main rotor only (will work for all sections of the hemisphere).
dedop_bandpass_sect2only_tailrotor.m	Performs all of the calculations to produce sounds used in this work for the tail rotor only and combines the data necessary to create the signals with characteristics of the combined main rotor and tail rotor (will work for all sections of the hemisphere).